CHARACTERISING THE PROTEIN-PROTEIN INTERACTIONS OF TACTA1-3 TOXIN-ANTITOXIN FAMILY

Rashi Kahan

A thesis presented for the degree of

Master of Philosophy

DEPARTMENT OF CHEMISTRY
IMPERIAL COLLEGE LONDON
July 2021

Declaration of Originality

I hereby declare that this thesis is my own work and is generated from the results of my original research. Any work that is the result of collaboration or the input of others has been specifically stated within the text. Information derived from the published or unpublished work of others has been acknowledged and referenced within the text.

Signed: 

Rashi Kahan

July 2021

Declaration of Copyright

The copyright of this thesis rests with the author and is made available under a Creative Commons Attribution Non-Commercial No Derivatives licence. Researchers are free to copy, distribute or transmit the thesis on the condition that they attribute it, that they do not use it for commercial purposes and that they do not alter, transform, or build up on it. For any reuse or redistribution, researchers must make clear to others the licence terms of this work.

Signed: 

Rashi Kahan

July 2021

Characterising the protein-protein interactions of TacTA1-3 Toxin-Antitoxin Family

Rashi Kahan

Abstract

Persisters are a small portion of a cellular population with heterogenous phenotypes, that switch to a dormant, growth arrested state upon antibiotic exposure allowing them to survive. Antibiotic persistence is a growing field of interest due to the recalcitrance of infection presenting a challenge to antibiotic therapy. Type II toxin-antitoxin systems have been implicated in persister cell formation. The TacT family of toxins containing a Gcn5 N-acetyltransferase fold have been identified to contribute to persistence in *Salmonella enterica.* Identifying pan peptide inhibitors of the TacT toxin family is a potential method to prevent the formation of persister cells in *Salmonella Typhimurium* and *Salmonella Enteritidis*. Towards this long-term goal, characterisation of the TacT interactions with their respective antitoxins has been reported in this thesis. Toxin-antitoxin affinities have been identified to be within the nanomolar to picomolar range, with a biphasic relationship observed. The protein-protein interaction demonstrated a high salt dependence suggesting primarily electrostatic interactions are involved. The results provide a starting point for the identification of a peptide compound to treat persistence by targeting the TacT toxins. In parallel this thesis reports the trial expression of the wild-type TacT proteins. This is crucial for the accurate characterisation of the proteins and for activity assays.

Acknowledgements

I would firstly like to thank my supervisors Dr Anna Barnard and Dr Louise Walport, you taught me so much about science and research. I so appreciate your support throughout my time at Imperial, and your understanding when I decided to convert to the MPhil.

Thank you to all the members of the Barnard group and Tate group for the support and fun times in the lab. I learnt so much from all of you and feel sad to be leaving so soon.

Thank you to my parents, siblings, and parents-in-law for your constant support and for trying to understand my research!

Finally, a huge thank you to my wonderful Mikey and Liora. Mikey you knew my project so well you could probably have done it yourself! Your support means the world. Liora, your little cuddles make everything perfect love mama.

Contents

1. Introduction . . . . . 14 – 25

1.1. Bacterial Persistence 14

1.1.1. The Persister Hallmark 14

1.1.2. Mechanisms of Bacterial Persistence 15

1.1.3. Toxin-Antitoxin Systems and their Role in Persistence . 15

1.1.4. GNAT Toxins 17

1.1.5. GNAT Toxins in Salmonella 17

1.2. Targeting PPIs in Bacteria 21

1.2.1. Discovery of Novel PPI Inhibitors 21

1.2.2. PPIs as Antibacterial Targets 21

1.2.3. PPIs of TA systems as Antibacterial Targets . . . 22

1.2.4. Strategy of Targeting TacTA family 24

1.3. Thesis Aims 24

2. Development of Toxic Protein Expression and Purification for the TacT1 – 3 Toxins . . . . . 26 - 47

2.1. Introduction to Toxic Protein Expression 26

2.2. Method 1: Expression and Purification of TacT1-3 YF Mutants . 30

2.2.1. Literature Approach 30

2.2.2. Optimised Expression Via Autoinduction . . . 31

2.2.3. Optimised purification of $(His)_7$-$TacT1^{Y140F}$ . . . 34

2.3. Method 2: Expression of WT TacT1-3 in the Presence of Pth . 37

2.3.1. Plasmid Design and Construction 38

2.3.1.1. Plasmid Design 38

2.3.1.2. Plasmid Construction 39

2.3.2. Trial Expression of Pth 41

2.3.3. Trial Expression of WT TacT1-3 in the Presence of Pth . 43

2.4. Chapter Summary and Conclusions 47

3. Characterising the Protein-Protein Interactions of TacTA1-3 . . 49-68

3.1. Introduction to Biophysical Characterisation of PPIs . . 49

3.1.1. Characterisation of PPIs 49

3.1.2. Characterisation of PPIs of TA systems . . . 50

3.1.3. Methods 52

3.1.3.1. Differential Scanning Fluorimetry . . . 52

3.1.3.2. Florescence Anisotropy 53

3.1.3.3. Surface Plasmon Resonance 53

3.1.4. Chapter Aims 54

3.2. Antitoxin Peptide Design and Synthesis 54
3.2.1. Introduction to Solid Phase Peptide Synthesis . . 55
3.2.2. Synthesis, Purification and Analysis of Peptides (**TAMRA_**)**1**, **2** and **3** 55
3.3. Binding of TacT1-3 to peptides of TacA1-3 58
3.3.1. Binding analysis of the TacT proteins to their antitoxin peptides by DSF 58
3.3.2. Binding analysis of the TacT proteins to their antitoxin peptides by SPR 62
3.3.3. Binding analysis of the TacT proteins to their antitoxin peptides by FA 65
3.4. Chapter Summary and Conclusions 67

4. Conclusions and Outlook . . . . . 69 – 71
4.1. Summary of Findings 69
4.2. Future Directions 70
4.2.1. Random non-standard Peptide Integrated Discovery . 70
4.2.2. In Vitro Fluorescence Acetylation Activity Assay . . 71

5. Biological Methods . . . . . 72 – 74
5.1. Plasmid Construction 72
5.2. Mutant Protein Expression 72
5.3. Mutant Protein Purification 72
5.4. Pth Expression Trials 73
5.5. Toxic Protein Expression Trials 74

6. Synthetic Methods . . . . . 75 – 76
6.1. General Methods 75
6.2. Solid Phase Peptide Synthesis 75
6.3. Peptide Purification 76

7. Affinity Assays Methods . . . . . 77 – 78
7.1. Differential Scanning Fluorimetry 77
7.2. Surface Plasmon Resonance Assay 77
7.3. Fluorescence Anisotropy 78

List of Figures

1.1. Antibiotic persistence is characterised by a biphasic killing curve 14
1.2. Features of a generic type II TA complex 16
1.3. GNAT toxin activity 18
1.4. Crystal structure of the TacT1 toxin dimer 19
1.5. Overlays of TacT1-3 crystal structures 20
1.6. PPIs of TA systems as antibacterial targets 23
2.1. Schematic of recombinant protein production 26
2.2. Recombinant expression of the Doc_{STm} toxin in bacteria. 28
2.3. Co-ordination of acetyl group of Ac-CoA by Y140 in WT TacT1 29
2.4. Recombinant expression of (His)7-TacT1^{Y140F} protein (20.9 kDa) 31
2.5. Trial expression of TacT proteins ((His)7-TacT1^{Y140F}: 20.9 kDa, (His)7-TacT2^{Y143F}: 20.9 kDa and (His)7-TacT3^{Y137F}: 22.2 kDa 32
2.6. Recombinant protein expression of TacT proteins ((His)7-TacT1^{Y140F}: 20.9 kDa, (His)7-TacT2^{Y143F}: 20.9 kDa and (His)7-TacT3^{Y137F}: 22.2 kDa 33
2.7. Schematic of recombinant protein purification 34
2.8. SDS-PAGE gel analysis of cell lysis of (His)7-TacT1^{Y140F} protein Expression 35
2.9. SDS-PAGE gel analysis of (His)7-TacT1^{Y140F} IMAC purification 35
2.10. SDS-PAGE gel analysis of (His)7-TacT1^{Y140F} IMAC purification 36
2.11. SDS-PAGE gel analysis of (His)7-TacT1^{Y140F} SEC purification 37
2.12. Design of primers using in silico construct of final plasmid product 39
2.13. Agarose gel analysis of PCR products prior to HiFi DNA ligation 40
2.14. Agarose gel analysis following site-directed mutagenesis 41
2.15. Expression of Pth protein (22.9 kDa) 42
2.16. Growth curves of TacT trial expression in BL21-AI *E. coli* cell culture in LB and TB media 45
2.17. SDS-PAGE analysis of total cell protein expression of TacT proteins with Pth at 24 hrs 46
3.1. Minimum antitoxin sequences 54
3.2. General scheme for peptide synthesis 56
3.3. UV chromatogram of purified peptide **1** at 280 nm 58
3.4. DSF with TacT1 protein at different conditions 60
3.5. DSF with TacT proteins and their minimum antitoxin peptides 61
3.6. SPR sensograms of the minimum antitoxin peptides **1-3** with their respective TacT1-3 toxin proteins 63
3.7. SPR sensograms of the minimum antitoxin peptides 1 and 2 with their respective TacT toxin proteins 63

3.8. Fluorescence anisotropy for binding of the toxin proteins to their respective minimum antitoxin peptide labelled with TAMRA 65
3.9. Fluorescence anisotropy for binding of the TacT2 protein to its respective minimum antitoxin peptide labelled with TAMRA 66

List of Tables

3.1. Melting temperature measured by DSF for each of the TacT proteins 59
3.2. Change in melting temperature measured by DSF for each of the TacT proteins binding to their minimum peptide 62
3.3. Binding data measured by SPR for each of the TacT proteins binding to their minimum peptide 64

Acronyms and Abbreviations

(p)ppGpp	Guanosine Tetraphosphate and Guanosine Pentaphosphate
Ac-CoA	Acetyl Coenzyme A
ACN	Acetonitrile
AMR	Antimicrobial Resistance
β-ME	β-Mercaptoethanol
BAM	β-Barrell Assembly Machine
CD	Circular Dichroism
CV	Column Volumes
DCM	Dichloromethane
DIC	N, N'-Diisopropylcarbodiimide
DIPEA	N,N-Diisopropylethylamine
DMF	Dimethylformamide
DMSO	Dimethylsulfoxide
DNA	Deoxyribonucleic Acid
DODT	2,2'-(ethylenedioxy)diethanethiol
dsDNA	Double Stranded Deoxyribonucleic Acid
DSF	Differential Scanning Fluorimetry
DTT	Dithiothreitol
FA	Fluorescence Anisotropy
FIT	Flexible in vitro Translation
Fmoc	Fluoren-9-ylmethyloxycarbonyl
GNAT	Gcn5 N-Acetyltransferases
HBTU	N-[(1H-benzotriazol-1-yl)(dimethylamino)methylene]-N-methylmethanaminium hexafluorophosphate N-oxide
HTS	High Throughput Screening
IMAC	Immobilised-Metal Affinity Chromatography

IPTG	Isopropyl β-D-1-Thiogalactopyranoside
ITC	Isothermal Calorimetry
K_D	Equilibrium Disscociatioin Constant
k_{off}	Dissociation Constant
k_{on}	Association Constant
LB	Luria-Bertani
LC-MS	Liquid Chromatography-Mass Spectrometry
Lpt	Lipopolysaccharide Transport
MALDI	Matrix-Assisted Laser Desorption/Ionisation
MCK	Multi-Cycle Kinetics
mRNA	Messenger Ribonucleic Acid
MS	Mass Spectrometry
MST	Microscale Thermophoresis
NUS	N-Utilisation Substances
OD_{600}	Optical density at 600 nm
ORFs	Open Reading Frames
Oxyma	Ethyl 2-Cyano-2-(Hydroxyimino)Acetate
PCR	Polymerase chain reaction
PMSF	Phenylmethanesulfonyl Fluoride
PPI	Protein-Protein Interaction
Pth	Peptidyl-tRNA Hydrolase
RaPID	Random non-standard Peptide Integrated Discovery
RNAP	RNA Polymerase
SCK	Single-Cycle Kinetics
SDS	Sodium Dodecyl Sulfate
SDS-PAGE	Sodium Dodecyl Sulphate-Polyacrylamide Gel Electrophoresis
SEC	Size Exclusion Chromatography
SEC-MALS	Size Exclusion Chromatography – Multi-Angle Light Scattering

SPPS	Solid Phase Peptide Synthesis
SPR	Surface Plasmon Resonance
SSB	Single-Stranded DNA-Binding Protein
TA	Toxin-Antitoxin
TacT	tRNA Acetylating Toxin
TAMRA	Tetramethylrhodamine
TB	Terrific Broth
TFA	Trifluoroacetic acid
TIS	Triisopropyl Silane
T_m	Melting Temperature
tRNA	Transfer Ribonucleic Acid
WT	Wild-Type

Chapter 1

Introduction

1.1. Bacterial Persistence

The increasing failure of antibiotics is a well-documented threat to the modern healthcare system. The WHO have published a Global Action Plan aiming to quell the impending crisis due to the growing lack of infection control as a result of increasing antimicrobial resistance (AMR).[1,2] Alongside AMR, antibiotic persistence is a related emerging field of interest.[3] It is increasingly recognised as a second causative factor in the failure of antibiotic treatments and recalcitrant infection, although the underlying mechanisms and biological pathways remain somewhat elusive.[4]

1.1.1. The Persister Hallmark

Bacterial persistence is a defence mechanism in which a small portion of a cellular population switch to a dormant, growth arrested state upon antibiotic exposure allowing them to survive, likely resulting in recalcitrance of infection.[5,6] By the most recent definition and understanding, persister cells all have the same genotype but heterogenous phenotypes. All the bacteria of the population have the ability to persist, but a small population are triggered to enter the dormant persister state upon stress conditions such as antibiotic treatment.[7] The persister hallmark is a biphasic antibiotic killing curve indicating that not all bacteria are killed at same rate with some surviving in the culture (**Figure 1.1**).[8] Bacteria such as *Salmonella Typhimurium* have been observed to produce persisters that can reinitiate infection after

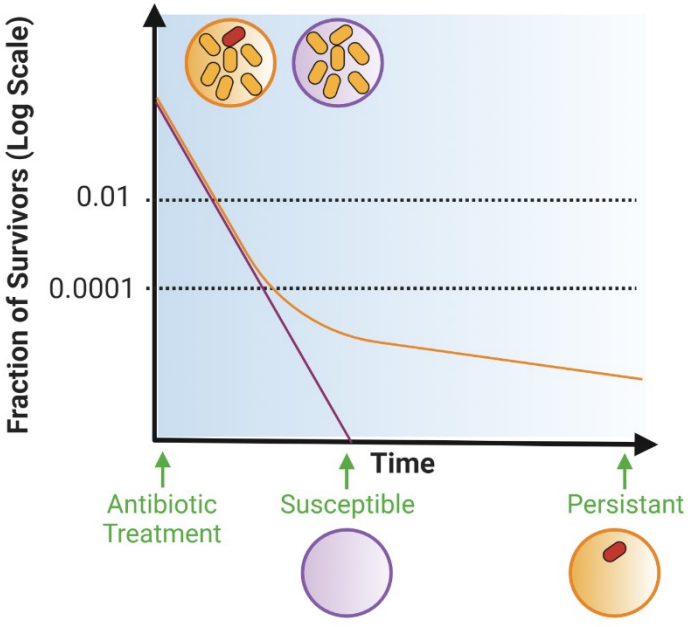


Figure 1.1: Antibiotic persistence is characterised by a biphasic killing curve. *Following antibiotic treatment, a homologous population of bacteria are all killed (purple). Following the same treatment, within a population of bacteria with heterogenous phenotypes, persisters are identified by a classic biphasic kill curve (orange). An initial rapid kill curve of the susceptible population is first observed, followed by a slower decrease in the persistent bacteria population.*

treatment. They are predicted to result in multidrug resistance due to increasing survival and mutation rates as long courses of antibiotics for relapsing infections may increase selection of resistant strains.[9,10]

1.1.2. Mechanisms of Bacterial Persistence

Most of the molecular pathways implicated in persister formation are controlled by stress signalling.[4] The stringent response pathway is the main stress signalling pathway conserved across nearly all mechanisms of persister formation. It is proposed to work together with the general stress response pathway or with the SOS response pathway.

The stringent response pathway is a highly conserved response in bacteria and is triggered by nutrient deprivation or other stresses such as antibiotic exposure.[4] It triggers survival functions via the alarmones guanosine tetraphosphate (ppGpp) and guanosine pentaphosphate (pppGpp).[11] Accumulation of (p)ppGpp alters protein activities and reprograms transcriptional functions, resources are instead redirected toward functioning in a dormant state to allow the survival of cells in stressful conditions.[4] The molecular basis and full mechanism of persister formation by (p)ppGpp is not fully understood.[11,12] It is currently hypothesised that (p)ppGpp signalling is activated either by stochastic activation of the (p)ppGpp signalling in cell growth, or environmental activation of (p)ppGpp production.[13] This then leads to entry into the persister state.

The environmental activation of (p)ppGpp production and subsequent entry into the persister state also relies on other pathways. These include the general stress response pathway or the SOS response pathway. The general stress response pathway relies on the alternative sigma factor RpoS.[14,15] RpoS has a dual role, as well as mediating the general stress response pathway, it also regulates bacterial persister formation.[14] As a result, under conditions that induce the general stress response, bacteria can also enter the persister state if there are high levels of RpoS. The SOS response system is maintained by a DNA-binding protein RecA and a transcriptional repressor protein LexA.[16] DNA damage activates expression of the RecA gene which triggers the SOS response. The response repairs damaged DNA allowing resuscitation of persister cells. Additionally, the response has been implicated in direct persister formation, although the pathway is not understood.[13]

1.1.3. Toxin-Antitoxin Systems and their Role in Persistence

Multiple studies have found a link between toxin-antitoxin (TA) systems and persister formation.[17,18] TA modules are small genetic elements usually comprised of two genes. The genes encode for a stable toxin which inhibits essential cellular functions and subsequently cell growth, and an unstable antitoxin that inhibits toxin activity (**Figure 1.2**).[19] There are a large variety of TA systems present in bacterial cells.[17] There are eight distinct types (I-VIII) of TA systems categorised based on the nature of the corresponding antitoxin and the method of neutralisation of the toxin function by the antitoxin.[20-22]

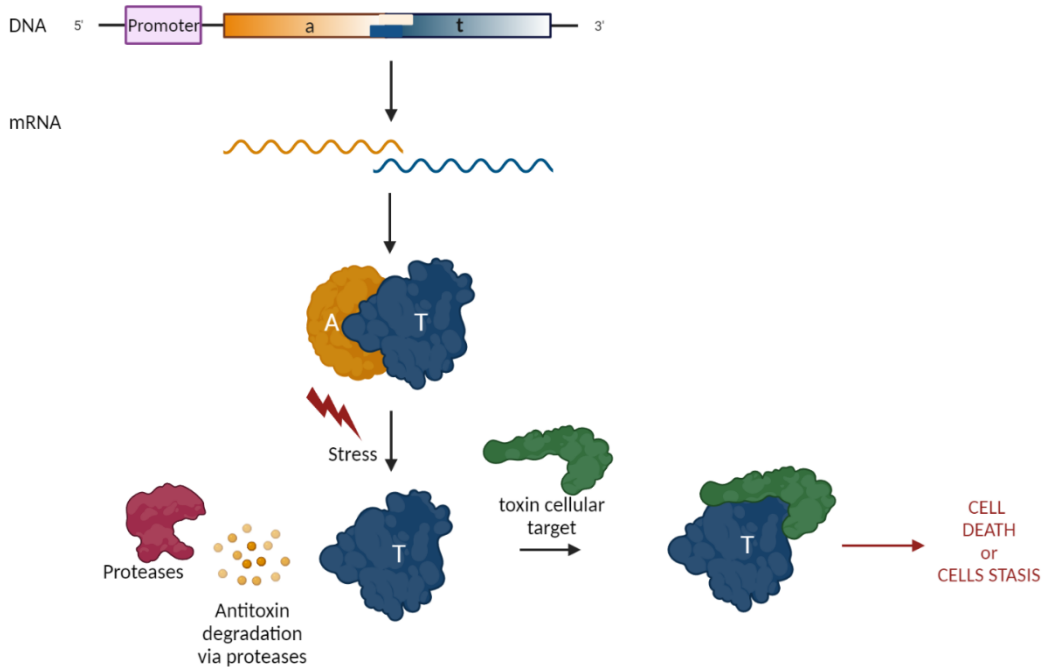


Figure 1.2: Features of a generic type II TA complex: *The antitoxin and toxin genes (a and t) are organised as an operon, the antitoxin gene (orange) precedes the toxin gene (blue), although the genes overlap. The antitoxin (A, orange) and toxin (T, blue) are expressed from the genes generating a harmless complex under normal cellular conditions. As a result of stress, the antitoxin protein is degraded. The toxin is liberated and acts on its cellular target resulting in cell stasis or cell death.*

The type I and III TA systems involve a non-coding RNA (sRNA) antitoxin.[23,24] The type I toxin is a hydrophobic peptide, in these systems the sRNA antitoxin binds to the mRNA of the toxin and prevents translation of the toxin.[25] The sRNA antitoxin of type III TA systems binds directly to the proteic toxin inhibiting its function.[26] The type II, IV and VI TA systems are composed of a proteic toxin and a proteic antitoxin molecule.[27] The type II antitoxin directly binds and inhibits the toxin.[28] The antitoxin of type IV systems indirectly counteracts the toxin protein, it binds to the target of the toxin and prevents toxin binding.[29] The antitoxin protein of VI systems forms a complex with a specific protease that facilitates the degradation of the proteic toxin.[30] In type V and VII TA systems the antitoxin is an enzyme. The type V antitoxin is an RNase which degrades the mRNA of the toxin and prevents translation of the toxin.[31] In type VII systems the enzymatic antitoxin directly targets the toxin and inactivates its function.[32] The type VIII TA system was most recently classified.[22] The toxin and antitoxin are sRNAs, the antitoxin directly binds and inhibits the sRNA toxin.

Type II TA systems composed of two proteins are the best described. In normal growth conditions the stable toxin is prevented from exerting its lethal effect through tight binding with its less stable antitoxin partner (**Figure 1.2**).[33] They are suggested to contribute to formation of persisters under stress conditions. The type II TA systems are often mutated in high-persistence screens and the toxins increase persister frequency in a population when overexpressed.[34-36] Originally a mutagenesis-screen in *Escherichia coli* led to the discovery

that a mutation in the *hipA* toxin gene of the HipAB type II TA system resulted in increased persister frequency.[37] Evidence was increased with transcriptomics carried out on *E. coli* fractions enriched for persister cells which resulted in upregulated expression of TA modules.[38,39] Additionally the deletion of TA modules in *E. coli* led to a decrease in the formation of persisters.[38,39]

Persistence is suggested to occur upon overexpression of the toxin in a bacterial cell or degradation of the antitoxin.[40] The predicted mechanism suggests that under stress conditions type I toxins are activated by the SOS response triggered by (p)ppGpp.[7,41] In the case of type II TA systems, the stringent response mediated by (p)ppGpp is triggered.[41,42] These signalling pathways can activate expression of the TA systems. They can also trigger degradation of the antitoxin by Lon or Clp proteases.[42] The resulting high level of toxin in bacterial cells promotes persister formation.[43] The toxins can inhibit cellular growth by targeting crucial cellular functions, this allows the cell to enter a dormant state and be tolerant to stress conditions.[17] The cells then persist in their dormant state until the stressor is removed, upon which they can return to their native state and grow.

1.1.4. GNAT Toxins

The majority of type II toxins effect translation and they can exert their toxicity in several ways.[18] The RelE, MazF and HicA toxin families are mRNA endonucleases; the VapC toxin family cleave rRNA and tRNA molecules; the Doc toxin family inactivates elongation factors and the HipA toxin family inactivates tRNA synthetases by posttranslational modification.[18,39,44-48]

Recently a new class of type II TA systems has been reported that belongs to the Gcn5 N-acetyltransferases (GNAT) family.[49,50] AtaTR and ItaTR in *E. coli,*[51-53] GmvAT in *Shigella flexneri,*[54] KacAT in *Klebsiella pneumoniae,*[55,56] and the TacTA family in *Salmonella enterica.*[57,58] The GNAT family of toxins inhibit translation by acetylation of the primary amino groups on aminoacyl-tRNAs using acetyl-coenzyme A (Ac-CoA) as an acetyl group donor (**Figure 1.3**). These acetylated aminoacyl-tRNAs are still recognised by the ribosome. They therefore halt translation as the alpha amino group cannot form a peptide bond with the carboxyl group of adjacent amino-acyl tRNA.[57]

1.1.5. GNAT Toxins in Salmonella

In humans *Salmonella enterica* serovars Typhimurium and Enteritidis (*S. Typhimurium* and *S. Enteritidis*) bacteria cause localised gastroenteritis, or a more invasive disease in HIV-infected patients.[59,60] The bacteria cause disease by proliferating in human cells including macrophages. Following antibiotic treatment 20-43% of patients have a recurrence of the disease.[61] This recurrence is closely associated with resuscitation of persistent bacteria cells.

Studies have shown that a large proportion of *Salmonella* bacterium taken up by macrophages enter a persister state.[36] A macrophage presents a stressful environment for *Salmonella* bacterium cells, and a subpopulation are induced into a dormant non-growing state.[13,36] There are 14 known TA systems in *Salmonella*, of which the majority were shown to contribute to persister formation inside macrophages. Deletions of each of the TA genes resulted in a decrease in persister cells.[36] This includes the TacT toxins, which have since been identified as GNAT toxins.[57]

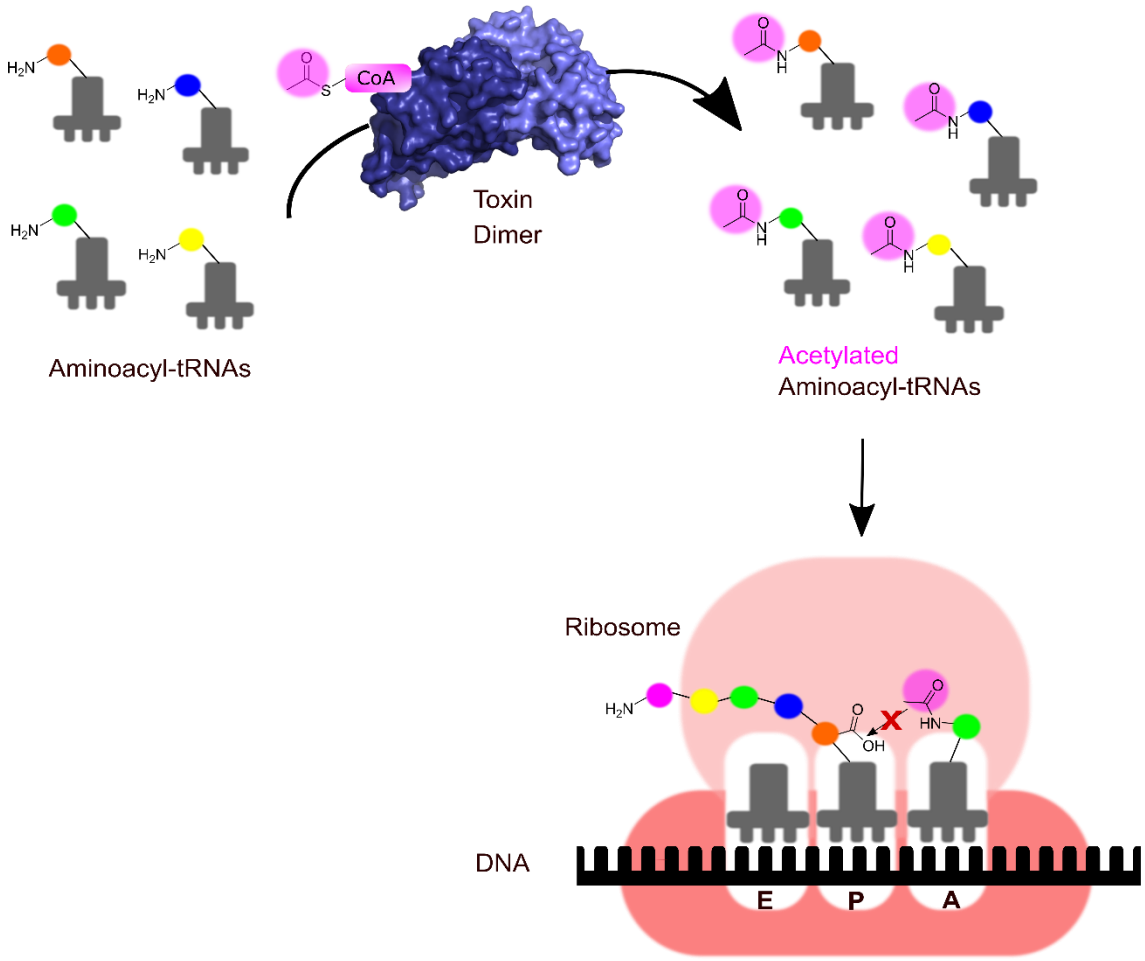


Figure 1.3: GNAT toxin activity: *The GNAT toxins acetylate the primary amine group of amino acids on amino-acyl tRNAs using Ac-CoA as the acetyl group donor. The alpha amino group of the acetylated tRNA in the ribosomal A site cannot form a peptide bond with the carboxyl group of the adjacent charged tRNA in the P site. Subsequently, protein translation is inhibited.*

Further experiments demonstrated that for strains of *S. typhimurium* and *S. enteritidis* isolated from humans a similarly large proportion of cells formed persisters compared to the cells taken up by macrophages.[58] The whole TacTA family of GNAT toxins, composed of the toxins TacT1, TacT2 and TacT3 and their respective antitoxins were implicated in the development of persister cell formation in the isolated strains of *S. typhimurium* and *S.*

enteritidis.[57,58] Overexpression of the TacT toxins into the single deletion mutant of the corresponding TacTA module led to an increase in the proportion of persisters in a population.[57,58]

TacT1 and TacT3 have been characterised by crystallography and TacT2 has been modelled computationally.[57,58] Additionally, the similar GNAT toxins AtaT and KacT have published crystal structures.[52,55] All are proposed to be dimeric in solution (**Figure 1.4**) and dimerisation is deemed necessary for toxicity. The residues for dimerisation are well conserved in TacT1, TacT2 and TacT3. There is a positively charged groove extending from the active site of one monomer to the α2 of the second monomer corresponding to the dimensions of a tRNA molecule (**Figure 1.4**).[57,58]

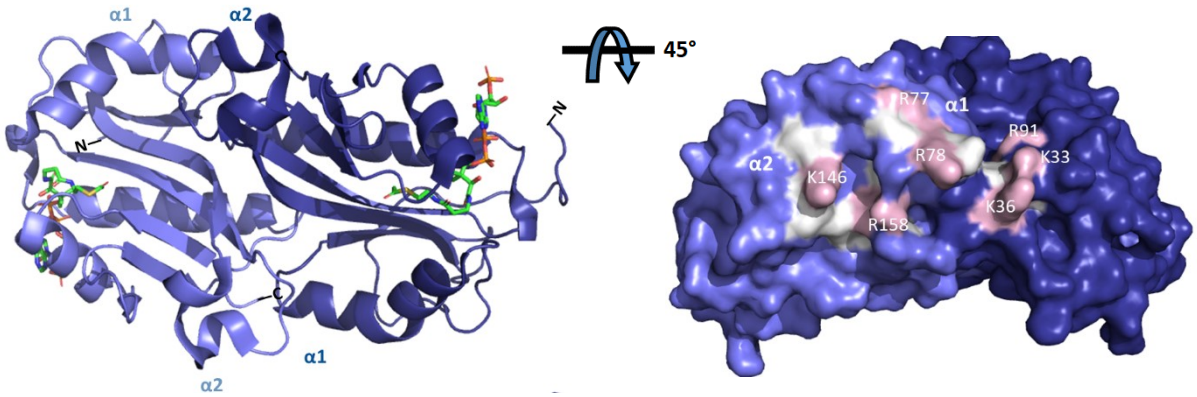


Figure 1.4: Crystal structure of the TacT1 toxin dimer a) *TacT1 toxin is represented as a cartoon, each monomer coloured different shades of blue. Ac-CoA is presented as stick representation.* ***b)*** *TacT1 toxin rotated 45°, and represented as a surface. The positively charged tRNA binding groove is labelled and highlighted in pink. (PDB:5FVJ).*

Substitution of amino acids in the binding groove confirmed binding by electrostatic interactions of the negatively charged tRNA in the positive groove.[58,50] It is proposed that the primary amine group of the amino acid bound to the tRNA sits in this active site. To identify whether the TacTs have a preference for certain charged tRNAs and if there are differing tRNA preferences within the TacT family a cell-free expression assay was carried out.[58,62] The assays were supplemented with Ac-CoA, and the acetylated tRNA molecules were extracted. A total of 13 different amino acids were detected from experiments with all the toxins demonstrating that the TacT family can target some but not all charged tRNAs. There is some overlap of preference within the family, TacT1-3 all show a bias towards $tRNA^{Gly}$, $tRNA^{Leu}$, and $tRNA^{Ile}$. TacT1 and TacT2 have a greater preference towards $tRNA^{Gly}$ and TacT3 has greater preference towards $tRNA^{Leu/Ile}$ indicating a lack of redundancy within the family.

TacT3 was identified to have the highest potency compared to TacT1 and TacT2 and it exhibited the greatest persister inducing effect.[58] TacT1 and TacT2 have the closest structural similarity, whilst TacT3 has an extra helix and more disordered loop (**Figure 1.5**). The

difference in structure allows a different conformation of Ac-CoA in the binding pocket. It has been hypothesised that this may allow for faster release of the CoA after transfer of the acetyl group, increasing the possible rate of acetyl transfer.

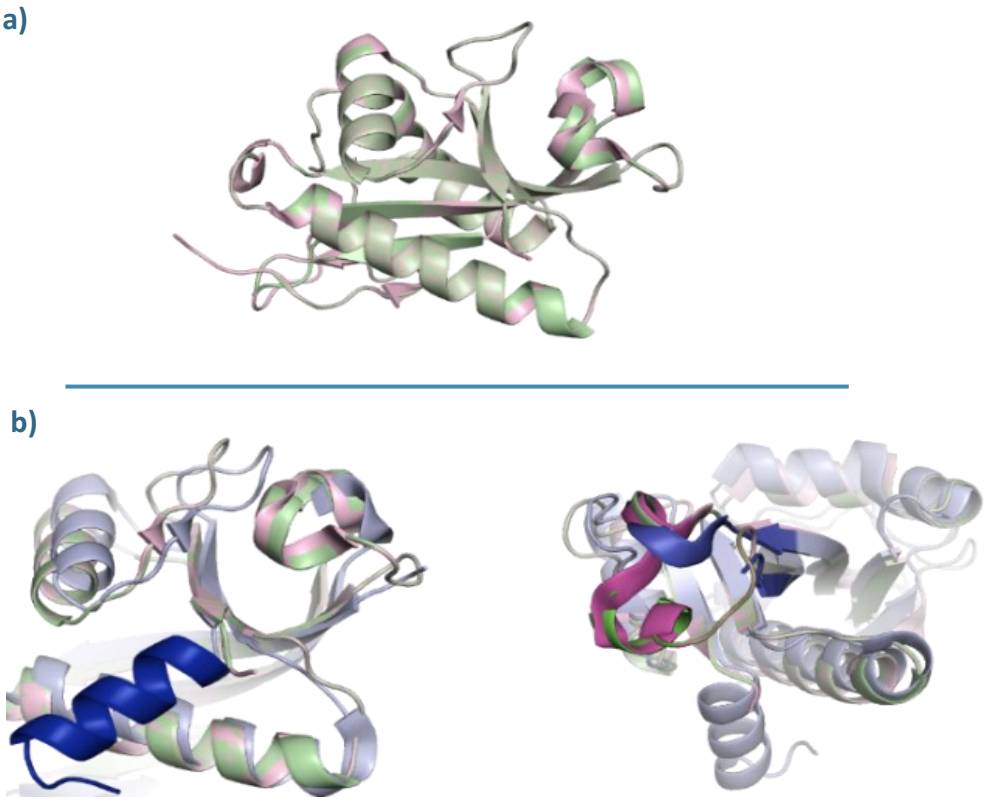


Figure 1.5: Overlays of TacT1-3 crystal structures a) *Crystal structure of a single monomer of TacT1 (pink) overlayed with a single modelled monomer of TacT2 (green) represented as a cartoon.* ***b)*** *crystal structure of a single monomer of TacT3 (blue) overlayed with single monomers of TacT1 (pink) and TacT2 (green) with extra helix and disordered loop highlighted in dark blue. (Unpublished crystal structures).*

The binding modes of the TacT toxins with their associated antitoxins could differ within the family. Current unpublished data from the Helaine group (Harvard University), of the crystal structures suggests TacT1 binds with a 1:1 toxin:antitoxin stoichiometry, but forms a large matrix with each antitoxin bound to two monomers at different binding sites; TacT2 binds in a 1:2 toxin:antitoxin stoichiometry, the dimer formation being fully interrupted by four bound antitoxins; and TacT3 binds in a simple 1:1 stoichiometry with an uninterrupted dimer formation. Interestingly the published crystal structures of AtaTR and KacAT are heterohexameric, two toxin monomers bound by four monomers of the antitoxin by direct protein-protein interactions (PPIs).[52,55] How the TacTA toxins and antitoxins interact in solution is yet to be confirmed, but, similar to other GNAT toxins it is likely that the toxin dimer is disrupted.

1.2. Targeting PPIs in Bacteria

In recent years it has been found that despite the large interaction surfaces of PPIs, often just a few 'hotspot' amino acid residues drive their formation.[63] As a result PPIs have increasingly been identified as druggable targets for novel therapeutics in areas such as cancer treatment and infections. Crucial cellular bacterial functions often rely on PPIs, many of which do not have close eukaryotic homologues.[64] They are therefore attractive drug targets for the development of selective drugs with no adverse side effects to humans and activity against a broad range of bacteria.[65] Many PPIs in bacteria have been identified as highly promising targets, with potential compounds currently in development.[66]

1.2.1. Discovery of novel inhibitors of PPIs

Both small molecules and peptides have been used to target PPIs. Well established discovery processes such as high throughput screening (HTS), fragment-based lead discovery and rational structure-activity based design have all been used to identify small molecule compounds that target clusters of 'hotspot' residues in bacterial PPIs.[67-69] Small molecules are likely to be orally bioavailable, stable in biological environments and cheap to synthesise.[69] Peptides, cyclic peptides and peptidomimetics have all been identified as PPI inhibitors, usually against PPIs that have 'hotspot' residues distributed over a large surface area as they can confer greater selectivity.[70,71] Cyclic peptide analogues or peptidomimetics have greater bioavailability and biological stability compared to linear peptides.[71,72] There are two typical methods of identifying novel drug-like peptide inhibitors of PPIs. In one approach, the interaction and selectivity of a linear peptide is characterised followed by further optimisations and development into cyclic peptides or peptidomimetics.[72] In a second approach HTS is performed using large libraries of macrocyclic peptides, often including non-standard amino acids.[73,74]

1.2.2. PPIs as antibacterial targets

A number of PPIs of pathogenic bacteria have been targeted, with different approaches used to identify and develop novel small molecule and peptide inhibitors.[66,75] These PPIs are all involved in essential cellular processes.

Inhibitors have been developed for PPIs involved in division and replication. Firstly, interfering with the PPI network of the single-stranded DNA-binding protein (SSB);[76-78] secondly blocking binding of essential enzymes to the β-sliding clamp protein;[79-85] finally, inhibiting the FtsZ-ZipA PPI.[86-89] Bacterial transcription is regulated by a number of transcription factors which form PPIs, two of these, the RNA polymerase (RNAP) and N-utilisation substances (Nus) B and E have been targeted, with promising inhibitors in development.[90-104] Inhibitors have also been developed that block crucial pathways involved in outer membrane protein synthesis.

Namely the BamA-BamD PPI in the β-barrell assembly machine (BAM) and the PPIs in the 7-protein macromolecular lipopolysaccharide transport (Lpt) complex.[105-114]

1.2.3. PPIs of TA systems as antibacterial targets

The role of TA systems in the formation of persisters was described in detail in sections 1.1.3-1.1.5. Whilst there is a growing pool of evidence for this theory, TA systems are also known for their bactericidal effects.[115] The TA modules are encoded in plasmids and chromosomes.[27] The plasmid-encoded TA modules were considered 'addiction' molecules for bacterial population.[25,116] Once the daughter cells acquired the plasmid, if they then lost the plasmid they could not survive. The antitoxin is unstable and eventually degrades, enabling the toxin to exert its toxic bactericidal effect. This results in cell death since the TA gene is no longer present for production of new antitoxin. If the cells retained the plasmid they survived. The chromosomal-encoded TA modules have been postulated to act in altruistic cell death.[117] In stressful conditions some cells will sacrifice themselves by triggering their TA systems. Eventual death and cell lysis provides greater availability of nutrients for other cells and the population can survive extinction.

Based on the evidence that toxins can cause cell death, disrupting the PPIs of type II TA systems is a proposed strategy for the treatment of bacterial infections with the aim of activating the toxin, resulting in cell suicide (**Figure 1.6**).[18,118,119] Targeting the TA PPI liberates the toxin either by competitive binding to the antitoxin or dissociation of the TA complex. Many experiments with a variety of known TA systems have been carried out to identify small molecule or peptide inhibitors of TA PPIs. Of these systems, compounds have been discovered that target the VapBC family, PemK-like protein family and HicBA complex.[47,48,120-133] The ζ-toxin of the TA system $\varepsilon_2\zeta_2$ (also known as PezAT) targets cell wall synthesis and a series of peptides have shown promise to trigger ζ-toxin mediated autolysis.[134,135] TplE is a toxin with lipolytic activity neutralised by the TplEi antitoxin and a peptide has been rationally designed to liberate this toxin.[136]

In a similar vein, targeting TA systems is a potential strategy for the treatment of bacterial persistence. Possible approaches include identifying molecules that bind to the toxin of a TA system, either mimicking the antitoxin binding at the PPI or targeting an allosteric position (**Figure 1.6**). The aim is that toxin activity will be inhibited even in the absence of its antitoxin which will reduce persister formation. This is a relatively new approach, with very few studies available. Li *et al.* have carried out a computational screen to identify small molecules inhibitors of the type II toxin HipA.[137] They demonstrated that inhibition of the toxin greatly reduced persister formation. This strategy first involved characterising the structural and biochemical properties of the toxin-antitoxin binding, then the design of molecules that target the toxin.

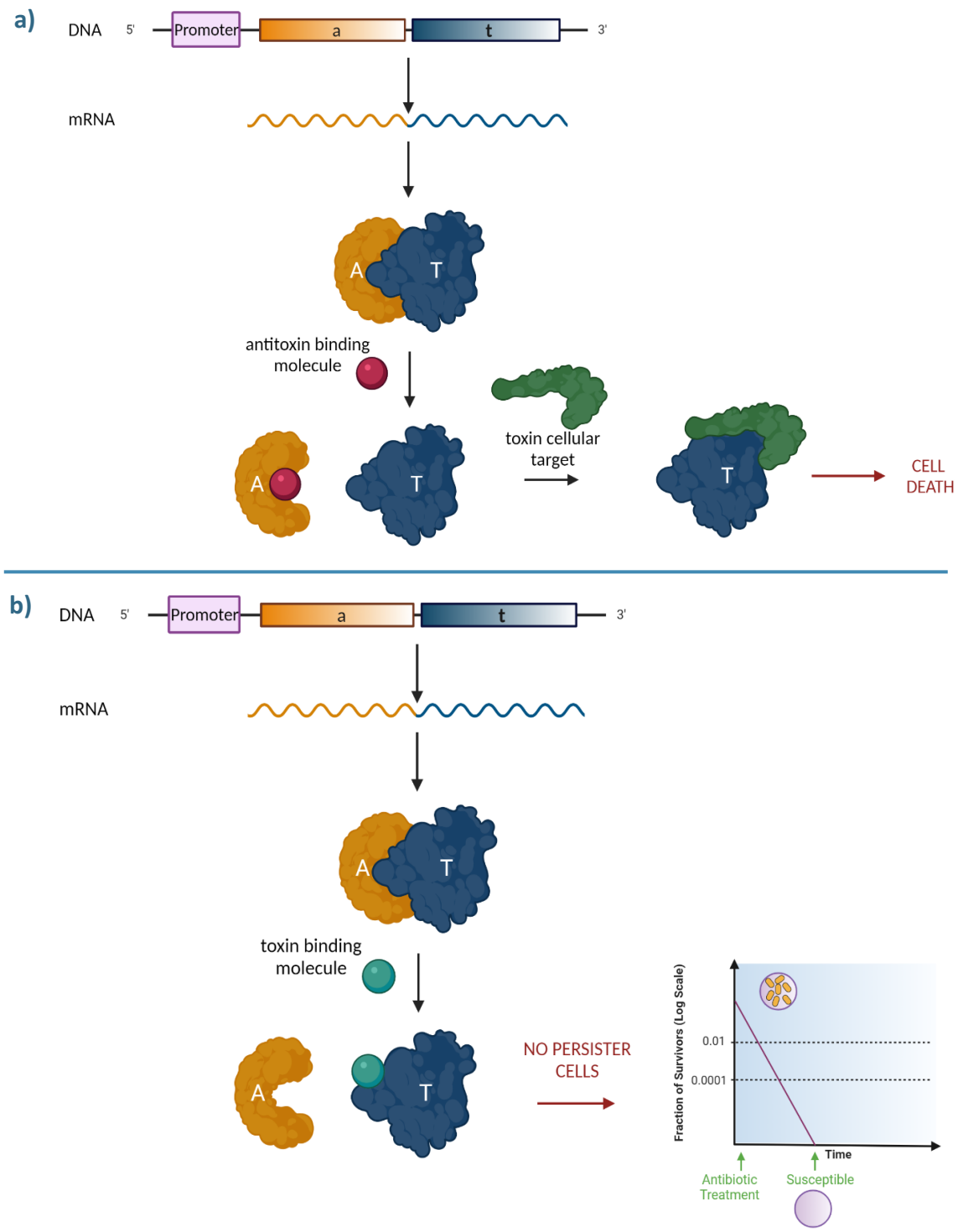


Figure 1.6: PPIs of TA systems as antibacterial targets: a) *Exploiting the TA systems for development of an antibiotic compound. An antitoxin inhibitor is developed that disrupts the TA PPI and binds to the antitoxin. As a result, the toxin is liberated and acts on its cellular target resulting in cell death.* ***b)*** *A compound is developed that binds to the toxin (here at the PPI, but allosteric sites would be possible). Even if the antitoxin is degraded under stress conditions such as antibiotic treatment, the toxin cannot carry out its toxic function. The bacteria cells do not enter a persister state, and all the cells die from the antibiotic treatment.*

1.2.4. Strategy of Targeting TacTA family

Inhibiting the toxic activity of TacT1-3 toxins, even in the absence of their respective antitoxin, will likely reduce persister formation in *S.Typhimurium* and *S.Enteritidis.* Based on the concepts in the study by Li *et al.* the TacTA family can be targeted using information derived from the crystal structures together with one or many inhibitor discovery methods with the aim of inhibiting TacT toxin activity.[137]

The crystal structures of the TacT toxins and the TacTA complexes give insight into the binding interactions of the toxin-antitoxin proteins. The PPI exists across a large surface area and involves many electrostatic interactions. The crystal structures also allow visualisation of the location, size, and shape of the active site for the charged tRNA molecules and the Ac-CoA. This information is a crucial starting point for the identification of possible points for inhibitor binding. Biophysical characterisation is then necessary to identifying the affinity of the toxins and antitoxins for one another. The information from the crystal structure and biophysical characterisation can then be combined with discovery methods such as HTS, fragment-lead design and rational structure-based design to identify an inhibitor for the toxin.

Identifying a compound that acts as an inhibitor of the toxin is just one step in the long process of drug discovery. Uptake of the compound into the bacteria and access to the PPI target is the biggest challenge in the development of antibacterial drugs. Small molecules make up the majority of antimicrobial drugs such as penicillin and nitrofurantoin, and with some small developments they can be optimised easily for cellular uptake. However, when considering large surface area targets such as PPIs, peptides are likely more selective. With recent developments cyclic peptides are increasingly able to penetrate cell membranes.[70,71] To target the large surface area of the TacTA PPI, cyclic peptides will likely have a greater selectivity over small molecules and can be optimised for cellular uptake. Highly selective drug-like peptide inhibitors can be identified using HTS methods with libraries of cyclic peptides, which can be further adapted to improve cellular uptake.

1.3. Thesis Aims

In this MPhil the aim was to characterise the PPIs of the TacTA1-3 systems in *Salmonella* as a starting point for their targeting for the treatment of persistence. This was broken down into three interconnected aims as described below:

1) Protein expression of TacT1-3 toxins. Toxin protein expression is exceptionally difficult as they result in growth arrest in a large proportion of the culture therefore very little protein can be isolated. Two strategies were attempted:
    - **a)** The expression of mutant forms of the toxins displaying reduced toxicity but an unchanged structure.
    - **b)** Trial expressions of the WT toxins in the presence of an antidote protein.

2) Solid phase peptide synthesis (SPPS) of the minimum antitoxins required to inhibit the toxicity of the toxins.

3) Biophysical characterisation of the TacTA1-3 PPIs. Preliminary affinity measurements were carried out for each of the minimum antitoxin peptides bound to the toxin proteins using fluorescence anisotropy (FA), differential scanning fluorimetry (DSF) and surface plasmon resonance (SPR).

Chapter 2

Development of Toxic Protein Expression and Purification for the TacT1 – 3 Toxins

Abstract

In this chapter attempts to express and purify the TacT1-3 proteins are described. Two different methods were used to express the TacT1, TacT2 and TacT3 toxin proteins. The first method is a tried and tested method to express a mutant inactive form of the proteins that have no toxic effect on the cells. Each of the mutant toxins were expressed in autoinduction media and the purification of the TacT1 mutant toxin was optimised. The second method is adapted from a novel method to express the Doc toxin developed in the Barnard group. Trial expressions were carried out expressing the WT toxins in the presence of an antidote protein. TacT3 was successfully overexpressed, and it is hypothesised that with further optimisation TacT1 and TacT2 can be expressed using a similar method.

2.1. Introduction to Toxic Protein Expression

Recombinant protein expression technology allows large-scale production of proteins. The basic workflow using bacteria as a host is shown in **Figure 2.1.**[138,139] Firstly the gene coding for the protein is inserted into a host plasmid, this plasmid is then transformed into competent cells. The cells are propagated in rich medium and then protein expression is induced. The protein can then be purified from the cells.

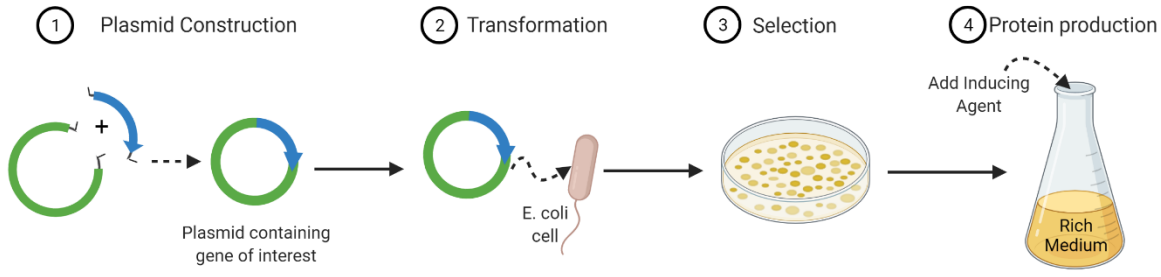


Figure 2.1: Schematic of recombinant protein production

The reality is less straightforward: each protein requires optimisation for expression and the correct environment to fold into its secondary, tertiary, and quaternary structures. In particular, there are some proteins that are toxic to the host bacteria. Upon induction of a toxic protein the bacteria cells will die, and high level of protein expression cannot be achieved. When expressing toxic proteins, it is necessary to carefully develop methods that result in high levels of protein expression. The TacT1-3 proteins are toxins, and though the toxin gene is isolated from *S. Typhimurium* the toxins still exhibit strong toxicity in *E. Coli* and severely inhibit bacterial growth.[57,58] This is a likely result of the tRNA in all bacteria being genomically comparable. Consequently, the toxins are difficult to express alone without their antitoxin. In standard conditions only trace amounts of toxin is expressed which is then challenging to purify.

This challenge of expressing and isolating TacT proteins applies to most toxins in type II TA systems.[140] To overcome these issues several strategies have been established for the expression of type II toxins, although each with its limitations. The first, most common strategy involves inactivation of the toxin by site-directed mutagenesis to reduce catalytic activity. This has been achieved for many type II toxins including Doc, RelE, MazF, KacT and AtaT.[45,52,56,141,142] However, with this strategy the non-functional toxins can only be used for structural and biophysical studies, they cannot be used in activity assays. Another common strategy involves co-expression of the toxin with the antitoxin. The stable complex is then denatured to isolate the toxin and then the toxin is refolded into its native state. This has been achieved for many type II toxins including Doc, MazF, ParE2, HigB2, ItaT and AtaT2.[51,140,143] However, the refolding of the toxins following denaturation requires extensive optimisation and is a laborious, time consuming process. Other less common strategies involve cell free expression, this can be very expensive and is usually only used to express toxic proteins on a small scale.[144] Alternatively, a yeast expression system could be used as the toxins may not be toxic to eukaryotic cells.[145] This strategy is limited by the longer doubling time of yeast compared to bacteria, so expression is more time consuming. Furthermore, the laborious protein refolding of bacterial proteins is often required.

Members of our group have developed a novel strategy to overcome the limitations of expression strategies in bacteria to obtain the *S. Typhimurium* Doc toxin. Doc blocks bacterial protein translation *via* phosphorylation of a conserved residue T383 in the elongation factor EF-Tu. Co-expressing Doc with an EF-Tu mutant (T383A or T383V) that cannot be phosphorylated by the toxin counteracted the toxicity of Doc. In these co-expression experiments bacterial growth was rescued and Doc was overexpressed and could be isolated in good yield (unpublished data, Dr Guilherme Castro, **Figure 2.2**).

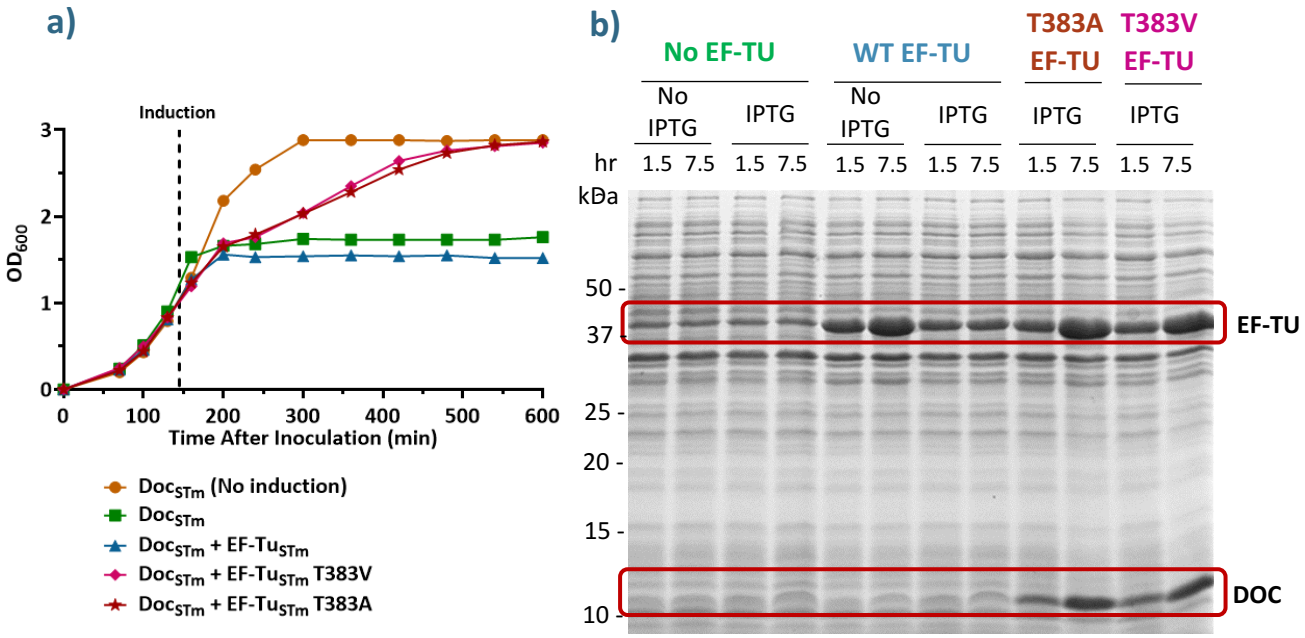


Figure 2.2 Recombinant expression of the Doc_{STm} toxin in bacteria. a) *Growth curves of E. coli BL21-AI expressing Doc_{STm} (green) or co-expressing Doc_{STm} with $EF\text{-}Tu_{STm}$ wild-type (blue), T383A (red) and T383V (pink). A control sample of cells carrying the Doc_{STm} vector in the absence of IPTG (orange) was measured for comparison.* ***b)*** *SDS-PAGE analysis of Doc_{STm} expression trials varying the addition of IPTG and the presence of $EF\text{-}Tu_{STm}$ encoding plasmids: wild-type, T383A and T383V. Time-points correspond to aliquots collected 1.5 h and 7.5 h after induction.*

For the expression of TacT1-3 each of the current known strategies were considered. Data has already been published for the expression of YF mutant TacT toxins which render the proteins non-toxic. The Y140 of TacT1 is conserved in many proteins containing a GNAT domain. It coordinates an oxygen atom of Ac-CoA to ensure correct orientation of the acetyl group for transfer (**Figure 2.3**). The Y140F TacT1 mutant has been shown to prevent transfer of the acetyl group to the acceptor tRNA molecule.[57] The residue is also conserved in TacT2 and TacT3. $TacT1^{Y140F}$, $TacT2^{Y137F}$ and $TacT3^{Y143F}$ all display reduced toxicity, and the mutation does not affect the native structure.[58] As this method was available and published it was used in this thesis to express proteins for biophysical and biochemical evaluation as the structural properties of the protein remain identical. However, no activity assays can be carried out on the protein due to the loss of functionality.

This project lies as the foundation of a larger aim to identify a pan inhibitor for the three toxins TacT1-3. An important development was to have the active protein, as it would be necessary to evaluate the activity not just the affinity of inhibitors. A novel approach to express the native toxic proteins was considered based on the work in our group to express active Doc protein which circumvents the limitations of other expression strategies. The approach with Doc was to express the toxin in the presence of a protein that prevents toxic activity. In an

expansion of this idea, in order to express the wild-type (WT) TacT toxins, an idea was developed to express the toxins in the presence of a known 'antidote' for the TacTs, peptidyl-tRNA hydrolase (Pth).

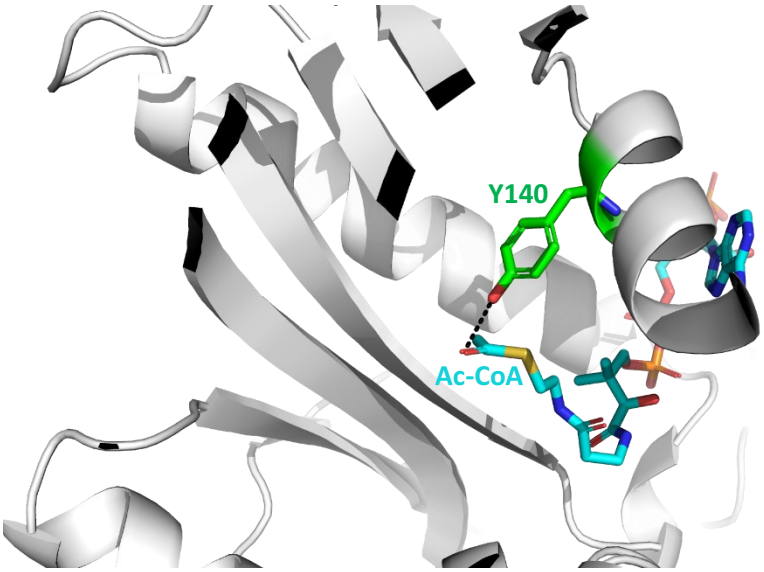


Figure 2.3: Co-ordination of acetyl group of Ac-CoA by Y140 in WT TacT1: *TacT1 is represented as a cartoon coloured grey, Y140 is represented as sticks coloured green and Ac-CoA is represented as sticks coloured cyan. The hydrogen co-ordination interaction is respesented with black dashes. (PDB:5FVJ).*

Pth was discovered to be an 'antidote' for TacT1 in a screening experiment of the ASKA collection of plasmids containing *E. coli* open reading frames (ORFs).[146] TacT1 toxicity is observed by slow colony recovery when cells are plated on LB agar as TacT1 induces an extension of lag phase. The screen involved transforming cells containing TacT1 in a vector with a pooled mixture containing the ASKA plasmid library, followed by spreading cells on plates. The pCA24N::*pth* plasmid from the library was selected for since it repressed TacT induced toxicity, observed by faster colony recovery.[57] Furthermore, *in vitro* acetylation detection assays incubating acetylated aminoacyl-tRNA with or without Pth demonstrated a reduction in acetylation signal in the presence of Pth.[57] Pth has previously been reported to hydrolyse peptidyl-tRNA and acetylated aminoacyl-tRNA molecules are recognised as dipeptidyl-tRNA. [147,148] Pth hydrolyses the ester bond between the 3' hydroxyl of tRNA and the C – terminal of the peptide. During translation some peptidyl-tRNA molecules are released if translation terminates prematurely, possibly due to ribosome stalling. Pth rescues a cell from the presence of toxic peptidyl-tRNA molecules and prevents the shortage of tRNA molecules which would stall cell growth.

It was therefore predicted that if Pth is expressed before the TacT toxin expression is induced it will be able to rescue or prevent growth toxin induced inhibition. As the TacT toxins are expressed, they acetylate charged tRNA inhibiting translation and causing cell stasis. The Pth

will detoxify the charged tRNA, reducing the toxic effect of the TacTs. The experiment was designed to allow for expression of Pth in *E. coli* cells followed by the expression of the TacT toxins in the same cells.

In the remainder of this chapter attempts to use these two methods to express the TacT toxins will be described.

a) Incorporation of the YF mutation that results in a loss of toxic function but with no effect on the structural properties of the protein (**2.2**).

b) Expression of the toxin in the presence of Pth, an 'antidote' protein (**2.3**).

2.2. Method 1: Expression and Purification of TacT1-3 YF Mutants

To express the TacT1-3 proteins that are toxic to the bacteria cells a YF mutation was incorporated resulting in a loss of toxic function but with no effect to the structural properties of the protein. The mutant renders the protein non-toxic to the host and can be expressed on a large scale. The aim was to express and purify these three mutant proteins: TacT1^{Y140F}, TacT2^{Y137F} and TacT3^{Y143F}.

2.2.1. Literature Approach

The expression of the $(His)_7$ tagged TacT1-3 YF mutants has been previously published,[57] so initial expression carried out replicating the published conditions. The gene for each protein carrying the YF mutation was cloned into a pQlinkH plasmid, by our collaborators in the Helaine group. The TacT genes were inserted into the plasmid with a $(His)_7$ tag at the N-terminus of the gene. The His tag can be exploited for efficient purification of the protein using affinity chromatography with Ni-NTA beads and imidazole. The pQlinkH plasmid has an ampicillin resistant gene for use as a selective marker.

The pQlinkH plasmid was originally chosen as it can prevent 'leaky' expression of proteins which could cause a problem as the mutant toxins may still carry some toxicity. The plasmid has a T5-derived lac promoter which is isopropyl β-D-1-thiogalactopyranoside (IPTG) inducible. Upon induction RNA polymerase is recruited and binds to the promoter and transcribes the gene of the desired protein into mRNA. Of note, the plasmid also has a *cis-lacIq* gene that overexpresses the lac repressor. The lac repressor prevents the binding of RNA polymerase to the promoter and therefore suppresses the expression of the toxic protein before the addition of IPTG for induction. This prevents 'leaky' expression. Any expression of toxic protein may prevent cells reaching high density, preventing 'leaky' expression allows a chance for high level expression of the toxic protein.

In attempts to replicate the expression using the published conditions none or only trace expression was observed. Each plasmid was used to transform chemically competent *E. coli* BL21 cells, and the cells were propagated in Luria-Bertani (LB) medium. *E. coli* BL21 cells are engineered for protein expression cultures, they are deficient in *lon* and *ompT* proteases and therefore less likely to digest recombinant proteins. The cell cultures were induced by IPTG early in the log phase - when OD_{600} reached 0.6 – 0.8. A large increase in growth was observed but SDS-PAGE analysis showed no overexpression bands for a protein at ~20 kDa (**Figure 2.4**), therefore expression of the mutants had to be optimised.

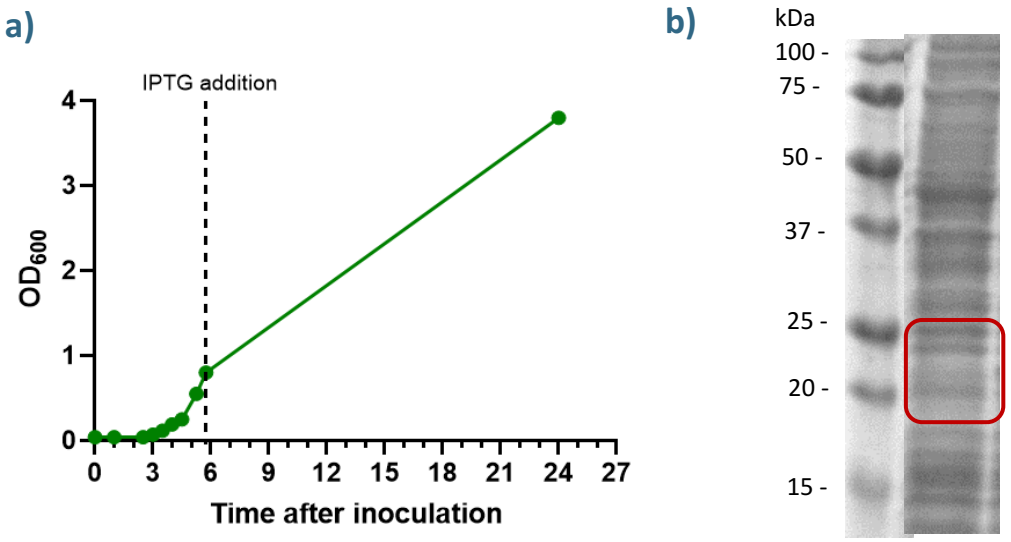


Figure 2.4 Recombinant expression of $(His)_7$-TacT1 ^{Y140F} protein (20.9 kDa): a) *Growth curve of BL21 E. coli cell culture transformed with pQlinkH-$(His)_7$-TacT1^{Y140F} plasmid. The time after inoculation is plotted against OD_{600}, the dotted line indicates induction by IPTG early in the log phase when OD_{600} reached 0.6, an increase in growth is observed following induction.* ***b)*** *The electrophoretic pattern of total cell protein expression is shown at 26 hrs. No overexpression was observed at ~20 kDa, circled in red.*

2.2.2. Optimised Expression via Autoinduction

Autoinduction was then employed to try to express the mutant toxin proteins. Autoinduction is a method of induction of the lac operator without the addition of IPTG. The culture medium can be LB, Terrific Broth (TB) or another rich media. LB media is the typical growth broth for bacteria cell cultures. It is a complex broth composed of tryptone, yeast extract and NaCl. Its exact composition is not defined, but it contains all the amino acids, small peptides, nitrogen, sugars and other components essential for cell growth. TB is a richer media, with a higher ratio of yeast extract to tryptone. It also contains glycerol and a potassium phosphate solution.

Autoinduction media is supplemented with glucose, lactose and other essential salts. The lac promoter is inhibited by the glucose and is only accessible when all the glucose in the media is used up. At this point the cells switch to lactose as an energy source and the lactose induces cell expression. The cells grow to a significantly higher density than cultures using IPTG induction, so there is more target protein per volume of culture. Even with trace expression a significant amount of protein can be isolated per litre.

To express the TacT1^{Y140F}, TacT2^{Y137F} and TacT3^{Y143F} proteins, the same pQlinkH plasmids and BL21 *E. coli* cells were used as in 2.2.1. Small-scale expression trials were carried out. Firstly, the relevant plasmid was transformed into the competent cells. Then overnight precultures were carried out in LB media. Finally, the preculture was inoculated at a 1:15 dilution into 15 mL of autoinduction expression cultures. This is a very high ratio compared to the standard dilution of 1:100. The aim was that a higher cell density could be achieved before the expression of the toxic protein that would cause cell death or cell stasis. The small scale autoinduction expression cultures had cell densities up to 10-fold greater than with the original IPTG induction, as well as strong overexpression of the TacT1^{Y140F}, TacT2^{Y137F} and TacT3^{Y143F} proteins (**Figure 2.5**). Inexplicably scaling up to 1 L did not yield the same overexpression. Trace bands were observed but an attempt to purify the trace amount of toxin was unsuccessful.

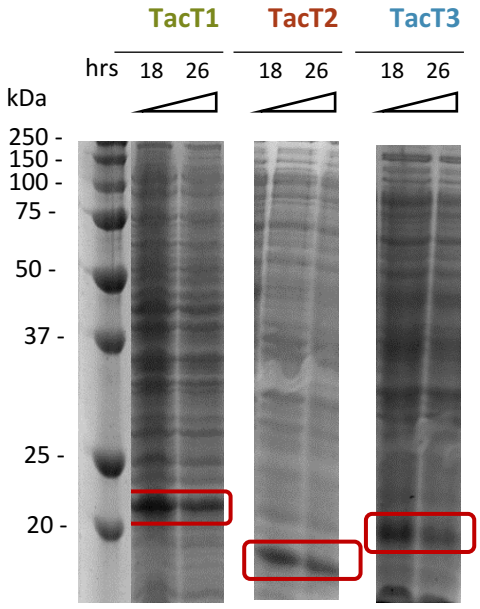


Figure 2.5: Trial expression of TacT proteins ((His)$_7$-TacT1 ^{Y140F}: 20.9 kDa, (His)$_7$-TacT2^{Y143F}: 20.9 kDa and (His)$_7$-TacT3^{Y137F}: 22.2 kDa*: SDS-PAGE analysis of total cell protein expression of trial expressions of (His)$_7$-TacT1^{Y140F}, (His)$_7$-TacT2^{Y143F} and (His)$_7$-TacT3^{Y137F} using autoinduction media at 18 hrs and 26 hrs. Overexpression bands are circled in red indicating successful overexpression of the target proteins.*

Supplementing media and LB agar gels with glucose is important when expressing toxic proteins with a lac operator. The glucose inhibits the lac operator and prevents leaky expression up until the point of induction. In the first trial expressions of TacT1^{Y140F}, TacT2^{Y137F} and TacT3^{Y143F} using autoinduction, the precultures and expression cultures were all supplemented with glucose. However, the LB agar gels were not. In a final attempt to improve expression the cells were primed with glucose from the earliest point. The *E. coli* cells transformed with relevant plasmid were now spread on LB agar plates containing glucose. As earlier, the precultures and autoinduction media used contained glucose.

These new small-scale expression cultures resulted in strong overexpression, as seen by the strong overexpression bands of each of the TacT mutants in SDS-PAGE analysis. This time, the electrophoretic pattern of total cell proteins during large-scale growth of auto-inducing cultures at 37 °C for each TacT1-3 YF mutant expression also demonstrated overexpression of a protein roughly corresponding to the predicted molecular weight (TacT1: 20.9 kDa, TacT2: 20.9 kDa and TacT3: 22.2 kDa) (**Figure 2.6a)**. The electrophoretic mobility of the proteins was compared to purified proteins provided by our collaborators to confirm expression (**Figure 2.6b**).

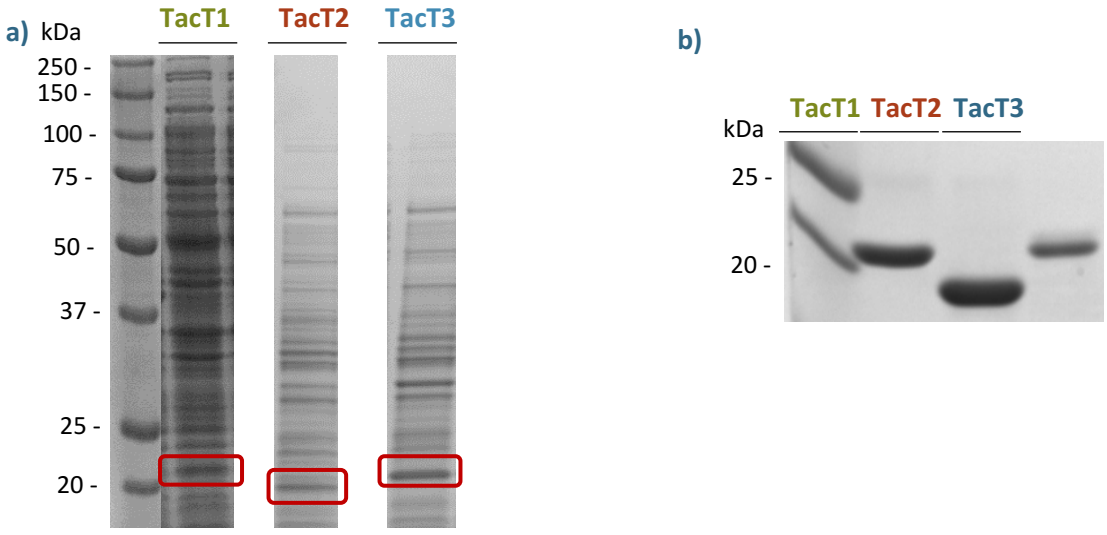


Figure 2.6: Recombinant protein expression of TacT proteins ((His)$_7$-TacT1 ^{Y140F}: 20.9 kDa, (His)$_7$-TacT2^{Y143F}: 20.9 kDa and (His)$_7$-TacT3^{Y137F}: 22.2 kDa: a) *SDS-PAGE analysis of total cell proteins from large scale expressions of (His)$_7$-TacT1^{Y140F}, (His)$_7$-TacT2^{Y143F} and (His)$_7$-TacT3^{Y137F} using autoinduction media after fully priming the cells with glucose. Overexpression bands are circled in red indicating successful overexpression of the target proteins.* ***b)*** *SDS-PAGE analysis of the purified proteins from collaborators, (His)$_7$-TacT1^{Y140F}, (His)$_7$-TacT2^{Y143F}and (His)$_7$-TacT3^{Y137F}. Pure proteins are observed corresponding to the predicted molecular weight.*

Interestingly TacT2 runs lower on the gel. SDS molecules carry a negative charge and impart two negative charges for every two amino acids, hence protein-SDS complexes should have the same mass-charge ratio compared to the native state of the protein. However, the number of negatively charged residues in the protein could significantly affect migration time. TacT2 has a lower isoelectric point (pI) than TacT1 or TacT3 and at a neutral pH may carry more negative charges. It is possible that it therefore migrates faster in an electric field and appears smaller than it is.

2.2.3. Optimised Purification of $(His)_7$-TacT1^{Y140F}

As with protein expression, protein purification often requires optimisation. The main steps in the basic workflow of protein purification involve first harvesting the cells of the expression culture by centrifugation. The cells in the cell pellet are then lysed. The protein is then purified from the cell extract by various chromatographic methods. Finally, the protein is prepared for storage (**Figure 2.7**).

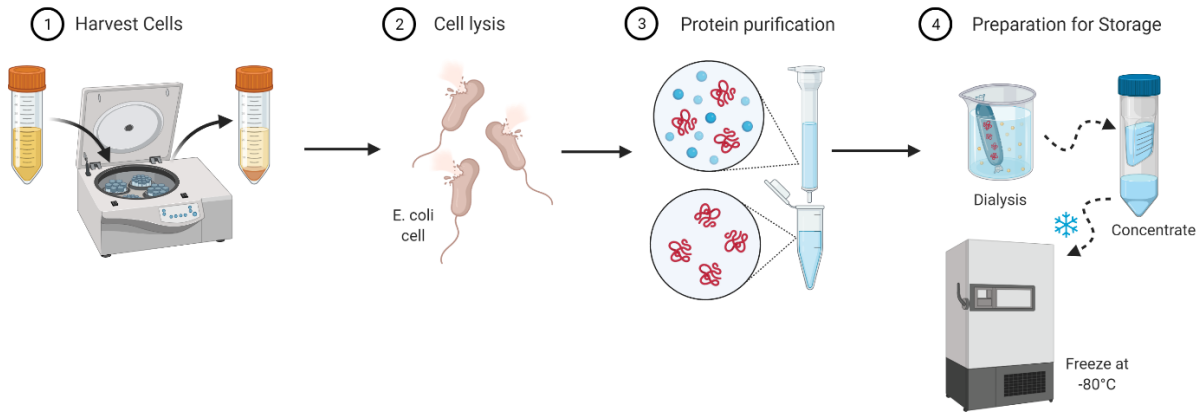


Figure 2.7: Schematic of recombinant protein purification

Methods for the purification of $(His)_7$-TacT1^{Y140F} and $(His)_7$-TacT2^{Y137F} have previously been published.[57,58] Using the published methods, the aim was to carry out trial purifications of the three proteins $(His)_7$-TacT1^{Y140F}, $(His)_7$-TacT2^{Y137F} and $(His)_7$-TacT3^{Y143F}. The purification of the recombinant $(His)_7$-TacT1^{Y140F} was carried out using the published methods with some optimisation, and pure protein was obtained. However, due to the coronavirus pandemic affecting laboratory access, the $(His)_7$-TacT2^{Y137F} and $(His)_7$-TacT3^{Y143F} proteins were not fully purified.

According to the published method, the cells were harvested by centrifugation and lysed in a buffer containing 500 mM NaCl. The literature methods used sonication for lysis, in this thesis a French press was used as it is the equipment of choice in our lab. Phenylmethanesulfonyl fluoride (PMSF) was added to the lysis buffer as reported in the literature. It is a protease inhibitor, specifically targeting serine proteases. In addition to the literature, cOmplete™ mini EDTA-free protease inhibitor cocktail (Roche) was added to the buffer to target a broader spectrum of proteases including cysteine and metalloproteases. DNase I was also added in

the presence of $MgCl_2$ to eliminate DNA in the lysis solution. Following cell lysis, electrophoretic analysis indicated that the protein was contained within the soluble fraction (**Figure 2.8**). High salt conditions were identified by our collaborators as optimal for solubilising the TacTs, so although not reported in the methods in the literature, buffers containing 500 mM NaCl were used for the remainder of the purification.

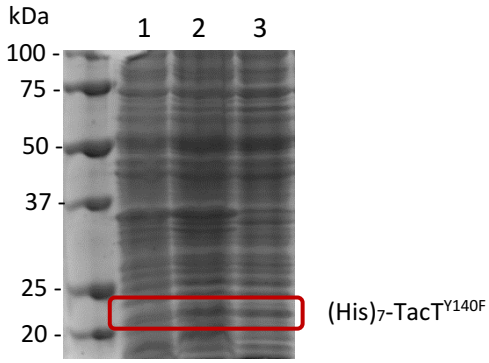


Figure 2.8: SDS-PAGE gel analysis of cell lysis of $(His)_7$-TacT1^{Y140F} protein expression: *Lane 1, $(His)_7$-TacT1^{Y140F} expression in BL21 cells; Lane 2, cell lysate following cell disruption; Lane 3 resulting supernatant (soluble fraction).*

In the published method $(His)_7$-TacT1^{Y140F} was firstly purified from the total cellular proteins by immobilised-metal affinity chromatography (IMAC) following incubation with Ni-NTA resin.[57] Two methods were used in this thesis for IMAC utilising the histidine tag. Firstly, a preloaded HiTrap TALON column was used as it is the column of choice for IMAC in our lab. The TALON column uses Co^{2+} ions which are more selective for histidine tags compared to Ni^{2+}, and less likely to bind randomly positioned histidines.[149] A preloaded column was used as it has the advantage of preventing possible degradation of proteins during the incubation time of the lysate with resin. Electrophoretic analysis demonstrated that a significant amount of $(His)_7$-TacT1^{Y140F} was lost in the flow through and column wash with 20 mM imidazole (**Figure 2.9**). The column was equilibrated with a starting concentration of 20 mM imidazole, it is possible that this was too high for a TALON column which can often elute a histidine tagged protein at a lower imidazole concentration. A starting concentration of 0 mM imidazole was therefore used in a second trial but no improvement was observed.

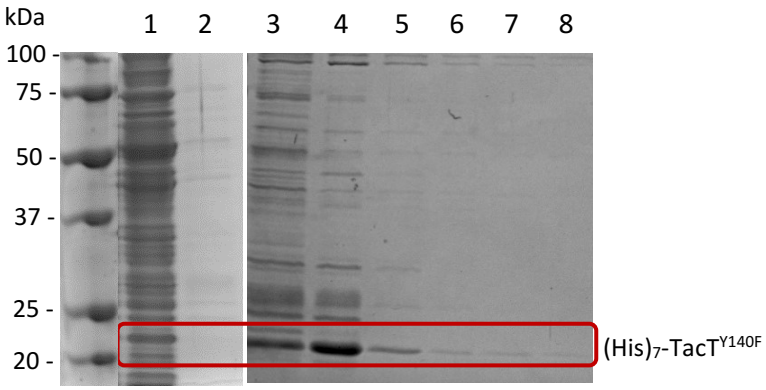


Figure 2.9: SDS-PAGE gel analysis of (His)$_7$-TacT1^{Y140F} IMAC purification: *Lane 1, flow through from loading of TALON column; Lane 2 - 3, column washes with 20 mM imidazole; Lane 4 - 8, elution with 500 mM imidazole*

To try improving the purification, gravity flow IMAC with Ni-NTA resin was tried as recorded in the literature. The crude lysate was incubated overnight with Ni-NTA resin without any imidazole, with the aim of allowing full binding of the toxin before purification by IMAC. Electrophoretic analysis of the purification identified no significant loss of (His)$_7$-TacT1^{Y140F} in the flow through or washes (**Figure 2.10**). The (His)$_7$-TacT1^{Y140F} was eluted with 500 mM imidazole, the fractions contained impurities but (His)$_7$-TacT1^{Y140F} was the main product. Fractions 9-13 were pooled for further purification.

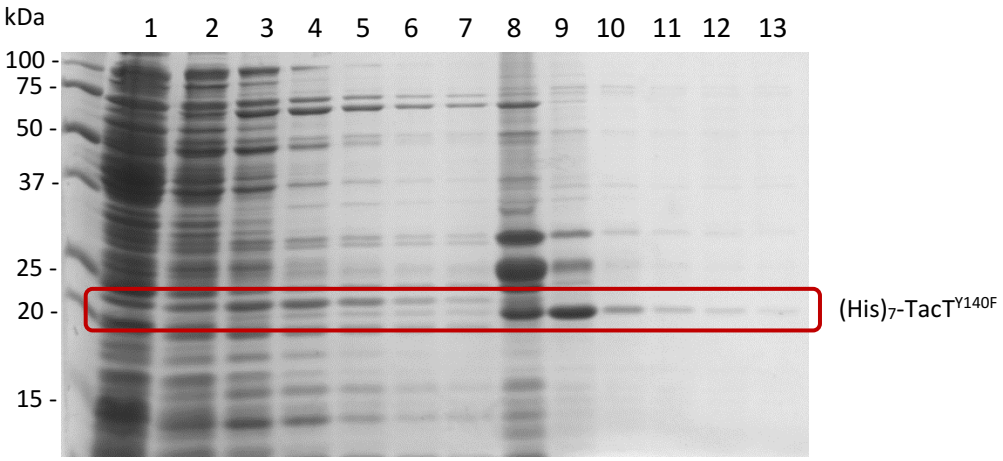


Figure 2.10: SDS-PAGE gel analysis of (His)$_7$-TacT1^{Y140F} IMAC purification: *Lane 1- 2, flow through from loading of TALON column; Lane 3-7, column washes with 20 mM imidazole; Lane 8-13, elution with 500 mM imidazole*

In the method reported in the literature for the purification of (His)$_7$-TacT1^{Y140F}, following IMAC the protein was then further purified by cation ion exchange (IEX) column chromatography, using a HiTrap SP HP column.[57] However, each of the three proteins (His)$_7$-TacT1^{Y140F}, (His)$_7$-TacT2^{Y137F} and (His)$_7$-TacT3^{Y143F} have a different isoelectric point so different

ion exchange columns would be required. The aim here was to optimise a purification method that can be used for all the TacT proteins, so this step was omitted.

Following the published method, size exclusion chromatography (SEC) using a HiLoad Superdex-75 column was carried out as the final purification step for $(His)_7$-TacT1^{Y140F}. The pooled protein following IMAC was dialysed to remove the imidazole and then concentrated. At this point most of the protein precipitated out of solution. The TacT1-3 proteins have two, four and three cysteines, respectively, making aggregate formation likely as a result of inter- and intra-molecular disulphide formation. To improve the yield in future, prior to concentrating, DTT or β-mercaptoethanol (β-ME) should be introduced at low concentrations as reducing agents to prevent the disulphide formation. The remaining solution was purified via SEC. The purified fractions eluted at retention volumes corresponding to a 40 kDa protein indicative of a dimeric state in solution. Electrophoretic analysis demonstrated that SEC can purify $(His)_7$-TacT1^{Y140F} to high purity (**Figure 2.11**). The fractions containing the pure protein were pooled and dialysed.

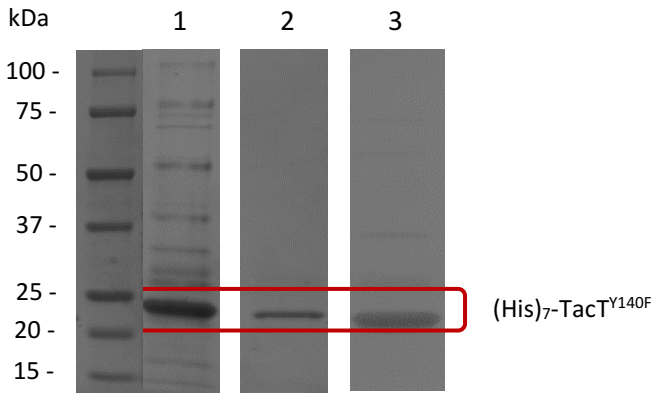


Figure 2.11: SDS-PAGE gel analysis of $(His)_7$-TacT1^{Y140F} SEC purification: *Lane 1, combined fractions following IMAC purification; Lane 2-3 two pure fractions of $(His)_7$-TacT1^{Y140F}* collected and later pooled together.

The protein concentration was determined by measuring absorption at 280 nm and calculating the concentration according to the Beer-Lambert law:

$$A = \varepsilon c l$$

Equation 1: *Beer – Lambert's law*

where A is the absorption; ε is the molar extinction coefficient of the protein, calculated using ExPASy ProtParam software with the amino acid sequence; and l is the optical path length – the distance of the sample through which the absorption is measured. In total just 1 mg of protein was isolated from 3 L of expression culture, but a much higher yield is expected without precipitation. Only $(His)_7$-TacT1^{Y140F} has so far been purified fully. $(His)_7$-TacT2^{Y137F} and

$(His)_7$-TacT3^{Y143F} have been expressed and will likely be able to be purified using the same optimised method.

2.3. Method 2: Expression of WT TacT1-3 in the Presence of Pth

In this section a second method to express the TacT1-3 proteins is described. The aim was to express the WT toxins TacT1-3 so that future activity and function assays can be carried out. The toxins were expressed in the presence of a known 'antidote' protein, Pth.[57] It was predicted that if Pth is expressed before the toxin expression is induced it will be able to rescue or prevent growth toxin induced inhibition. As the TacT toxins are expressed, they acetylate charged tRNA inhibiting translation and causing cell stasis. The Pth will detoxify the charged tRNA, reducing the toxic effect of the TacTs. The experiment was designed to allow for expression of Pth in *E. coli* cells followed by the expression of the TacT toxins in the same cells.

2.3.1. Plasmid Design and Construction

2.3.1.1. Plasmid Design

The choice of host plasmid for protein expression is very important. Mainly because of the promoter that controls expression, but also the plasmid copy number and the antibiotic resistance gene that acts as a selective marker. The promoter drives the transcription of the target gene and determines which cell types the gene can be expressed in. Promoters are usually IPTG inducible or arabinose inducible. When expressing two proteins simultaneously from different plasmids it is possible to induce one protein earlier by using a second plasmid with a different promoter. In this experiment the aim was to introduce Pth first as an 'antidote' for the toxic function of the WT TacT1-3 proteins and then express the WT TacT1-3 proteins. pBAD33 is one of the pBAD series of expression vectors which are arabinose inducible. It was proposed that Pth be cloned into a pBAD33 vector, and overexpressed first by the addition of arabinose. Each of the TacT proteins would then be inserted into the IPTG inducible pQE-80LC expression vector and expressed after the Pth by the addition of IPTG.

Antibiotic resistance genes can be used as selective markers for cells that have taken up the plasmid. The media is supplemented with the appropriate antibiotic and only cells with the plasmid containing the resistant gene can grow in the media. Since this experiment involves growing cells containing two plasmids, it was designed such that the two plasmids have different selectable markers. The pQE-80LC plasmid has an ampicillin resistance gene and the pBAD33 has a chloramphenicol resistance gene. The LB agar and all cultures could then be supplemented with both ampicillin and chloramphenicol, this ensures that the colonies selected to inoculate cultures have taken up both plasmids.

The pQE-80LC plasmid was chosen as it is a bicistronic expression vector, it also contains the gene to express BirA. BirA biotinylates proteins *in vivo* when they contain an AviTag™ and the media is supplemented with biotin.[150] The genes coding for each TacT1-3 protein were

inserted into the pQE-80LC plasmid with a $(His)_6$ tag and an AviTag™ at the N-terminus of the gene. The expression of the toxins is an important developmental step in the overall project to identify inhibitors of the toxins. The affinity of any new inhibitor to the toxins would need to be measured. The biotin – (Strept)Avidin interaction has been exploited for use in many in many biophysical assays such as surface plasmon resonance (SPR). For the expression of the TacT proteins, a biotin tag was used to allow for future development of inhibitors, it was chosen over other labelling options because the biotin molecule is stable and small and is unlikely to interfere with the function of the protein.

The final reason the pQE-80LC plasmid was chosen as the vector, was because 'leaky' expression of the toxins would be a problem. The pQE-80L expression vectors as with pQlinkH vectors have a *cis-lacIq* gene that overexpresses the lac repressor and suppresses the expression of the toxic protein before the addition of IPTG for induction. This prevents 'leaky' expression allowing a chance for high level expression of the toxic protein.

2.3.1.2. Plasmid Construction

Pth was cloned into a pBAD33 plasmid prior to this thesis by our collaborators in the Helaine group. The genes coding for each TacT1^{Y140F}, TacT2^{Y137F} and TacT3^{Y143F} toxins were cloned into a pQE-80LC plasmid using NEBuilder HiFi DNA assembly mix, the mutation was then restored to the WT so the active protein could later be expressed.

For NEBuilder HiFi DNA assembly careful design of primers is key. The primers had to have a gene specific sequence for template priming during amplification as well as an overlap sequence of 15-25 base pairs allowing for the assembly of the vector and insert. The final plasmid constructs were designed *in silico* and used to design the primers (**Figure 2.12**), primers are listed in **Table S1**. The insert gene and the vector plasmid were amplified using PCR, with appropriate overlaps. The agarose gel analysis of each PCR product suggested a single DNA product (**Figure 2.13**).



Figure 2.12: Design of primers using in silico construct of final plasmid product: *The overlapping sequences are the nucleotides coloured pink. The primers are the purple arrows, they each cover the whole overlapping region and a gene specific sequence.*

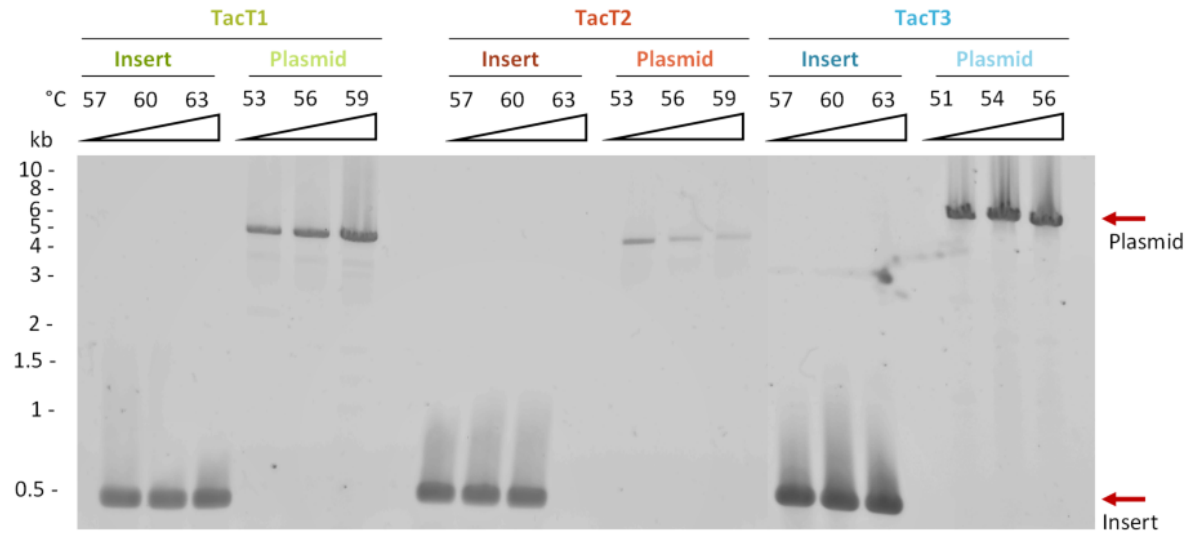


Figure 2.13: Agarose gel analysis of PCR products prior to HiFi DNA ligation: *A single PCR product for each insert and vector was obtained prior to ligation to form $(His)_6$-AviTag-TacT1, $(His)_6$-AviTag-TacT2 and $(His)_6$-AviTag-TacT3.*

In a single tube reaction, the NEB HiFi master mix was used to assemble the amplified double stranded DNA (dsDNA) insert sequence and dsDNA vector sequence with appropriate overlap sequences. The 5' exonuclease removes nucleotides at the 5' terminal leaving single stranded 3' overhangs. The overhangs of the vector and insert have complementary overlapping sequences and so the DNA anneals together. The DNA polymerase extends the 3' ends to fill in the gaps of the annealed fragments with nucleotide bases. The DNA ligase seals the nicks on the backbone of the assembled DNA. The ligated DNA was transformed into high efficiency competent cells and spread on LB agar gels. Colonies were observed for each ligation experiment for TacT1-3, indicating successful ligation. The final plasmid construct was confirmed with Sanger sequencing, demonstrating that each of the TacT1^{Y140F}, TacT2^{Y137F} and TacT3^{Y143F} genes were inserted successfully into pQE-80LC plasmid.

Following successful assembly, the mutant TacT genes were restored to the WT using single-point site-directed mutagenesis, primers are recorded in **Table S1**. The agarose gel analysis of each PCR product suggested a DNA product that corresponds to the size of the plasmid (**Figure 2.14**) and the success of mutagenesis was confirmed with Sanger sequencing.

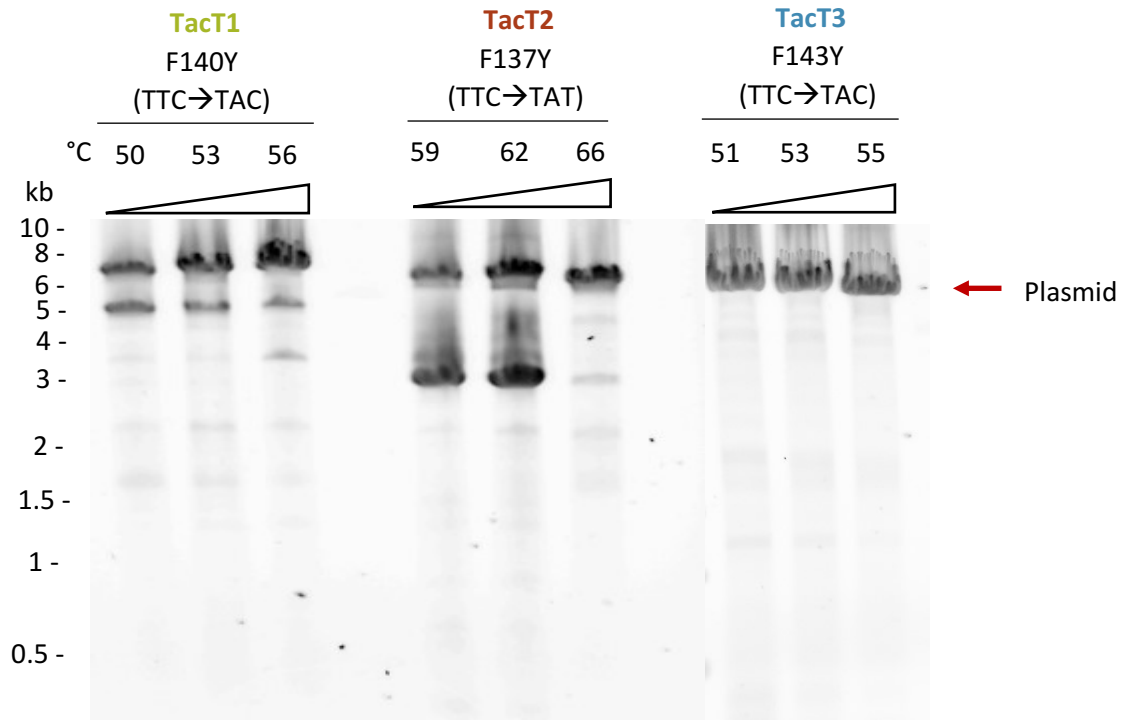


Figure 2.14: Agarose gel analysis following site-directed mutagenesis: *Product observed for mutation of mutant toxin gene: (His)$_6$-AviTag-TacT1^{Y140F}, (His)$_6$-AviTag-TacT2^{Y137F} and (His)$_6$-AviTag-TacT3 ^{Y143F} to WT genes (His)$_6$-AviTag-TacT1, (His)$_6$-AviTag-TacT2 and (His)$_6$-AviTag-TacT3.*

2.3.2. Trial Expression of Pth

The optimum conditions for Pth expression were investigated with small scale trial expressions before trial expressions with the TacT1-3 proteins. The pBAD33 plasmid containing the gene encoding Pth was used to transform chemically competent *E. coli* BL21-AI cells. *E. coli* BL21-AI cells differ from *E. coli* BL21 cells in that the replication machinery is only activated upon arabinose induction, preventing leaky expression of a toxic protein. The first method of expression of the TacT1-3 proteins (**2.2**) involved expression of the mutant toxins that have reduced toxic function. Since the aim of this method was to express the WT TacT1-3 proteins, *E. coli* BL21-AI cells were used to limit any expression of the protein until the cells have had a chance to grow to a high cell density. This is less important at this stage when just expressing the Pth, but important for trial expressions of the toxic proteins (**2.3.3**).

The cells were propagated in LB or TB media. The optimal time for induction differs from protein to protein. Usually, arabinose can be added to express non-toxic protein as early as the moment of inoculation up until the optical density of the bacterial culture at 600 nm (OD_{600}) reaches 0.6 – 0.8. For this trial the cell cultures were induced with arabinose either at the start or when the OD_{600} reached 0.4. Arabinose can be used in the range of 0.1 - 1 % (w/v), for these trial expressions a concentration of 0.4 % (w/v) was used. A large increase in growth was observed for each culture (**Figure 2.15a**). Cultures in TB media had a final cell density almost 3 times larger than the cultures in LB media. The cultures induced by arabinose at the start compared to at OD_{600} = 0.4 demonstrated no difference in cell density. SDS-PAGE analysis showed overexpression bands for a protein at ~23 kDa in each cell culture correlating to the size of Pth (**Figure 2.15b**). The overexpression band for Pth was not noticeably different with arabinose expression at OD_{600} = 0.4 compared to at the start.

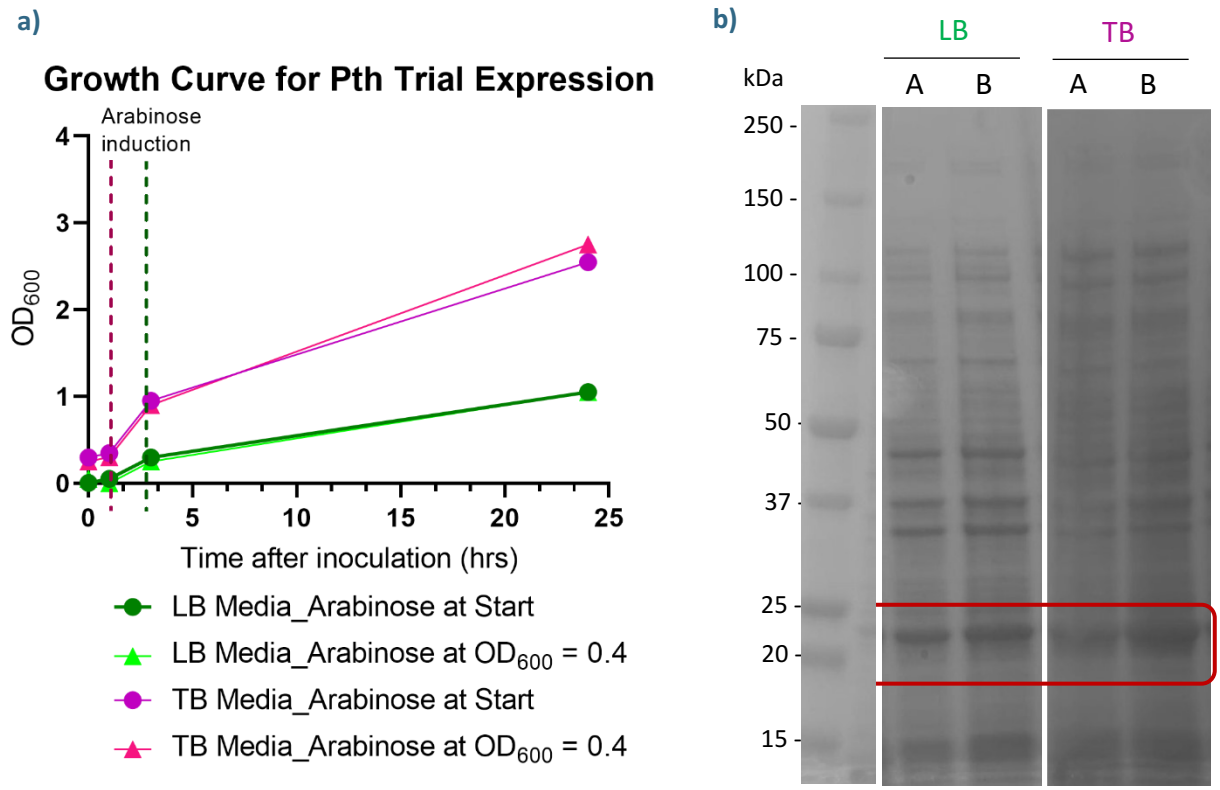


Figure 2.15: Expression of Pth protein (22.9 kDa): a) *Growth curve of BL21-AI* E. coli *cell culture transformed with pBAD33_Pth plasmid, in LB and TB media. The time after inoculation is plotted against OD_{600}, the dotted lines indicate induction by arabinose early in the log phase when OD_{600} reached 0.4, an increase in growth is observed following induction. Cultures in TB media compared to LB media have a greater cell density.* **b)** *SDS-PAGE analysis of total cell protein expression at 24 hrs. Lanes A: arabinose added at the start, Lanes B: arabinose added at OD_{600} = 0.4.* Overexpression bands were observed at *~23 kDa, circled in red, indicating successful overexpression of Pth.*

Based on this experiment Pth can be expressed well in both LB and TB media. There is no significant difference in expression between induction with arabinose at the start or at OD_{600} = 0.4. For the next stage of trial expressions of the toxic proteins together with Pth (**2.3.3**) the arabinose was added at the start as it makes little difference to the amount of Pth, but Pth will be expressed earlier. Both LB and TB media were used as they did not affect Pth expression but may affect TacT1-3 expression.

2.3.3. Trial Expression of WT TacT1-3 in the Presence of Pth

In these trial expression experiments the aim was to find optimum conditions to overexpress three proteins in each cell culture: Pth, BirA and one of TacT1, TacT2 or TacT3. The gene encoding the Pth protein was in a pBAD33 plasmid and the gene encoding BirA was in the bicistronic pQE-80LC plasmid with one of each TacT1, TacT2 or TacT3 genes. The method follows the normal workflow for bacteria-hosted protein expression. Chemically competent

E. coli BL21-AI cells were transformed with both plasmids and plated on LB agar plates containing the antibiotics which the plasmids carry resistant genes for (both ampicillin and chloramphenicol). Precultures were grown up from a single colony in LB or TB media containing the correct antibiotics. The cultures were then diluted 1:15 in the chosen media. As earlier with expression via autoinduction, a very high ratio of preculture to new media was used compared to standard dilution of 1:100. The precultures in TB media had reached a very high density, so the starting OD_{600} of the growth cultures were between 0.1 and 0.4. Arabinose was added at the start to induce Pth expression. The BL21-AI replication machinery was therefore also induced from the start because of the addition of arabinose. Usually, IPTG can be added when the OD_{600} reaches 0.6 and the induction of a toxic protein should be done at a time point as late as possible. IPTG was therefore added when the OD_{600} reached 0.6 – 0.8 to induce the expression of the TacT proteins. IPTG can be used in the range of 0.1 to 5 mM, for induction of toxins the IPTG concentration used should be on the lower scale end. Therefore, for these trial expressions 0.5 mM IPTG was added. The cultures were all supplemented with biotin to promote biotinylation by BirA.

Three variables were changed to try to find optimum expression conditions. Both LB and TB media were used; the presence or absence of glucose at a 0.4% w/v concentration; and the presence or absence of IPTG at 0.5 mM concentration. The growth of each culture was monitored by measuring the OD_{600} every hour and then every half an hour after OD_{600} of 0.4 was reached. A few patterns were noticed. In all cases cells grew to OD_{600} of 0.6 – 0.8 within 2 - 4 hours. After 24 hours the cultures in TB media had up to 3-fold higher cell density compared to the same cultures (with/without glucose and IPTG) in LB media (**Figure 2.16**). Because of the higher cell densities of TB cultures, the difference in growth in the cultures with or without glucose and IPTG is easier to observe and evaluate. The remainder of growth observations are of cultures in TB media.

Prior to induction the expression cultures of each of the TacT1-3 proteins grown in the presence of glucose had higher cell density compared to those without (**Figure 2.16**). Due to this head-start, after 24 hours the expression cultures of TacT1 had an OD_{600} value 0.5 - 1.0 higher; TacT2 had an OD_{600} value 3 times higher and the TacT3 had OD_{600} value 4 times higher. Glucose inhibits the lac operator of the T5- promoter in pQE-80LC, it therefore prevents leaky expression of the TacT toxins up until the point of induction. In the cultures with glucose the TacT toxins aren't present prior to induction, whereas without glucose the cells express a small amount of TacT toxins which inhibits growth. This prevents them growing to a higher density.

After 24 hours the expression cultures of the TacT1 and TacT2 proteins induced by IPTG had lower cell density compared to the cultures for which no IPTG was added (**Figure 2.16**). This suggests that the expression of the TacT1 and TacT2 toxins caused a toxic effect on the bacterial cultures and growth was hindered. It further suggests that Pth did not sufficiently

act as an ‘antidote’ to repair any acetylated tRNA. There was an overexpression band for a protein at ~23 kDa in each cell culture correlating to the size of Pth (**Figure 2.17**), suggesting that Pth was present but did not act as an antidote. There was a faint overexpression band for a protein at ~32 kDa in each cell culture correlating to the size of BirA, suggesting that the IPTG was active and some BirA was expressed. As the TacT1 and TacT2 genes were each in the same plasmid as BirA it is expected that the TacT1 and TacT2 proteins would also be expressed. No overexpression bands for TacT1 and TacT2 were observed suggesting that the proteins were too toxic to the cells and could not be overexpressed.

After 24 hours the expression cultures of the TacT3 protein induced by IPTG had identical cell density compared to the cultures for which no IPTG was added (**Figure 2.16**). This suggests that either TacT3 did not express, or the expression of the TacT3 toxins did not cause a toxic effect on the bacterial cultures. If TacT3 did express, it further suggests that Pth may have acted as an ‘antidote’ to repair the tRNA acetylated by TacT3. In each culture there was an overexpression band correlating to the size of Pth and a faint overexpression band correlating to the size of BirA (**Figure 2.17**). Encouragingly, there was also a strong overexpression band at ~20 kDa corresponding to the size of TacT3. This suggests that the IPTG was active and BirA as well as TacT3 were expressed. The continued cell growth upon induction as well as the overexpression band of TacT3 indicate that Pth was successful at acting as an ‘antidote’ to the toxic TacT3. Although the TacT3 was expressed and it is toxic to the cell, the cells could still grow and the TacT3 was still successfully overexpressed.

It is interesting that this method of expression was only successful for TacT3 and not for TacT1 and TacT2. It is possible that further optimising the conditions for expression would enable overexpression of TacT1 and TacT2. Possibly a higher level of glucose in the media would help keep tighter control of leaky expression. Varying the IPTG may also enhance expression, a lower amount of IPTG may limit the amount of toxin expressed and allow Pth more time to repair the acetylated tRNA. The temperature was not varied in this experiment, expression at 18 °C following induction may prevent IPTG from deactivating and keep the cell replication level slower so the Pth has a better chance of repair. The expression of TacT3 was successful and can be scaled up to find out if the experiment is feasible on a large scale.

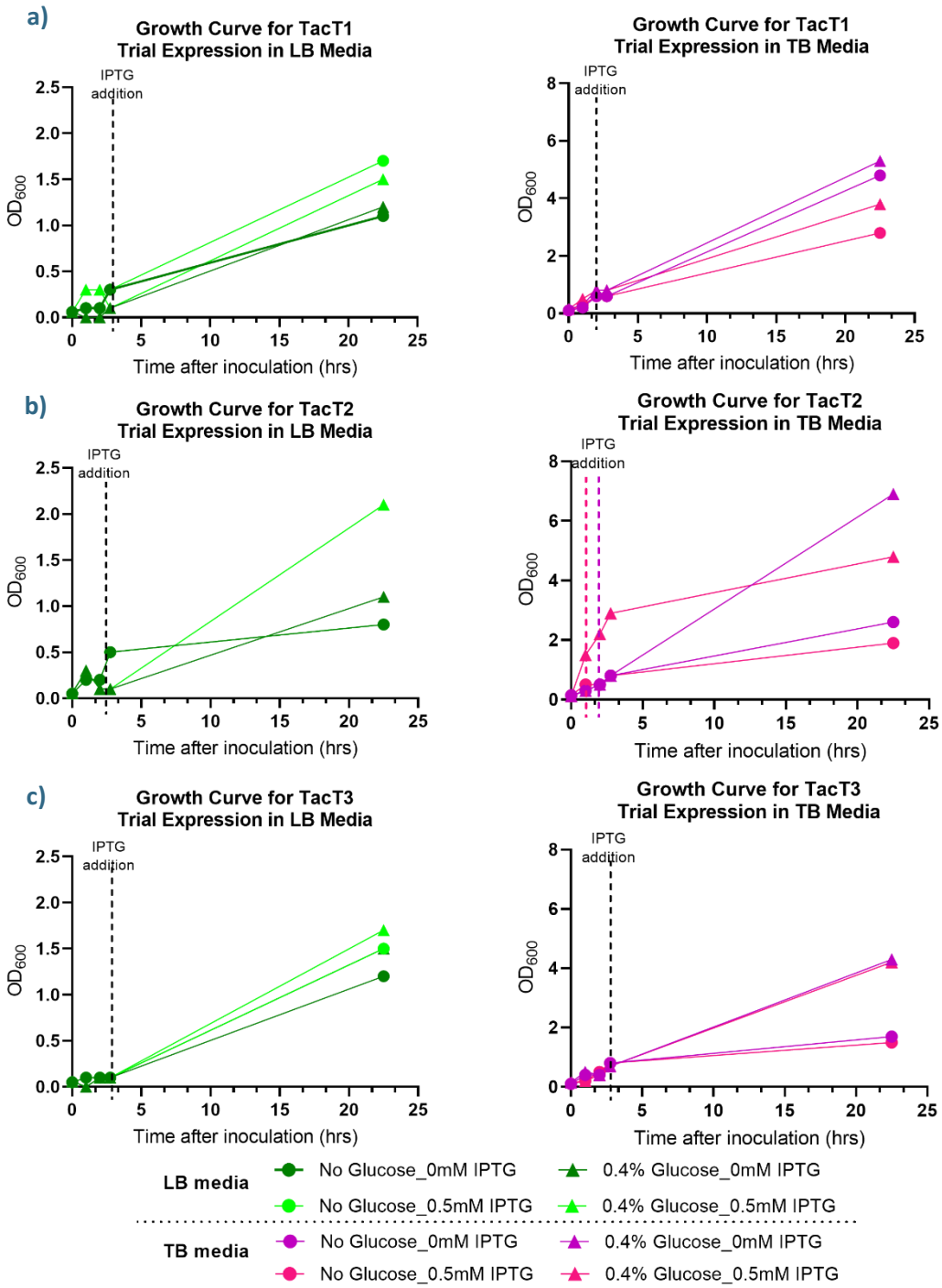
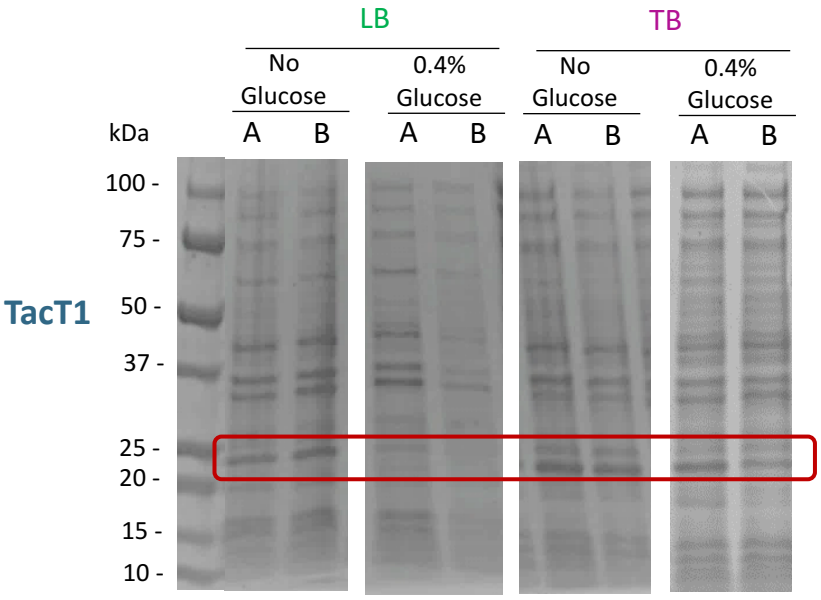
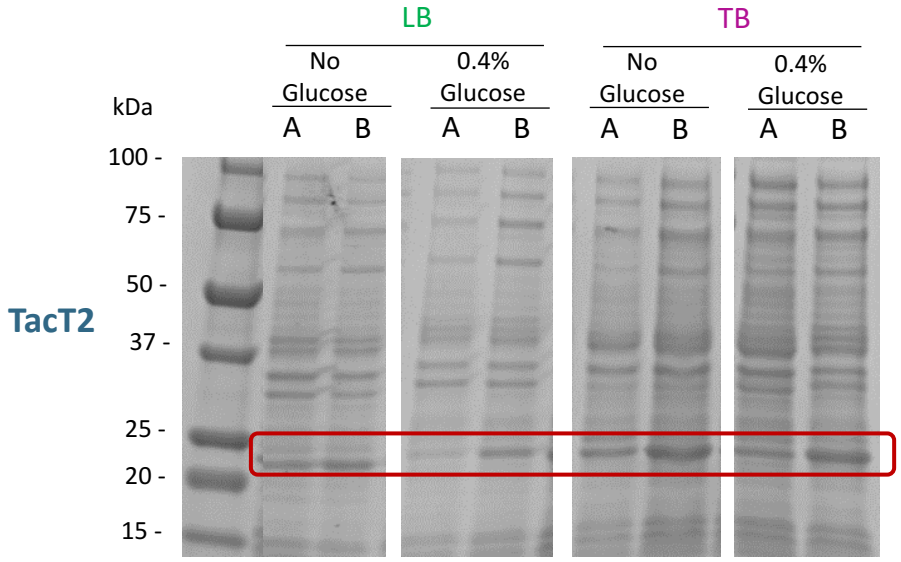


Figure 2.16: Growth curves of TacT trial expression in BL21-AI* E. coli *cell culture in LB and TB media*: Cells transformed with pBAD33_Pth plasmid and **a)** pQE80LC_$(His)_6$-AviTag-TacT1 **b)** pQE80LC_$(His)_6$-AviTag-TacT2 and **c)** pQE80LC_$(His)_6$-AviTag-TacT3. The time after inoculation is plotted against OD_{600}, the dotted lines indicate induction by IPTG early in the log phase when OD_{600} reached 0.4, an increase in growth is observed following induction. Cultures in TB media compared to LB media have a greater cell density. The expression cultures of the TacT1 and TacT2 proteins induced by IPTG had lower cell density compared to the cultures for which no IPTG was added. The expression cultures of the TacT3 protein induced by IPTG had identical cell density compared to the cultures for which no IPTG was added.*

a)


LB
TB
No Glucose
0.4% Glucose
No Glucose
0.4% Glucose
kDa
A B A B A B A B
100 -
75 -
50 -
37 -
25 -
20 -
15 -
10 -
TacT1

b)


LB
TB
No Glucose
0.4% Glucose
No Glucose
0.4% Glucose
kDa
A B A B A B A B
100 -
75 -
50 -
37 -
25 -
20 -
15 -
TacT2

c)

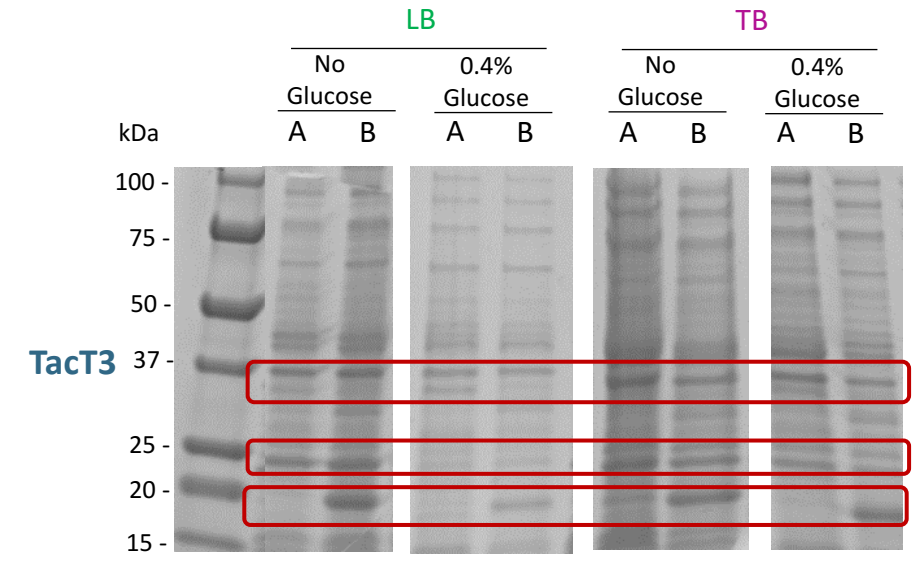

LB
TB
No Glucose
0.4% Glucose
No Glucose
0.4% Glucose
kDa
A B A B A B A B
100 -
75 -
50 -
37 -
25 -
20 -
15 -
TacT3

Figure 2.17: SDS-PAGE analysis of total cell protein expression of TacT proteins with Pth at 24 hrs: *Lanes A: no IPTG, Lanes B: IPTG added at OD_{600} = 0.4.* ***a)*** *expression of $(His)_6$-AviTag-TacT1 (22.1 kDa) in presence of Pth. Expression band observed for Pth at ~20 kDa, small expression band observed for BirA at ~35 kDa; and no expression band observed for$(His)_6$-AviTag-TacT1 at ~22 kDa.* ***b)*** *expression of $(His)_6$-AviTag-TacT2 (22.0 kDa) in presence of Pth. Expression band observed for Pth at ~20 kDa, small expression band observed for BirA at ~35 kDa; and no expression band observed for $(His)_6$-AviTag-TacT2 at ~22 kDa.* ***c)*** *expression of $(His)_6$-AviTag-TacT3 (23.4 kDa) in presence of Pth. Expression band observed for Pth at ~20 kDa, expression band observed for BirA at ~35 kDa; and expression band observed for $(His)_6$-AviTag-TacT3 at ~23 kDa.*

2.4 Chapter Summary and Conclusions

In this chapter the expression of TacT1-3 proteins has been discussed and demonstrated. In the first section of the chapter, the challenges of expressing type II toxins were discussed. The toxins are toxic to *E. coli* cells and expressing the WT form without its coordinating antitoxin is not possible. A number of methods have been reported to express type II toxins, and two of those methods were chosen to express the TacT toxins in this thesis. The first was expression of mutant forms of each toxin that cannot co-ordinate the Ac-CoA cofactor in the correct position for transfer of acetyl group to tRNAs. The TacTs cannot carry out their toxic function, so the cells survive and propagate in the presence of the protein. With some optimisation of the methods reported in the literature $(His)_7$-TacT1^{Y140F}, $(His)_7$-TacT2^{Y137F} and $(His)_7$-TacT3^{Y143F} were all overexpressed to a level that allows for purification. It was found that priming the cells with glucose from the earliest stage when plating cells on agar for growth recovery was crucial to prevent 'leaky' expression and allow cells to propagate. It was also found that using autoinduction in TB media gave the highest level of expression.

The second method used to express the TacT toxins in this thesis was to express the WT toxins in the presence of a known 'antidote' Pth. Since an antidote to TacT toxicity is known, it was proposed that TacTs could be expressed in the presence of this antidote Pth. The aim was that the toxic activity is overhauled by the presence of Pth, and TacTs can be overexpressed as cell death is not triggered. The experiment was carefully designed to allow for expression of Pth first, followed by the TacT proteins. Cell lines and plasmids were chosen to tightly control expression and prevent leaky expression of the very toxic WT proteins that would inhibit cell growth.

Due to time constraints just one trial expression experiment for each of the TacTs in the presence of Pth has been carried out so far. In this trial it was exciting to observe that on a small scale the WT TacT3 was overexpressed in the presence of Pth, suggesting the strategy is promising. The WT TacT1 and TacT2 toxins were not overexpressed, but further optimisation of the conditions may enable overexpression of the proteins. A higher level of glucose in the media may keep a tighter control of leaky expression. A lower amount of IPTG,

or later addition of IPTG may slow toxin expression and allow Pth more time to repair the non-functional tRNA.

This thesis is part of a larger project to identify a pan inhibitor of the three TacT proteins. It is important to be able to express the WT TacT proteins for future activity assays to assess the strength of inhibitors. First, further trials should be carried out to try express the toxins in the presence of Pth, varying the glucose concentration; the IPTG concentration and time of addition; and varying the temperature for expression. If this method does not work, other reported methods for toxin protein expression could be considered. Firstly, expressing the TacTs with their antitoxins, denaturing the complexes and then refolding just the TacTs. Expression in yeast cells is an alternative option, it would be a preferred method to expression with the antitoxins if no refolding has to be carried out. As a final resort cell free expression could be used, although it is expensive, so this would only be for a small scale expression.

In this chapter, the purification of $(His)_7$-TacT1^{Y140F} has also been presented. The purity was high enough for use in biophysical and biochemical assays to assess binding characteristics. Although $(His)_7$-TacT2^{Y137F} and $(His)_7$-TacT3^{Y143F} were expressed, due to time constraints as a result of the coronavirus pandemic, they have not been purified. It is expected that the established purification method for $(His)_7$-TacT1^{Y140F} can be applied to these two proteins with minimal optimisation required. Additionally, it is expected that the $(His)_6$-AviTag-TacT1, $(His)_6$-AviTag-TacT2 and $(His)_6$-AviTag-TacT3 can also be purified using this method if expression alongside Pth is successful.

Chapter 3

Characterising the Protein-Protein Interactions of TacTA1-3

Abstract

This chapter describes the use of purified TacT1-3 proteins for the biophysical and biochemical characterisation of the interaction between TacT1-3 and their respective antitoxins. The aim was to gain insight into the nature of the PPIs to provide a strong starting point for the development of compounds to inhibit the TacT toxins. Firstly, a series of peptides based on the antitoxin proteins TacA1-3 were designed and synthesised. Then the affinity of the antitoxin peptides to the TacT toxin proteins were determined using biophysical experiments. TacT1, TacT2 and TacT3 all demonstrated different affinities for their corresponding antitoxin peptides, supporting the published data that they display different potencies.

3.1. Introduction to Biophysical Characterisation of PPIs

Biophysical characterisation is the use of different biophysical analytical methods to investigate the biophysical behaviour of biomolecules. The analysis could involve understanding the structure and other biophysical properties of a single biomolecule. It also could involve characterising the structure and properties of an interaction of the biomolecule with a ligand or another biomolecule. It is important to characterise biophysical properties as the biophysical behaviour of proteins can impact many aspects of cellular function as well as drug function in relation to the molecule.

3.1.1. Characterisation of PPIs

The fundamental forces of binding; including electrostatic forces, hydrogen and van der Waals bonding and the hydrophobic effect; all determine the interaction characteristics of PPIs.[151] The specificity of the interaction generally comes from the molecular complementarity between the interaction site of the two proteins. Binding energies are not evenly distributed across the PPI surface, this is because of 'hotspot' residues or compact centralised regions that are crucial to the affinity of the interaction.[152]

In **Chapter 1** it was described that both small molecules and peptides have been used to target PPIs despite their large surface area. Whilst HTS has been used for the discovery of small molecule inhibitors of PPIs, rational structure-activity based design has shown the greatest success. Small molecule compounds have been discovered that target clusters of 'hotspot'

residues in bacterial PPIs.[67-69] Prior to the rational design of these molecules the structure, affinity and other biophysical properties in particular the identification of 'hotspot' residues of the PPI interface must be elucidated. This also applies to the identification of peptides, cyclic peptides and peptidomimetics as PPI inhibitors. These larger molecules are usually used to target PPIs that have 'hotspot' residues distributed over a large surface area as they can confer greater selectivity.[70,71] A peptide is often designed using the structure of one of the binding partners and further optimised and developed based on the biophysical properties of the interaction.

A robust understanding of the biophysical characteristics of a PPI is crucial for the successful development of drugs inhibiting a PPI or targeting a protein involved in a PPI. Structural characterisation by crystallography or NMR provides details of the interface size and the types of amino acids involved and therefore some indication of the type of bonding at the interface. Analysis of the structure can also indicate the shape complementarity. It may also highlight some conformational changes of the one or both proteins upon binding when comparing the protein alone and when bound. A number of other biophysical characterisation methods have been developed to investigate the affinity, thermodynamics, kinetic rates and salt sensitivities of a PPI. These can be used to elucidate the biological functional mechanisms of the proteins in PPIs. Additionally, 'hotspot' residues can be identified providing a starting point for the rational design of small molecules or peptides to target a PPI.

3.1.2. Characterisation of PPIs of TA systems

As explained in **Chapter 1** the type II TA systems consist of a toxin and an antitoxin protein pair that form a PPI.[20] Whilst the crystal or NMR structures of many type II systems have been elucidated, other biophysical characteristics of many TA pairs have not been reported.[153] Consequently, the biological functions of many TA pairs is not fully understood. For example, it is not well understood what properties of antitoxins allow them to exhibit a controlled neutralisation effect on the toxins.[154]

One of the obstacles to characterising TA pairs is the challenging recombinant expression of the toxins.[140] This was discussed in **Chapter 2** where two solutions were examined to express the TacT proteins and can be extended to other TA systems. Another barrier is the complexity of the antitoxin proteins. The antitoxins have been reported to bind to the toxin (in some cases at multiple sites), bind to the TA operon to regulate expression and form homodimers.[155] The antitoxins are generally intrinsically disordered proteins or have unstructured C-terminal regions.[156-160] When bound to the toxin or a target they may have a tertiary structure, in some cases they bind as a linear peptide. It is a challenge to identify which region of the antitoxin is responsible for the PPI.

Some work has been done to characterise the properties of some TA PPIs beyond the structural data.[161-164] The affinities between the antitoxins to their toxin pairs as well as to their other targets, specifically the TA DNA operators, have been reported.[161-167] The

equilibrium constant K_D is often used to rank strengths of bimolecular affinities. Affinities of either a ligand, DNA, peptide or protein to a protein are often measured and reported as a K_D. The K_Ds for some TA complexes have been reported in the nanomolar range indicative of high affinity PPIs.[161-164] This likely encourages proper cell growth in normal cell conditions. Experiments were carried out to identify the K_Ds between full length proteins of TA pairs: PezA-PezT (<1 nM), RelB-RelE (0.33 nM), Phd-Doc (0.35 µM and 31 µM) and MqsA-MqsR (<0.15 nM).[161,163,164,166] However, using the full length antitoxin does not give any information about which region is involved in the PPI. The affinity of CcdA-CcdB was assessed using truncated peptides of the antitoxin CcdA.[162] The peptides used were based on the structure of the TA complex. It is interesting that this complex had the lowest K_D of 0.03 nM, possibly a result of no interference from other regions of the antitoxin. Using truncated peptides can identify which area holds majority of the binding energies. In all these studies no further analysis was carried out to identify which residues are crucial for the interaction, this would give further information about the binding energies of the PPIs.

As mentioned in **Chapter 1** the structures of the mutant TacT1-3 proteins have been elucidated and published.[57,58] Additionally, our collaborators have unpublished crystal structures of each of the TacT proteins in a complex with a truncated antitoxin protein. The crystal structures provide some information of the region of the antitoxin involved in the PPI, as well as the amino acids involved. However, the affinities between the toxin and antitoxin pairs have not been measured. This is necessary to better understand the biological function and how the antitoxin neutralises the toxin. It is also a step in the process of discovering a pan inhibitor for the three TacT proteins. Each of the TacTs may have different mechanisms of neutralisations or rely on different 'hotspot' residues. Characterising the PPIs and the crucial interactions involved may identify whether an inhibitor can be designed to target the site of the interaction with the antitoxin or an allosteric site.

In this project, it was decided to characterise the affinities of the TacTs for their respective antitoxins as a starting point to elucidate the neutralisation mechanism of the TacA antitoxins. Future experiments could be carried out to compare this measured affinity to the affinity of the antitoxin to the TA DNA operon. This can provide information of whether the TA systems rely on conditional cooperativity as reported for some type II TA systems.[161-163,166]

TacA peptide sequences of the toxin binding-domain would be used as chemical tools to characterise the interaction. Using the sequence that is only involved in toxin binding reduces the influence from the remainder of the antitoxin that is involved in other functions. Additionally using peptides provides future opportunities to characterise the key residues which is not possible with proteins. This can be done by using an alanine scanning technique, wherein a series of peptides would be synthesised with each amino acid sequentially replaced with alanine. Since alanine has a small inert side chain, this allows the determination of the contribution of each amino acid to the binding affinity.

3.1.3. Methods

There are many methods available to measure the affinities of a protein-protein or protein-peptide interaction. Quantitative methods release a signal that indicates the strength of the interaction. Some of these can be extrapolated to obtain the binding affinity as a K_D value. Methods include isothermal titration calorimetry (ITC), microscale thermophoresis (MST), differential scanning fluorimetry (DSF (thermal shift)), fluorescence anisotropy (FA (fluorescent polarisation)) and surface plasmon resonance (SPR).[168] In this thesis three methods were used, DSF, FA and SPR. The advantages and considerations of each method used are discussed below.

3.1.3.1. Differential Scanning Fluorimetry

Using DSF, thermal shift assays are carried out where proteins are gradually heated in the presence of an external fluorescent probe. SYPRO® orange dye is commonly used as the probe.[169] As the temperature is increased the protein unfolds and hydrophobic areas are exposed. SYPRO® orange has an affinity for hydrophobic areas on a protein and binds to the protein at the increasingly larger hydrophobic surface areas inducing a fluorescent signal. As the temperature increases the fluorescence peaks just before protein aggregation and dye dissociation.

The fluorescent signal at 610 nm can be plotted as a function of temperature. The inflection point of the resulting sigmoidal curve is referred to as the observed melting temperature (T_m), the point at which 50% of protein is unfolded and is a measure of stability. In the presence of a binding partner a change in T_m is usually observed (ΔT_m). The protein complex may be more stable so the T_m is higher, or it may be less stable resulting in a decrease of the T_m. There are many reports that the stabilising effect of a compound when bound to a protein is proportional to the affinity of the compound.[170] This suggests a tighter binding compound will result in a greater increase in melting temperature. It is important to be cautious though as the ΔT_m is not an exact reflection of affinity. Enthalpic and entropic contributions affect the magnitude of the shift. Larger shifts will be observed for interactions that are hydrophobically (entropically) driven. An observed thermal shift is a good indicator of a binding interaction; however the exact binding affinity cannot be extrapolated from the data.

DSF is a very useful tool. It can be high-throughput when carried out in 96-well or 384-well plates. It is very quick, inexpensive and uses only small amounts of protein. It is important to consider that it cannot be used for every protein or binding partner. As the probe detects hydrophobicity, the assay is sensitive to hydrophobicity of a protein, a very hydrophobic protein will have large background noise. If the binding partner has fluorescence this will affect the readout as it will be difficult to distinguish the source of fluorescence.

3.1.3.2. Fluorescence Anisotropy

FA has been used since the early 1900's as an analytical technique to carry out biophysical characterisation experiments.[171] When a fluorescent label such as fluorescein or TAMRA is excited by polarised light it emits light with a degree of polarisation inversely proportional to the rate of molecular rotation. The emission of light from a labelled peptide alone in solution is largely depolarised, but upon binding to a protein the fluorophore has reduced rotational speed and therefore is more polarised. The observed polarisation upon introduction of the protein to the peptide solution is proportional to the fraction of bound peptide.

FA is a highly useful tool to determine the K_D of a ligand or peptide to a protein. It has been developed for high throughput use in 384-well plates, and is fast to carry out.[172,173] It is important to consider that a fluorescently labelled peptide or ligand is necessary, synthesis can be time consuming or expensive and, if the binding peptide or ligand is fluorescent (besides the label), this will affect the readout.

3.1.3.3. Surface Plasmon Resonance

The physical process of surface plasmon resonance was discovered in the early 1900s.[174,175] Later the knowledge of the SPR process was applied to sensing.[176,177] When plane-polarised light hits the sensor surface of a grating or prism, if total internal reflection (TIR) conditions are met, an electrical field of photons reflects from the surface. Surface plasmons are a result of these photons interacting with the electrons on the surface of a noble metal. When the momentum of the incoming light is the same as the momentum of the plasmons, resonance occurs.[178] The momentum is highly dependent on the angle of incident light. The angle of incident light is referred to as the resonance angle, it can be measured very precisely in SPR assays.[178] When the composition of the medium is changed, the refractive index is changed. This is detected as a change in the angle of resonance.

Using SPR, the protein of interest (ligand) is bound to a noble metal surface sensor. When a second biomolecule (analyte) binds to the surface of a sensor a change in refractive index is observed. This change is proportional to the number of molecules bound to the surface.[179] SPR can be used to detect biomolecular interactions, it can measure the K_D values for a peptide, protein or ligand interacting with a protein. The analyte is introduced in increasing concentrations by flowing over the noble metal surface. The change in refractive index upon peptide binding is measured and recorded in arbitrary units (RU). The resulting sensograms plot the RU against analyte concentration. The plot demonstrates an association phase from which the k_{on} is determined, and a dissociation phase from which the k_{off} is determined. The K_D can be calculated from these two constants.

SPR is a highly useful tool to determine the binding kinetics and binding affinity of two interacting biomolecules. It characterises reactions in real time using label-free detection. It is important to consider that it is not a very high throughput method. Additionally, any buffer that affects the refractive index of a sample, for example dimethylsulfoxide (DMSO), will alter an SPR readout.

3.1.4. Chapter Aims

In the remainder of this chapter the biophysical characterisation of the TacTA1-3 PPIs will be described. The chapter is divided into two main sections

a) Design and synthesis of antitoxin peptides (**3.2**).

b) Using various biophysical methods to measure the affinities and some other properties of the TacT1-3 interaction with peptides of TacA1-3 (**3.3**).

3.2. Antitoxin peptide design and synthesis

In unpublished data, our collaborators, the Helaine group in Harvard, have previously identified the minimum TacA antitoxin lengths necessary to inhibit the toxicity of their respective TacT toxins (**Figure 3.1**). They performed a series of 5 amino acid long N-terminal truncations for each antitoxin. They tested their abilities to restore the growth of *Salmonella* expressing their cognate toxin. The final sequences were minimal and sufficient to neutralize their cognate toxin. These were a good starting point to measure the affinity of TacT-TacA binding for TacTA1, TacTA2 and TacTA3 and were therefore targeted for synthesis using solid phase peptide synthesis (SPPS).

1: TacA1 52--**FNFNDEQYEEFINLLDAPVADDPVIEKLLARKPQWDV**-- 88

2: TacA2 54--**IEQRIIMADPEAYQEFLVRLDQTPSPNAALRKTMQTPAPWEQEK** 97

3: TacA3 58--**YLTERDTKMIMEILDNPPAPNEKLLAAAFALPDMKK**-- 93

Figure 3.1: Minimum antitoxin sequences: *minimum sequence found to inhibit the toxicity of the TacT toxins. Synthesised using SPPS and referred to in the text as peptides **1**, **2** and **3** respectively.*

The peptides were designed to have an acetyl group at the N-terminus to remove the positive charge on the peptide to better mimic the state of the native protein (**Figure S1**). The acetyl group also prevents N-terminal degradation by exopeptidases so increases peptide stability.[180] The acetyl capped peptides corresponding to TacA1-3 are referred to as **1**, **2** and **3**, respectively. FA was used initially for characterisation of the interaction between each minimum antitoxin peptide and their respective toxin, therefore each of the minimum peptides was also synthesised with a fluorescent label. Tetramethylrhodamine (TAMRA) was used and coupled to the N-terminus (**Figure S2**). The TAMRA capped peptides are referred to as **TAMRA_1**, **TAMRA_2** and **TAMRA_3** hereon in.

3.2.1. Introduction to solid phase peptide synthesis

SPPS has been developed and refined over the last 60 years, since the initial work of Merrifield *et al.* reporting that an amino acid could be anchored to a solid support.[181] It is now used in the synthesis of natural products and biopolymers, chemical ligation, and is constantly being developed for use in other fields. SPPS is used to reduce the synthesis time of peptides and because of the variety of synthetic products that can be produced.

The synthesis of a peptide, involves cycles of deprotection and coupling of two amino acids to form an amide bond. The first building block (amino acid) is anchored to a matrix (resin). Then protected amino acids are coupled in the C → N direction via repeat cycles of deprotection, coupling and washing. Finally, the peptide product is released from the matrix and the side chains are simultaneously deprotected (**Figure 3.2**).

3.2.2. Synthesis, Purification and Analysis of Peptides (**TAMRA_**) **1**, **2** and **3**

A Liberty Blue HT12^{TM} automated microwave peptide synthesiser was used to synthesise all peptides in this thesis. Microwave irradiation during SPPS has enabled the synthesis of longer or more challenging to synthesise peptide sequences. Heating prevents formation of secondary structures which are formed by difficult peptide sequences making the reactive sites on the growing peptide chain partially inaccessible. Heating also allows for improved coupling of bulky amino acids by reducing the steric hindrance. The result is greater yields and purity of challenging peptides and significantly reduced reaction times.

A linker is used to anchor the growing peptide chain to the resin. Depending on what linker is used a different C-terminus can be obtained when the peptide is cleaved from the linker. As peptides **1** and **3** are derived from the middle of the antitoxin proteins (not the C-terminus) a C-terminal amide was chosen to best mimic the protein. The Rink Amide linker on an MBHA resin was used which, when cleaved, results in a C-terminal amide. As peptide **2** is derived from the C-terminus of its antitoxin protein a C-terminal carboxylic acid was chosen to best mimic the native protein. Using a pre-loaded resin for synthesis of peptides with a C-terminal carboxylic acid prevents the formation of diastereomeric side-products. Therefore a pre-loaded Fmoc-Lys(Boc) Wang linker was used to synthesise peptide **2**.

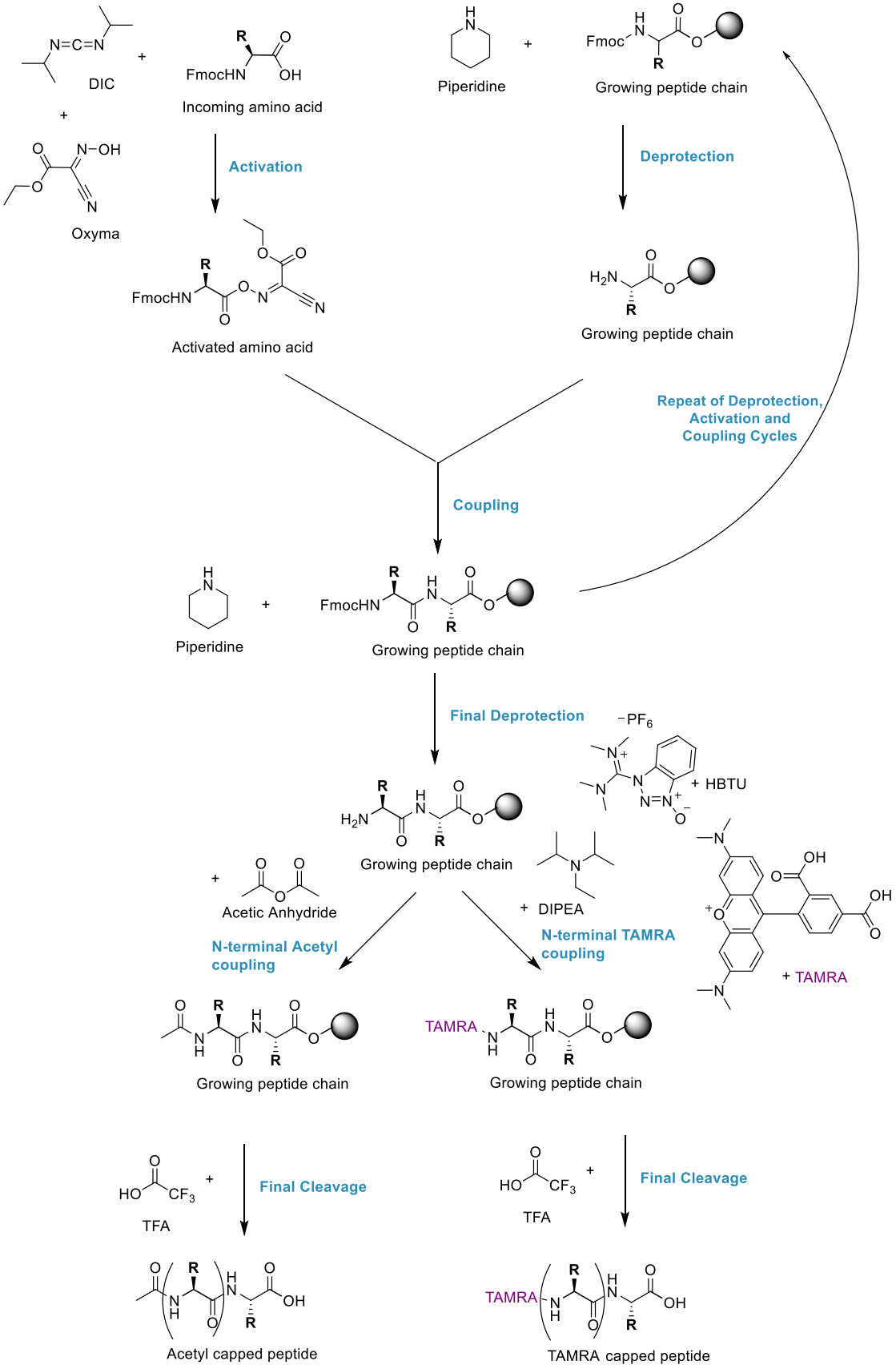

DIC
Incoming amino acid
Oxyma
Activation
Activated amino acid
Piperidine
Growing peptide chain
Deprotection
Growing peptide chain
Repeat of Deprotection, Activation and Coupling Cycles
Coupling
Piperidine
Growing peptide chain
Final Deprotection
Growing peptide chain
+ HBTU
Acetic Anhydride
+ DIPEA
+ TAMRA
N-terminal Acetyl coupling
N-terminal TAMRA coupling
Growing peptide chain
Growing peptide chain
TFA
Final Cleavage
TFA
Final Cleavage
Acetyl capped peptide
TAMRA capped peptide

Figure 3.2: General Scheme for Peptide Synthesis: *The synthesis begins with the removal of the Fmoc protecting group on the N-terminal amine group of a resin. In a coupling reaction the amine group binds to an Fmoc protected incoming amino acid at the activated carboxy terminus, forming a peptide bond. The Fmoc protecting group is removed under basic conditions by piperidine before the subsequent coupling. The deprotection, activation and coupling steps are repeated for addition of each amino acid in the peptide chain. The N-terminus can be capped with an acetyl group of fluorescent label prior to cleavage and side-chain deprotection in acidic conditions. R represents amino acid side chains.*

Following the synthesis of the linear sequences, acetic anhydride in DMF was used to acetylate the peptides to generate **1**-**3**. It is fast and convenient, and the reaction occurred under non-inert conditions. To synthesise **TAMRA_1-3**, TAMRA was manually added to each of the peptides in a similar way to the addition of each amino acid in the automated synthesis. TAMRA was first activated to an ester using the coupling reagent N-[(1H-benzotriazol-1-yl)(dimethylamino)methylene]-N-methylmethanaminium hexafluorophosphate N-oxide (HBTU) in the presence of the base N,N-Diisopropylethylamine (DIPEA). HBTU is an electrophile with a built-in auxiliary nucleophile that is released, it controls the chemical outcome preventing racemisation and prevents side reactions. The deprotected terminal Nα amine on the peptide chain can then couple with the activated carbonyl group of TAMRA creating an amide bond.

Prior to purification a test cleavage of each peptide was carried out to confirm that the desired product had been synthesised. A small amount of peptide was cleaved from the resin, dissolved in 25% acetonitrile (ACN) and run through an analytical liquid chromatography-mass spectrometry (LC-MS) column. In each case the observed mass of the main product was in agreement with the calculated mass of the peptides. The whole product was then cleaved from the resin using trifluoroacetic acid (TFA) and scavengers. The crude mixture was separated using preparatory LC-MS. Fractions containing the pure peptide were combined and a high purity of > 90% was obtained for all six peptides (**Figure 3.3** and **Figure S3**). The mass of each peptide was also confirmed using matrix assisted laser desorption ionisation (MALDI) MS.

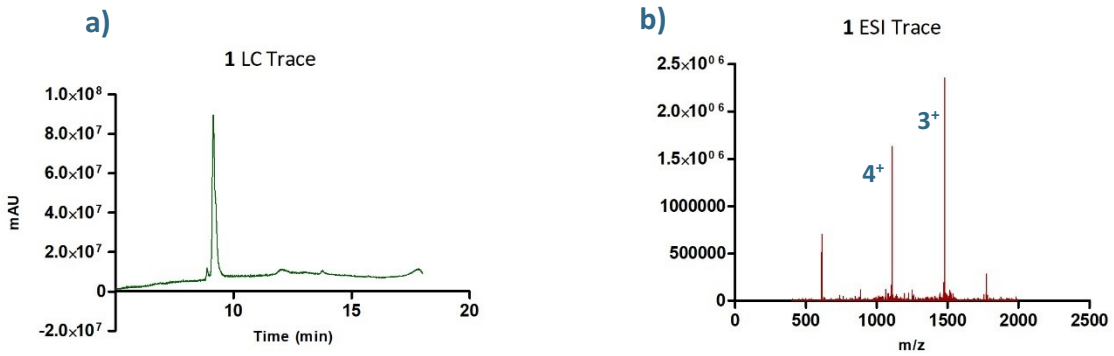


***Figure 3.3: Purified peptide** 1 **a) UV chromatogram at 280 nm;** a single peak was observed in the UV chromatogram corresponding to the desired product peptide **1. b) ESI trace;** the peaks in the mass spectrogram correspond to the charged peptide ions. The expected mass of **1** was 4434.4 Da, the following ions were observed: 4^+ (1109.9) and 3^+ (1478.1).*

The final yield was first measured using the weight of the dry pure peptide. Once dissolved in solution it was also calculated spectrophotometrically. Each of the peptides contain tryptophan and tyrosine residues, and the labelled peptides additionally contain TAMRA. Absorption was measured at 280 nm for each of the peptides, as well as 555 nm for the peptides with TAMRA. The molar extinction coefficient of peptides **1** - **3** at 280 nm were calculated using ExPASy ProtParam software. The molar extinction coefficient used for peptides **TAMRA_1 - 3** at 555 nm was 65000 $M^{-1}cm^{-1}$. The molar extinction coefficient used for peptides **TAMRA_1 - 3** at 280 nm was the same as that calculated for peptides **1** - **3** with the addition of 19500 $M^{-1}cm^{-1}$ to take into account TAMRA. The concentration was determined using the Beer-Lambert law. Whether measuring absorption at 555 nm or 280 nm the concentrations of the TAMRA peptide were almost identical, with a maximum 10% difference in final calculated values. Using spectrophotometrically calculated values, each peptide had a final yield of 25% or greater following purification.

3.3. Binding of TacT1-3 to peptides of TacA1-3

Following the successful synthesis of the labelled and unlabelled minimum antitoxin peptides, the interactions of the toxins TacT1-3 with their respective minimum antitoxin peptides were characterised. The binding affinity and other information about the interactions were measured using the experimental methods described in 3.1.2: DSF, FA and SPR.

3.3.1. Binding analysis of the TacT proteins to their antitoxin peptides by DSF

A thermal shift assay was used as an initial measure of the affinities of each YF mutant toxin TacT1-3 protein with its respective antitoxin TacA1-3 peptide. The experiments were carried out with protein provided by our collaborators.

The melting temperatures of $(His)_7$-TacT1^{Y140F}, $(His)_7$-TacT2^{Y137F} and $(His)_7$-TacT3^{Y143F} were first measured alone in solution. The conditions were optimised to find preferred salt conditions, dye concentration and protein concentration (**Figure 3.4** and **Figure S4**). Varying the

concentration of NaCl in the buffer had no effect on the strength of the fluorescence observed. Although at 500 mM NaCl the proteins all demonstrated at least a 2.5 °C higher T_m compared to measurements carried out at 150 mM NaCl (**Table 1**). It seemed the proteins were more stable in higher salt conditions so a buffer with 500 mM NaCl was used for subsequent measurements. Assays were trialled with dilutions of SYPRO dye from 1:500 – 1:2000. A 1:1000 dilution of SYPRO dye was chosen, this was enough dye to observe a clear sigmoidal increase in fluorescence as the protein melts. Assays were carried out with the TacT proteins between the range of 2.5 - 10 µM concentrations. At concentrations of protein higher than 5 µM the observed fluorescence was greater than background fluorescence and a strong fluorescence peak was observed (**Figure 3.4**). Therefore, 5 µM of protein was used in subsequent assays.

Protein		T_m (°C)							
		150 mM NaCl				500 mM NaCl			
		SYPRO 2.5X	**SYPRO 5X**	**SYPRO 7.5X**	**SYPRO 10X**	**SYPRO 2.5X**	**SYPRO 5X**	**SYPRO 7.5X**	**SYPRO 10X**
TacT1	2.5 µM	53	52	52.5	52	57	55.5	55.5	56
	5 µM	53	52.5	52.5	52.5	57	57	56	55.5
	10 µM	53	53	53	53	57	57	57.5	57
TacT2	2.5 µM	48.5	48	49	-	54	57	58	58.5
	5 µM	49	45	50	48	53	57	56	56.5
	10 µM	49	47	48	49	52	54	56	56
TacT3	2.5 µM	61	59	58.5	58	57	61	61	60.5
	5 µM	59	58.5	58	59.5	60.5	60.5	61	60.5
	10 µM	59.5	59	59	59	60	61	61	61

Table 1: Melting temperature measured by DSF for each of the TacT proteins *(2.5-10 µM) in solution in the presence of SYPRO-Orange dye (2.5 – 10 X (1:2000 -1:500)). Measured in two buffers at different salt concentrations 150 mM and 500 mM NaCl.*

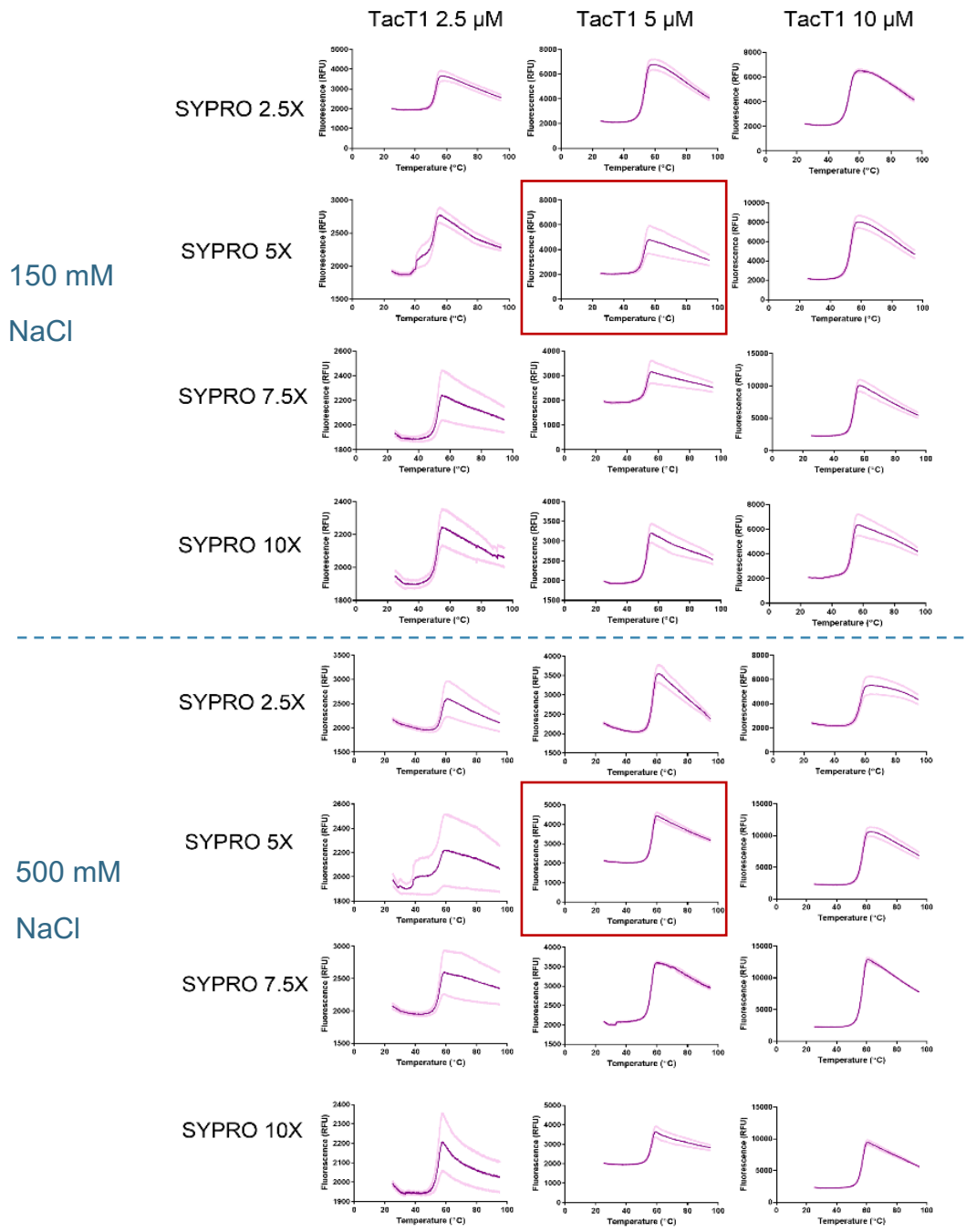


Figure 3.4: DSF with TacT1 protein at different conditions*. The change in fluorescence of TacT proteins (2.5-10 µM) in solution in the presence of SYPRO-Orange dye (2.5 – 10 X (1:2000 -1:500)) with increasing temperatures between 25-95°C. Measured in two buffers at different salt concentrations 150 mM and 500 mM NaCl. The average of triplicate measurements is shown with the dark purple line and the standard deviation shown with light purple lines.*

Alone in solution $(His)_7$-TacT1^{Y140F}, $(His)_7$-TacT2^{Y137F} and $(His)_7$-TacT3^{Y143F} all demonstrated high thermal stability with melting temperatures in the range of 55-65 °C, indicating stably folded proteins, and suggesting purification can be carried out at room temperature (**Figure 3.5a**). The three proteins were then measured in the presence of their corresponding antitoxin peptide (**1**-**3**). The peptides were added at two concentrations 5 µM and 25 µM, a 1:1 and 5:1 ratio with the TacT proteins.

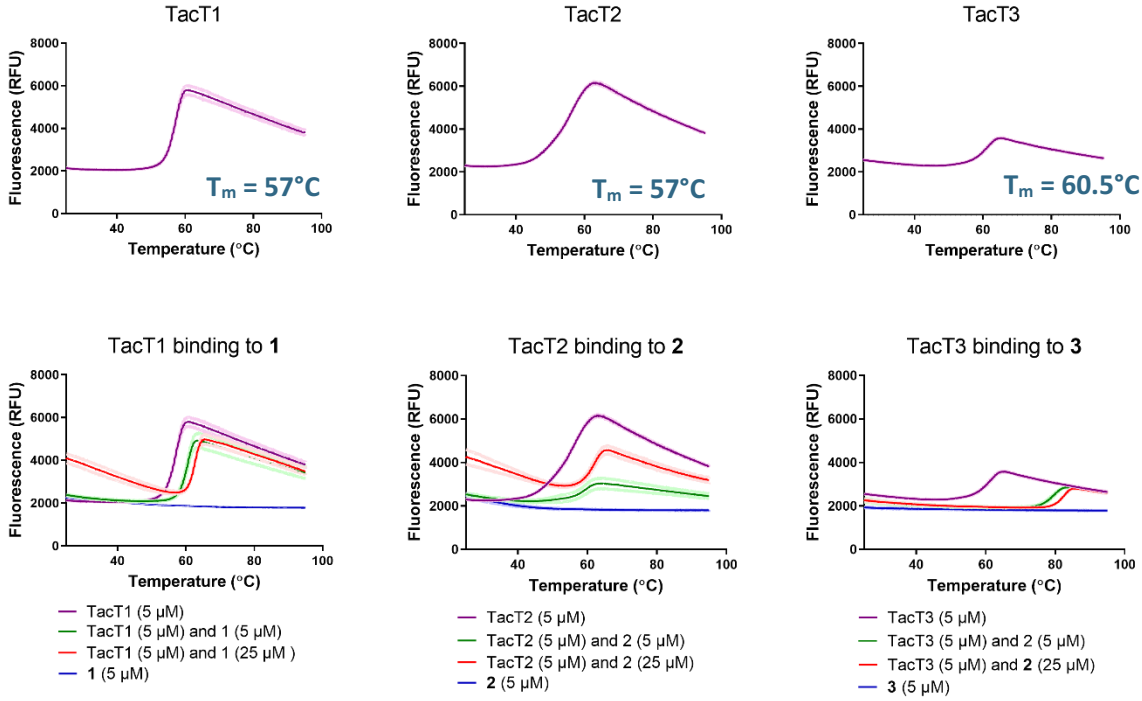


***Figure 3.5: DSF with TacT proteins and their minimum antitoxin peptides**. **a)** The change in fluorescence of TacT proteins (5 µM) in solution in the presence of SYPRO-Orange dye (1:1000) with increasing temperatures between 25-95°C. The average of triplicate measurements is shown with the dark purple line and the standard deviation shown with light purple lines **b)** The change in fluorescence of TacT proteins in the presence of their respective antitoxin peptides (5 µM or 25 µM) in the presence of SYPRO-Orange dye (1:1000) with increasing temperatures between 25-95°C. Measurements are plotted in the same graph as the TacT proteins alone in solution, a thermal shift can be observed for all three proteins binding to their respective antitoxin peptides.*

A rightward shift in T_m in the presence of the antitoxin suggests a binding event since this leads to increased stability of the protein, in general the greater the shift in temperature, the higher affinity of the binding event. TacT1 and TacT2 demonstrated a small shift of 3.2 °C and 3.5 °C, respectively, in the presence of 5 µM peptide (**Table 2, Figure 3.5b**). A much larger shift of 17.6°C was observed for TacT3 when bound to **3** suggesting that TacT3 binds with the highest affinity to its antitoxin **3**. In the presence of 25 µM of peptide (5:1 ratio) the ΔT_m of

each protein was increased by 2-3 °C. One possible explanation is the presence of a second binding site for the peptide, with a double or excess of peptide enabling more to bind to the protein. The protein is stabilised further and a greater shift in melting temperatures was observed. However, this slight shift is typical for thermal shift assays. It is likely that an excess of peptide ensured that more protein molecules were bound to a peptide and overall, more protein was stabilised at any given point. The overall fluorescent signal was therefore greater.

Protein (5 µM)	ΔT_m (°C)	
	5 µM peptide	25 µM peptide
TacT1	3.2	5.2
TacT2	3.5	5.9
TacT3	17.6	20.4

Table 2: Change in melting temperature measured by DSF for each of the TacT proteins binding to their minimum peptide.

3.3.2. Binding analysis of the TacT proteins to their antitoxin peptides by SPR

SPR was then used to measure the K_D values for each of $(His)_7$-TacT1^{Y140F}, $(His)_7$-TacT2^{Y137F} and $(His)_7$-TacT3^{Y143F} proteins to their respective antitoxin peptides (**1**-**3**). Each protein was bound to an Ni-NTA chip via its $(His)_7$ tag, and the antitoxin was introduced in increasing concentrations by flowing over the chip. The achieved response (steady state) was plotted against analyte concentration (**Figure 3.6** and **3.7**). For initial SPR measurements a buffer containing 500 mM NaCl was used. A 1:1 kinetic model could be applied to the results of TacT3 bound to its antitoxin (**Figure 3.6**). The model could not be fit to the results of TacT1 and TacT2 binding to their antitoxin at this concentration (**Figure 3.7**). Only in reduced salt conditions with NaCl concentrations of 250 mM could a K_D be accurately measured (**Figure 3.6**). Binding of **1** to $(His)_7$-TacT1^{Y140F} was measured using multi-cycle kinetics (MCK). The complex was allowed to associate and fully dissociate because the dissociation time was quick and within a measurable time frame. For the affinity measurements of **2** and **3** binding to $(His)_7$-TacT2^{Y137F} and $(His)_7$-TacT3^{Y143F} respectively, the k_{off} was found to be significantly slower. This long dissociation time of the peptide was too long to allow for full dissociation between each concentration measurement. Instead, these measurements were carried out using single-cycle kinetics (SCK) and the chip was fully regenerated between each measurement.

The calculated K_D values indicated moderate to high binding affinities of the toxins to their antitoxin peptides (**Table 3, Figure 3.6**). TacT1 bound the weakest to its antitoxin peptide with K_D of 360 nM, TacT2 ranked second with K_D of 54 nM, and TacT3 bound with the highest affinity to its antitoxin peptide with a K_D of 700 pM, confirming the predicted affinity ranking from the thermal shift assay.

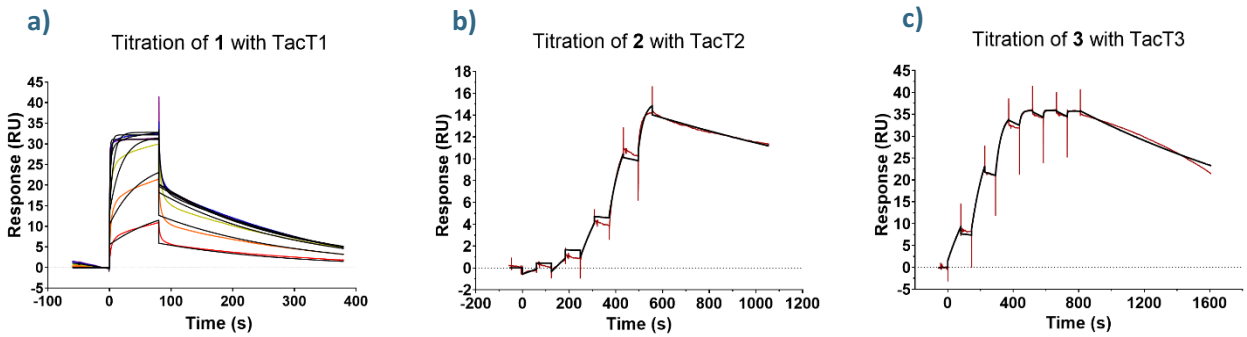


***Figure 3.6: SPR sensorgrams of the minimum antitoxin peptides** 1-3 **with their respective TacT1-3 toxin proteins**. **a)** Response curve for the titration of **1** (100-0.04 µM) with TacT1 measured using MCK. Experiment carried out in buffer containing 250 mM NaCl. **b)** Response curve for the titration of **2** (5-0.06 µM) with TacT2 measured using SCK. Experiment carried out in buffer containing 250 mM NaCl. **c)** Response curve for the titration of **3** (1000-4 nM) with TacT3 measured using SCK. Experiment carried out in buffer containing 500 mM NaCl. A kinetic 1:1 binding model was applied to each experiment.*

TacT_A	K_D	k_{on} (M^{-1} s^{-1})	k_{off} (s^{-1})
TacT1_1	360 nM	1.30^{4}	4.60^{-4}
TacT2_2	54 nM	8.50^{3}	4.60^{-4}
TacT3_3	700 pM	6.90^{5}	4.80^{-4}

***Table 3: Binding data measured by SPR for each of the TacT proteins binding to their minimum peptide**.*

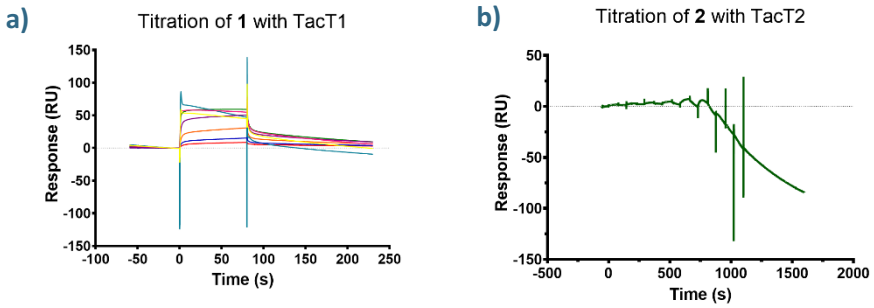


***Figure 3.7: SPR sensorgrams of the minimum antitoxin peptides 1** and **2 with their respective TacT toxin proteins a)** Response curve for the titration of **1** (100-0.04 µM) with TacT1 measured using MCK. **b)** Response curve for the titration of **2** (5-0.06 µM) with TacT2 measured using SCK. Both experiments carried out in buffer containing 500 mM NaCl. A kinetic model could not be fit to this data.*

The sensitivity to salt in the buffer indicated that the TacTA toxin-antitoxin binding is, in some instances, very salt dependent. Salts can block charged residues that mediate electrostatic interactions. The interactions cannot form and, if the binding of two molecules relies on many transient electrostatic interactions, the binding is significantly hindered. This is the case with the TacTA PPI. The TacT proteins have a unique structural feature. When in the active dimer conformation, it has two adjacent positively charged patches at the surface (**Figure 1.4**), this is the tRNA binding site. The negatively charged phosphate groups of tRNA molecules interact with side chains of positively charged amino acids. Unpublished data from collaborators identified that the minimum antitoxin peptides bind to the tRNA binding site. The toxin-antitoxin PPI is therefore mediated by electrostatic interactions. This is the method by which the antitoxin inhibits the toxin function, it prevents the TacT toxin binding to tRNA.

The binding of TacT1 and TacT2 with their minimum antitoxins was most significantly affected by high salt conditions. The antitoxin peptides **1** and **2** have 9 and 7 negatively charged residues, respectively, compared to the 4 negatively charged residues in peptide **3.** It appears that these antitoxin peptides rely on electrostatic interactions at the positively charged surface binding site of tRNA and that these interactions are strongly influenced by the presence of competing salts. Furthermore, the thermal shift and affinity data suggests that the TacTA1 and TacTA2 PPIs are held together less strongly than that of TacTA3. This correlates well to the fact that the interaction of TacTA1 and TacTA2 is mediated by electrostatic interactions which are weak and not very specific.

TacT3 binding with **3** was the least affected by high salt conditions. Interestingly the minimum antitoxin **3** has the least negatively charged residues compared to **1** and **2**. It seems the interactions with the antitoxin are not dominated by electrostatic interactions, and it therefore makes sense for peptide **3** to be less effected by high salt conditions. Additionally, thermal shift and SPR data demonstrated that TacT3 has the highest affinity for its minimum antitoxin. The interaction likely relies on additional, more specific interactions. *In vivo* data has shown TacT3 to have the most potent persister effect in *Salmonella.*[58] TacT3 has an extra helix and loop as explained in Chapter 1.1.5. This was predicted to enhance potency by enabling better binding to cofactor Ac-CoA. It is interesting that the TacT3 toxin has the highest affinity to its antitoxin, it is possible that the extra loop and helix allow it to bind more strongly to TacA3 without relying on electrostatic interactions at the positively charged tRNA binding site.

The high salt dependencies of the TacTA1 and TacTA2 PPIs highlights the importance of carrying out *in vitro* assays in relevant physiological conditions. In a cellular environment the physiological ionic strength varies but averages around 150 mM.[182,183] All future affinity experiments as well as activity assays should therefore be carried out at 150 mM so that the strength of electrostatic interactions is comparative to *in vivo* conditions.

3.3.3. Binding analysis of the TacT proteins to their antitoxin peptides by FA

To further characterise the binding of TacTs to their antitoxin peptides, FA assays were carried out using the TAMRA labelled peptides. The antitoxin peptides were prepared at 1 nM, above the fluorescence detection limit of the instrument (0.5 nM) and less than twice the predicted K_D for any of the toxin-antitoxin interactions. It is important that the fluorophore ligand concentration used is significantly lower than the K_D as otherwise a stoichiometric titration of the ligand will be measured. The $(His)_7$-TacT1^{Y140F}, $(His)_7$-TacT2^{Y137F} and $(His)_7$-TacT3^{Y143F} proteins were titrated within a range of 5 µM–0.075 nM, with the aim to have the lowest concentration (0.075 nM) less than 10% of the K_D if it reaches within the picomolar range.

A biphasic relationship was observed for TacT1 binding to **TAMRA_1** giving K_D values of 3 nM and 2200 nM for each binding event (**Figure 3.8a**). When this same interaction was measured by SPR a 1:1 kinetic model was used to fit the data as it wasn't possible to know for certain whether a biphasic relationship was present, it is likely, therefore, that the calculate K_D is an average of the two binding events. Notably, the average of the two K_D values calculated from the FA assay is close to the value of 360 nM obtained by SPR.

The affinity of TacT3 binding to **TAMRA_3** was calculated to be 54 nM, much higher than expected from the large thermal shift in the thermal shift assay and the value of 700 pM from SPR characterisation (**Figure 3.8b**). As seen in the graph, at lower concentrations of TacT3 towards 0.075 nM the anisotropy measurements dipped significantly. It appeared that if the anisotropy was measured at even lower concentration a second binding event would be observed. It is predicted therefore that there is also biphasic relationship with this TA pair with a second lower K_D value not observed in this range. To confirm this, a titration at lower concentrations would be required. This may be challenging as normally the lowest protein concentration value should be less than 10% of the K_D. If the value is less than 750 pM then this has not been covered. If the K_D is less than 500 pM then the tracer peptide concentration of 1 nM is too high. Since the instrument detection limit is 500 pM, the lowest K_D that can be measured is 250 pM. **TAMRA_3** should be prepared at a concentration of 500 pM, and TacT3 titrated with a range reaching 0.025 nM.

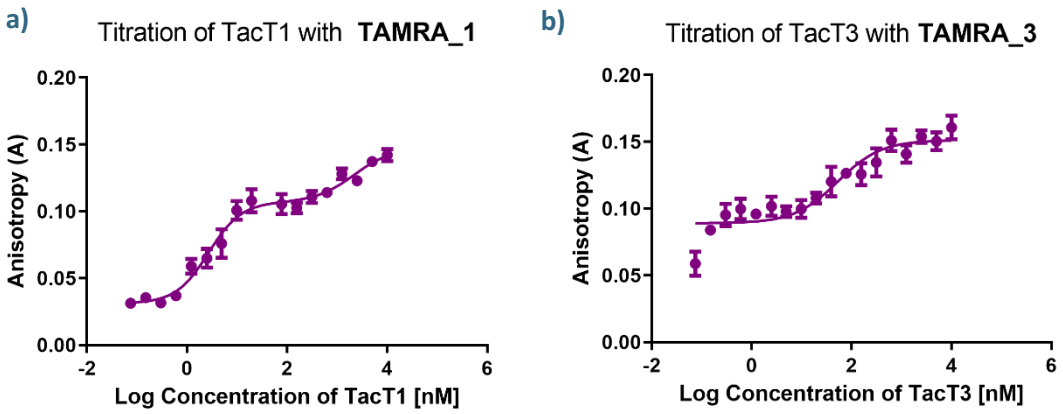


Figure 3.8: Fluorescence anisotropy for binding of the toxin proteins to their respective minimum antitoxin peptide labelled with TAMRA*. The log concentration of protein is plotted against anisotropy (A).* ***a)*** *response curve for the titration of TacT1 (5µM-0.075 nM) with* ***TAMRA_1*** *(1 nM).* ***b)*** *response curve for the titration of TacT3 (5µM-0.075 nM) with* ***TAMRA_3*** *(1 nM).*

It was not possible to observe a curve for binding of TacT2 to its minimum antitoxin peptide **2** (**Figure 3.9**). It is possible the peptide was too long. Usually a molecular weight of 1500 Da is the recommended cut off point for a fluorescent peptide to accurately measure binding by FA. All the peptides were larger than the recommended molecular weight. **TAMRA_1** had a molecular weight of 4800 Da and **TAMRA_3** had a molecular weight of 4500 Da, but **TAMRA_2** had a much greater molecular weight of 5580 Da. It is possible that the peptide was not well folded, although this is unlikely as binding was measured by DSF and SPR. It is most likely that the binding could not be measured because a high salt buffer containing 500 mM NaCl was used. This is similar to the observation with SPR measurements where a binding model could not be fit to data measured in buffers containing 500 mM NaCl. The high salt may have masked the charged residues involved in toxin-antitoxin binding. Peptide folding should be investigated by circular dichroism (CD) in the future and different salt conditions used to try and optimise the assay.

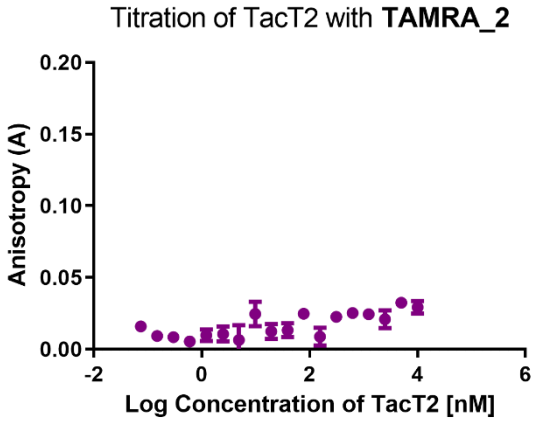


Figure 3.9: Fluorescence anisotropy for binding of the TacT2 toxin protein to its minimum antitoxin peptide labelled with TAMRA*. The log concentration of protein is plotted against anisotropy (A) and the response for the titration of TacT2 (5µM-0.075 nM) with* ***TAMRA_2*** *(1 nM) is shown.*

4.3. Chapter Conclusions and Summary

The antitoxin peptides **1 - 3** and **TAMRA_1 - 3** were successfully synthesised using automated microwave SPPS. They were all isolated in high purity and with a yield above 25%, despite their very long lengths.

Initial characterisation of the binding affinities confirmed the minimum antitoxin peptides bind to their respective TacT proteins and indicated that TacT3-**3** has the highest affinity interaction. The lower affinities of the TacT1 and TacT2 proteins to **1** and **2** respectively is surprising. Type II TA pairs are commonly of very high affinity.[161,162] Additionally a large difference in affinities was not expected given the similarity within the TacTA family. It is predicted that folding of the peptides plays a role in this interaction, and as the peptides are very long, they may not have folded to their native configuration. This should be confirmed by CD measurements, and if necessary, a method to refold the peptides may be needed to obtain an accurate measure of affinity.

Additionally, FA and SPR results suggest that electrostatic interactions are likely to play a large role in the interaction. The interactions between the toxin proteins and their respective antitoxin peptides that had the lowest affinities likely have the most electrostatic interactions. They are therefore highly interrupted by salt and most greatly affected by high salt conditions. The values obtained for the affinities in each assay may be much greater in lower salt conditions of 100 mM or 250 mM NaCl that mimic the cellular environment better.

Finally, a biphasic binding relationship was observed for TacT1 binding to its minimum antitoxin peptide. This relationship is also predicted to occur for TacT2 and TacT3 binding to their antitoxins, further work using FA is needed to clarify this. The biphasic relationship

corresponds to a predicted interaction of the toxin with two different peptides at each binding site. Our collaborators (the Helaine group from Harvard) have obtained crystal structures demonstrating that two antitoxins bind to each toxin. It is speculated that in a first slow interaction one helix binds to the protein in its active site, this then causes the shift and disordering of a loop allowing a second fast binding event of the second helix to the disordered loop. It is possible that both helices belong to one antitoxin, or the second binding event is by a second antitoxin molecule binding. It is not clear which binding event would have the highest affinity, and it is still unknown whether the crystal structure mimics the activity in solution.

Based on these results there is a lot of future work that can be carried out to further characterise the interaction and identify whether a biphasic relationship is truly involved. It would be useful to also identify which helix binds first and if there is an interdependency. One experiment could involve alanine scanning to determine the contribution of each amino acid to the binding affinity and in this case, particularly those that are essential for the biphasic interaction. Each minimum antitoxin sequence has two helices. Therefore, DSF, SPR and FA could all be carried out following synthesis of each of the helices separately. The change in K_D and titration curves comparing the presence of one or both helices may identify which has the highest affinity, and whether one helix binds first and allows a second binding event. The crystal structure may not actually mimic the activity in solution. To find out the stoichiometry of the interaction and confirm what happens in solution, size exclusion chromatography – multi-angle light scattering (SEC-MALS) could be employed. In this experiment, the toxin would be mixed with the antitoxin peptides and then separated via SEC. The mass of proteins or protein complexes eluted would then be measured by MALS and the mass would be indicative of the ratio of antitoxin peptide to toxin protein.

Chapter 4

Conclusions and Outlook

The principal contribution of this thesis was to characterise the PPI between each of the TacT1-3 proteins and their antitoxins. This thesis has built upon the work of the Helaine group, identifying the TacT proteins and their contribution to persistence.[57,58] Their published crystal structures of the TacT proteins and unpublished structures of the TacT proteins bound to a minimum antitoxin sequence gave some insight into the characteristics of the TacT structure and the TacTA1-3 PPIs. At the start of this thesis the binding mode and affinities of the TacT proteins to their antitoxins were not known. This MPhil used biophysical characterisation to extend current understanding of the nature of the TacTA1-3 PPIs. This project is part of a greater project to identify a pan inhibitor of the three TacT proteins. Understanding the nature of the TacTA complexes is a crucial step in the development of inhibitors of the TacT proteins to counter persistence. It is of particular importance to identify the differences and similarities between the three TacTA1-3 complexes in the TacTA family to identify where a pan inhibitor could target the proteins.

4.1. Summary of Findings

In **Chapter 2** the expression of TacT1-3 proteins was demonstrated. Firstly, with some optimisation of the methods reported in the literature, mutant non-active TacT constructs ($(His)_7$-TacT1^{Y140F}, $(His)_7$-TacT2^{Y137F} and $(His)_7$-TacT3^{Y143F}) were overexpressed to a level that allows for purification. Next one set of trial expressions were carried out to express the WT TacT constructs ($(His)_6$-AviTag-TacT1, $(His)_6$-AviTag-TacT2 and $(His)_6$-AviTag-TacT3). The trials involved expressing the WT toxins in the presence of a known 'antidote' Pth. It was exciting to observe that on a small scale the WT TacT3 was overexpressed in the presence of Pth, suggesting the strategy is promising. The WT TacT1 and TacT2 toxins were not successfully overexpressed in this trial.

In **Chapter 3** the minimum antitoxin peptide sequences necessary to inhibit the TacT functions were successfully synthesised using automated microwave SPPS. As a means to measure the TacTA PPI, the interaction between the minimum antitoxin peptides and their respective TacT proteins were characterised by DSF, FA and SPR assays. Each of the minimum antitoxin peptides bound to their respective TacT proteins and TacT3-**3** was found to have the highest affinity interaction. Additionally, the salt dependency in obtaining FA and SPR results suggest that electrostatic interactions are likely to play a large role in the interaction. Finally, a biphasic binding relationship was observed for TacT1 binding to its minimum antitoxin peptide. This relationship is also predicted to occur for TacT2 and TacT3 binding to their

antitoxins. The biphasic relationship corresponds to a predicted interaction of the toxin with two different peptides at each binding site.

Overall, these results demonstrate the strong affinity of the TacTA PPIs. The results also suggest that the interactions between each of the three TacT toxins to their TacA antitoxins are not identical. The affinities vary and the number of electrostatic interactions involved vary. Finally, they may not all have a biphasic interaction. Even if they all do have a biphasic interaction, some may depend on the second interaction for inhibition of toxin function and some may not. Future work developing a pan inhibitor for the three antitoxins will need to consider these biophysical differences as well as the *in vivo* functional similarities.

4.2. Future Directions

At the end of each chapter future developments of experiments carried out have been discussed. This included improving the experiment to achieve more robust data or other experiments that would reinforce the current data. In this short section future experiments are discussed with respect to the future direction of the project.

This project was originally undertaken for a PhD qualification with the aim to identify pan peptide inhibitors of the TacT toxin family, preventing the formation of persister cells in *S. Typhimurium* and *S. Enteritidis*. Due to personal circumstances the project was terminated early, and in this thesis just the initial characterisation of the structural and biochemical properties of the TacTA toxin-antitoxin binding were reported. There are many type II TA systems implicated in persister formation, targeting just one may result in upregulation of other toxins. A pan inhibitor is ideal to target multiple toxins, especially those with strong sequence identity. The aim was to discover inhibitors using RaPID (Random non-standard Peptide Integrated Discovery). RaPID is used to screen libraries of macrocyclic peptides and identify high affinity binders. An *in vitro* acetylation assay was designed to then measure the effect of high affinity binding compounds on toxin function and identify true inhibitors.

4.2.1. Random Non-Standard Peptide Integrated Discovery

The RaPID screening technology is ideal to identify potent inhibitors; extremely diverse libraries of $>10^{12}$ cyclic peptides can be synthesised for affinity screening of drug like molecules.[184] The RaPID technology allows for identifying highly selective inhibitors, but given the diversity of the libraries can likely also be adapted to find a pan inhibitor to target all multiple related toxins. RaPID uses an *in vitro* expression system coupled with mRNA display.[185] The use of ribozymes (RNA-based enzymes) in a process named Flexible *in vitro* Translation (FIT), allows the synthesis of macrocyclic peptides containing non-canonical residues.[186] The peptides can contain D-stereochemistry, N-alkyl, β- and α-disubstituted residues, all observed in secondary metabolites which are a rich source of drugs. Biotinylated active TacT proteins have been shown to be in production in **Chapter 2**. Using RaPID, the TacT proteins can be screened for affinity towards compounds in the RaPID libraries to find a pan

inhibitor. Peptide hits from the screen are then characterised and the effect on functional activity of the toxins following peptide binding is then assessed.

4.2.2. *In Vitro* Fluorescence Acetylation Activity Assay

Currently in the literature all well-developed assays to measure the acetyltransferase activity of the TacT toxins or related type II GNAT toxin involve radioactive signalling. This is not ideal as it generally carries safety issues. An *in vitro*, fast and high-throughput fluorescence assay to measure the activity of WT TacT1-3 was therefore designed. This would be an excellent tool to measure the change in activity of the TacTs upon binding to the minimum antitoxin peptides. This could be used alongside alanine scanning mutations or experiments with two separate antitoxin peptides that were discussed in the conclusion of **Chapter 3**. It could subsequently be used to measure the effect of high affinity binding compounds, identified by RaPID, on toxin function and identify true inhibitors.

The principle of the assay is the determination of the Ac-CoA concentration by a commercially acquired kit for a coupled enzyme assay, which results in a fluorometric (λex = 535/λem = 587 nm) product, proportional to the concentration of Ac-CoA present. This assay can be set up to determine Ac-CoA in either the nanomole or picomole range. As explained in **Chapter 1**, Ac-CoA is used by the TacT proteins to transfer an acetyl group to aminoacyl tRNAs. Measuring the concentration of Ac-CoA following incubation of aminoacyl tRNAs, a TacT toxin and a known concentration of Ac-CoA indicates the activity of the TacT toxin.

The assay would involve a number of steps. Firstly, commercially acquired tRNAs would be aminoacylated using tRNA synthetase directly before use in the assay. Next, the aminoacyl tRNAs would be incubated with a defined concentration of Ac-CoA and TacT (with or without antitoxin peptides or inhibitors). After a short time (10 min) the reaction is quenched. The reaction mixture is then added to the assay kit components. The fluorescence is measured and the amount of Ac-CoA remaining in solution is calculated and compared to the starting concentration. The toxin alone will use a high concentration of the Ac-CoA in the solution, it will transfer the acetyl group from Ac-CoA to aminoacyl tRNAs. The result would therefore be a low final fluorescence signal. The presence of the antitoxin or a true inhibitor will prevent the activity of the toxin and the use of Ac-CoA. A higher concentration of Ac-CoA in solution will present with a quantifiably higher fluorescence signal.

Chapter 5

Biological Methods

5.1. Plasmid Construction

General: *Escherichia coli* calcium competent DH5α cells were used for cloning. Plasmids were purified using the Thermo Scientific GeneJET Plasmid Miniprep Kit. All primers were synthesised by New England Biolabs and have been listed in Table S.1. Sanger sequencing was carried out by Genewiz (UK).

The DNA coding for *Salmonella Typhimurium* TacT1^{Y140F}, TacT2^{Y137F} and TacT3^{Y143F} were previously cloned into pQlinkH bacterial expression vector to encode the N-terminal $(His)_7$ fusion proteins.[58] This DNA coding for *S.Typhimurium* TacT1^{Y140F}, TacT2^{Y137F} and TacT3 ^{Y143F} were each inserted into the pQE80LC bicistronic vector using NEBuilder HiFi DNA Assembly Master Mix (New England Biolabs). The gene sequences were verified by sequencing of the entire coding region for each protein by using pQE65 and pQE276 primers.

Missense mutations of *S.Typhimurium* TacT1^{Y140F}, TacT2^{Y137F} and TacT3 ^{Y143F} back to the wild-type gene were introduced using PCR site directed mutagenesis. Firstly, non-overlapping forward and reverse primers were designed for each mutation. Then each plasmid and its respective primers were added to the reaction mix with KOD Hot Start DNA Polymerase (Sigma-Aldrich) according to the standard reaction setup provided by the manufacturer. The cycling conditions for the reaction were setup according to the protocol provided by the manufacturer. The linear products of the PCR reaction were analysed with samples run for 1 hr on a 1% agarose gel. Then, to phosphorylate and ligate the linear product and degrade the template DNA, KLD enzyme mix (New England Biolabs) was added to the PCR product according to the manufacturers protocol. Mutations were confirmed by sequencing the entire coding region for each mutant by using pQE65 and pQE276 primers.

5.2. Mutant Protein Expression

1 µL of the desired plasmid for expression of the N-terminal $(His)_7$ fusion TacT1-3 YF mutant proteins (50–100 ng/µL) was added to 50 µL of chemically competent *Escherichia coli* BL21 cells. Cells were incubated on ice (5 min), then incubated at 42 °C (40 sec) and finally returned to ice (2 min). 600 µL of Luria-Bertani (LB) media was added, followed by incubation at 37 °C (45 min). 100 µL of the cell suspension was spread over an LB agar plate containing 100 µg/mL of ampicillin and 0.5% (v/v) glucose. Successfully transformed cells were selected from the observed colonies. The cells were used to inoculate a preculture of 10 mL LB media (100 µg/mL ampicillin, 0.5% (v/v) glucose, 2 mM $MgSO_4$, trace metals 1X). To increase protein production the precultures were transferred to 2 L growth flasks after 24 hours and induced

by growth in 1 L liquid auto-induction medium supplemented with 400 µg/ml ampicillin at 37 °C for 24 hours using the lac expression system.[187] Cells were harvested by centrifugation at 4200 x g (25 min at 4 °C) in a Sorvall LYNX 4000 superspeed centrifuge (ThermoFisher Scientific) with a Fiberlite™ F12-6 x 500 LEX Fixed Angle Rotor (ThermoFisher Scientific).

5.3. Mutant Protein Purification

Cell pellets were resuspended in lysis buffer (50 mM Tris pH 7.5, 500 mM NaCl, 1 mM PMSF) with the addition of cOmplete™ mini EDTA-free protease inhibitor cocktail (Roche, 1 tablet per 50 mL of lysate), DNase I (Sigma-Aldrich, 3 U/mL) and $MgCl_2$ (5 mM). The mixture was incubated for 30 min (4 °C with agitation), then lysed by three passes at 25 kpsi through a cell disruptor (Constant Systems). The soluble fraction of the lysate was collected by centrifugation at 17000 rpm (45 min, 4 °C) in Sorvall LYNX 4000 superspeed centrifuge (ThermoFisher Scientific) with a Fiberlite™ F21-8 x 50y fixed-angle rotor attached (ThermoFisher Scientific). Clarified lysate was made up to 20 mM imidazole and incubated with 1 mL Ni-NTA agarose (Quiagen) overnight at 4 °C with agitation. The mixture was applied to a polypropylene column (1 mL, Qiagen) and washed with 10 column volumes (CV) of wash buffer (50mM Tris pH 7.5, 500 mM NaCl, 20 mM imidazole) and the protein eluted in 10 CV of elution buffer (50mM Tris pH 7.5, 500 mM NaCl, 500 mM imidazole). Fractions containing the target protein were pooled and dialysed (3.5 K MWCO SnakeSkin™ Dialysis Tubing (ThermoFisher Scientific)) against dialysis buffer (50 mM Tris pH 7.5, 500 mM NaCl, 10 mM β-ME) overnight at 4 °C, then concentrated using 3 kDa MWCO centricon (Amicon® Ultra-15) at 4000 rpm, 4 °C. Using an ÄKTA pure (GE Healthcare) protein purification system the pooled fractions were subjected to size exclusion column chromatography using HiLoad Superdex-75 16/600 column (GE Healthcare) equilibrated with (50 mM Tris pH 7.5, 500 mM NaCl, 10 mM β-ME). Expression and purification of the proteins was analysed by SDS-PAGE with samples run for 55 min on a 12% SDS-PAGE gel. Protein concentration was measured spectrophotometrically using a NanoDrop™ One/OneC Microvolume UV-Vis Spectrophotometer (ThermoFisher Scientific) using an extinction coefficient calculated by ExPASy,[188] then flash-frozen with liquid nitrogen in aliquots, and stored at -80 °C.

5.4. Pth Expression Trials

A microcentrifuge tube containing BL21-AI™ One Shot™ chemically competent *E. coli* cells (ThermoFisher Scientific) was kept on ice (20 min), followed by the addition of 1 µL of the pBAD-33 plasmid for expression of Pth at 50–100 ng/µL. After 10 minutes in ice, the cells were incubated in a 42 °C water bath (45 sec), then returned to ice (5 min). The microcentrifuge tube was removed from ice and 450 µL of SOC medium (ThermoFisher Scientific) was added, followed by an incubation at 37 °C (45 min). After this period, 100 µL of this cell suspension was spread over a LB agar plate (40 µg/mL of chloramphenicol, +/- 0.1% (v/v) glucose) and left to grow overnight at 37 °C.

The cells were used for two purposes. Firstly, a preculture of 5 mL LB media (40 µg/mL of chloramphenicol) in a 15 mL conical tube was inoculated with one colony and left shaking overnight at 37 °C. The following morning 1 mL of each preculture was added to two 50 mL conical tubes (labelled A and B) containing 10mL of LB media (40 µg/mL of chloramphenicol). Culture A was supplied with 0.2% (w/v) arabinose. The cultures were grown at 37 °C until the optical density of the bacterial culture at 600 nm (OD_{600}) reached 0.4. At this stage culture B was supplied with 0.2% (w/v) of arabinose. The cultures were grown at 37 °C for a further 24 hours. Expression of the protein was analysed by SDS-PAGE with samples run for 55 min on a 12% SDS-PAGE gel. The same experiment was carried out using TB (terrific broth) media.

Secondly these cells were made chemically competent again using the following procedure: colonies from the transformation were used to inoculate 10 mL of TB media (40 µg/mL of chloramphenicol). After shaking overnight at 37 °C the resulting high-density culture was transferred to a 2 L conical flask containing 1 L of TB medium (40 µg/mL of chloramphenicol). The flask was left shaking at 37 °C OD_{600} reached 0.35–0.40. At this stage the cells were chilled on ice (30 min) and harvested by centrifugation at 3000 x *g* (30 min, 4 °C). The pellet was gently resuspended in 100 mL of an ice-cold solution of 0.1 M $MgCl_2$ and the cells were harvested by centrifugation at 2000 x *g* (15 mi, 4 °C). The pellet was gently resuspended in 200 mL an ice-cold solution of 0.1 M $CaCl_2$ and kept in ice (20 min). After this period the cells were harvested by centrifugation at 2000 x *g* (15 min, 4 °C) and the pellet was gently resuspended in 50 mL of an ice-cold solution of 15% glycerol and 0.085 M $CaCl_2$. The cells were harvested by centrifugation at 1000 x *g* (15 min at 4 °C) and the pellet was gently resuspended in 50 mL of an ice-cold solution of 15% glycerol and 0.085 M $CaCl_2$. This suspension of chemically competent cells was, flash frozen with liquid nitrogen, in 0.5 mL microcentrifuge tubes as 50 µL aliquots, and stored at -80 °C.

5.5. Toxic Protein Expression Trials

Newly chemically competent BL21-AI *E. coli* cells containing pBAD33 Pth were transformed with the following set of plasmids using standard protocols, generating in total three transformants: 1) pBAD33 Pth + pQE80LC TacT1; 2) pBAD33 Pth + pQE80LC TacT2; 3) pBAD33 Pth + pQE80LC TacT3. Successfully transformed cells were used to inoculate two 15 mL conical flasks (labelled A and B) containing 5 mL of LB media (with 40 µg/mL of chloramphenicol and 100 µg/mL ampicillin). Culture B was supplied with 0.4% w/v glucose. The cultures were grown shaking overnight at 37 °C. The following morning, for each transformant, two 50 mL conical flasks (labelled 1 and 2) containing 5 mL of LB (with 40 µg/mL of chloramphenicol, 100 µg/mL ampicillin, +/- 0.4% w/v glucose) were inoculated with 0.25 mL of the overnight culture. In all cases flasks were supplied with 0.2% (w/v) of L-arabinose and all flasks were left shaking at 37 °C. Growth was monitored and once the bacterial cultures in conical tubes labelled 2 reached OD_{600} of 0.6–0.8, IPTG was added to a final concentration of 0.5 mM. Aliquots at this time point were collected and lysed for SDS-PAGE following standard

protocols. Growth was continued for a further 12 h, where a final aliquot was collected for SDS-PAGE. The same experiment was carried out replacing LB media with TB media.

Chapter 6

Synthetic Methods

6.1. General Methods

Solid phase peptide synthesis (SPPS) was carried out using a Liberty Blue HT12™ Automated Microwave Peptide Synthesizer (CEM). 9-fluorenylmethoxycarbonyl (Fmoc)-protected amino acids were purchased from AGCT Bioproducts, CEM and Fluorochem. Preloaded Wang resins and Fmoc-Rink Amide MBHA resin were purchased from Advanced Chemtech and Novabiochem, respectively, and DIC was from Fluorochem. Piperidine, acetic anhydride, 2,2'-(ethylenedioxy)diethanethiol (DODT) and triisopropyl silane (TIS) were from Sigma-Aldrich. Oxyma Pure was obtained from CEM. ACN, DMF and diethyl ether were purchased from VWR and DCM and TFA were obtained from Fisher Scientific UK. Peptide purification using LC-MS was carried out using a Waters RP-HPLC system containing: a Waters 2767 auto-sampler; a Waters 515 HPLC pump; a Waters 2998 photodiode array detector; a Waters 3100 mass detector and a preparative reversed-phase XB-C18 column. A flow rate of 20 mL/min was used with different gradients of eluent A (0.1% (v/v) formic acid (FA) in water) and eluent B (0.1% (v/v) FA in ACN). LC-MS analysis of the purity and identity of the peptides was carried out with the same system using an analytical reversed-phase XB-C18 column (100 mm × 4.6 mm, 5 µm, 100 Å, 1.2 mL/min) and a linear gradient of 20% to 98% eluent B in eluent A over 10 min. Chromatograms were recorded at λ = 220 nm and the masses of the products were detected in the range from 400-2000 m/z. The identity of the pure peptides were additionally confirmed by MALDI-ToF mass spectrometry (Micromass, Waters). Peptide product solutions where dried by lyophilisation on an Alpha 2-4 LD plus Freeze dryer (Christ Freeze Dryers).

6.2. Solid Phase Peptide Synthesis

Minimum TacA1-3 antitoxin peptides (TacA1: 52-88; TacA2: 54-97; TacA3: 58-93) referred to as 1, 2 and 3 respectively were synthesised using the high-swelling protocol of the Liberty Blue. Derivatives used were 9-fluorenylmethoxycarbonyl/tert-Butyl (Fmoc/tBu) protected amino acids. Fmoc-Rink Amide MBHA resin (50 µmol scale, peptides 1 and 3) was used to obtain peptides as C-terminal amides and Fmoc-Lys Wang resin (50 µmol scale, peptide 2) was used to obtain the peptide as a C-terminal acid. For automated SPPS, the resin was first

swelled with DMF, then deprotected with the addition of 10% piperidine, 0.1 M Oxyma in DMF. Amino acid coupling was carried out with 5-fold molar excess of amino acid (250 µmol, 0.2 M), 10 eq. DIC (500 µmol, 0.5 M) and 5 eq. Oxyma (250 µmol, 0.2 M) in DMF for 2 min (single coupling) or 4 min (double coupling) at 90 °C. Single couplings carried out for each amino acid, with the exception of: all amino acids after 20 residues; **1**: residues R and VIE; **2**: residues RI and **3**: residues EKL and NDL which were double coupled. The N-terminus was Fmoc deprotected as the last step with the addition of 10% (v/v) piperidine, 0.1 M Oxyma in DMF for 1.5 min at 90 °C. After completion of automated synthesis, the resin was split in half by weight. To one half manual N-terminal acetyl capping was carried out with 5% (v/v) acetic anhydride in DMF (3 mL) for 3 x 15 min at RT with agitation. To the second half N-terminal 5(6)-TAMRA coupling was carried out with 2 eq. 5(6)-TAMRA (50 µmol, 21.5 mg), 2 eq. HBTU (50 µmol, 18.95 mg) and 2 eq. DIPEA (50 µmol, 8.75 µL) in DMF (0.6 mL) overnight at RT with agitation. The resins were washed with DMF (5x) and DCM (5x), shortly dried on the vacuum pump and stored at 4 °C. Cleavage of peptide from resin and side chain deprotection was carried out with addition (TFA 92.5% (v/v), H_2O 2.5% (v/v), TIS 2.5% (v/v), DODT 2.5% (v/v), 3 mL) for 30 min at 40 °C in the CEM Razor rapid peptide cleavage system. The solution was evaporated to a third of the final volume under a stream of N_2 followed by precipitation of the crude peptide by addition of ice-cold diethyl ether (10 eq.). The precipitate was then isolated by centrifugation and washed with additional ice-cold diethyl ether. Peptides were dissolved in 20-50% ACN with 0.5% TFA and lyophilised to give solid powders of crude peptides.

6.3. Peptide Purification

Each peptide was dissolved in ACN 25% (v/v) with TFA 0.01% (v/v) and filtered followed by separation using preparatory LC-MS, mass-directed fraction collection was used to isolate the desired products. Fractions containing the pure peptide were combined and dried by lyophilisation to give solid white (**1**, **2** and **3**) or purple powder (**TAMRA_1**, **TAMRA_2** and **TAMRA_3**). The observed masses were in agreement with the calculated masses and a purity of > 90% was obtained for all compounds by LC-MS analysis.

Chapter 7

Biophysical Methods

7.1. Differential Scanning Fluorimetry

Experiments were performed in a Mx3005P qPCR System (Agilent) collecting fluorescence data with a temperature ramp of 25 °C to 95 °C. Samples were prepared in buffer T (10 mM HEPES (pH 7.8), 500 mM NaCl). The SYPRO® Orange dye (Sigma-Aldrich, 5000X stock in DMSO) was used to monitor protein denaturation and was diluted to a final concentration of 5X. For the binding experiments the final concentration of the TacT proteins and minimum antitoxin peptides were 5 µM. Every condition was performed in triplicate and the melting curves were plotted using GraphPad Prism 5 (GraphPad Software, USA). The melting temperatures were obtained by fitting the sigmoidal section of the curves to a Boltzmann sigmoid function.

7.2. Surface Plasmon Resonance

Experiments were performed using a Biacore S200 (GE Healthcare) equipped with a Series S sensor chip NTA (GE healthcare). The data was analysed using the Biacore Evaluation Software (GE Healthcare) and curves were plotted using GraphPad Prism 5 (GraphPad Software, USA). All experiments were performed at 22 °C with one of the following running buffers: buffer A (10 mM HEPES (pH 8.0), 500 mM NaCl, 50 µM EDTA and 0.005% (v/v) TWEEN® 20), buffer B (10 mM HEPES (pH 8.0), 250 mM NaCl, 50 µM EDTA and 0.005% (v/v) TWEEN® 20) or buffer C (10 mM HEPES (pH 8.0), 750 mM NaCl, 50 µM EDTA and 0.005% (v/v) TWEEN® 20). The surface was conditioned following the standard manufacturer's guidelines. The $(His)_7$-TacT1-3 proteins (20.9 kDa, 20.9 kDa and 22.2 kDa respectively) were immobilised using Ni-NTA affinity capturing. Surface regeneration was performed with a one-minute pulse of 0.5 M imidazole followed by a one-minute pulse of 0.35 M of EDTA at pH 8.0. The proteins in running buffer A, B or C at a concentration of 100 nM were immobilised with a 30–60 second pulse (flow rate of 5 µL/min) on flow cell 2 and flow cell 1 was left blank as a reference surface. Binding of 1 (4.4 kDa) to TacT1 was measured using MCK. 1 was injected with a flow rate of 30 µL/min over the two flow cells at six increasing concentrations. The complex was allowed to associate and fully dissociate for 80 sec and 3 min, respectively. Binding of 2 (5.2 kDa) and 3 (4.1 kDa) to TacT2 and TacT3 respectively was measured using SCK. In the SCK experiments, 2 or 3 were injected with a flow rate of 30 µL/min over the two flow cells with 6-8 concentrations with 80 sec association. The surface was fully regenerated in between measurements for each protein. In both setups the double-referenced sensorgrams (raw data subtracted from a blank injection and reference surface responses) were fit to a simple kinetic 1:1 binding model.

7.3. Fluorescence Anisotropy

Measurements were conducted using an EnVision® multimode microplate reader using a low-volume TAMRA FA protocol. The excitation wavelength was set to 485 nm (with attenuated excitation filter) and emission was detected at 520 nm. For each independent experiment, the gain of the parallel and perpendicular channel was calibrated for the whole plate (using the wells with the highest TAMRA-peptide concentration) so that 0.6-1.25 nM of peptide had a polarization value of ~27 mP. A flash number of 100 was used for each well. The tracer peptide was used at 1 nM and 5 nM and the data measured for a 50% dilution series of protein between 5 µM – 0.075 µM. The final volume per well in the 384-well plate format was 15 µL and the plate was incubated in the dark (20 min, RT, with agitation) prior to imaging. Protein background of both channels was subtracted from each replicate measurement of protein and TAMRA-peptide. The polarimetry values were converted to anisotropy (A) for each well using the background-corrected channel values: A = (S–(G*P))/(S+(2*G*P)) with S = S-channel, P = P-channel and G = instrument correction factor.[189] Anisotropy (y-axis) was then plotted against logarithmic TacT concentration (x-axis) using GraphPad Prism 5 (GraphPad Software, USA). The EC_{50} (K_D) values were obtained fitting the curves to a sigmoidal or biphasic dose-response curve.

References

1. World, H. O. *Global action plan on antimicrobial resistance;* World Health Organization: Geneva, 2015; .

2. Brown, E. D.; Wright, G. D. Antibacterial drug discovery in the resistance era. *Nature* **2016***, 529*, 336-343.

3. Balaban, N. Q.; Gerdes, K.; Lewis, K.; McKinney, J. D. A problem of persistence: still more questions than answers? *Nat. Rev. Microbiol.* **2013***, 11*, 587-591.

4. Harms, A.; Maisonneuve, E.; Gerdes, K. Mechanisms of bacterial persistence during stress and antibiotic exposure. *Science* **2016***, 354*, 10.1126/science.aaf4268.

5. Gollan, B.; Grabe, G.; Michaux, C.; Helaine, S. Bacterial Persisters and Infection: Past, Present, and Progressing. *Annu. Rev. Microbiol.* **2019***, 73*, 359-385.

6. Balaban, N. Q.; Helaine, S.; Lewis, K.; Ackermann, M.; Aldridge, B.; Andersson, D. I.; Brynildsen, M. P.; Bumann, D.; Camilli, A.; Collins, J. J.; Dehio, C.; Fortune, S.; Ghigo, J.; Hardt, W.; Harms, A.; Heinemann, M.; Hung, D. T.; Jenal, U.; Levin, B. R.; Michiels, J.; Storz, G.; Tan, M.; Tenson, T.; Van Melderen, L.; Zinkernagel, A. Definitions and guidelines for research on antibiotic persistence. *Nat. Rev. Microbiol* **2019***, 17*, 441-448.

7. Fisher, R. A.; Gollan, B.; Helaine, S. Persistent bacterial infections and persister cells. *Nat. Rev. Microbiol* **2017***, 15*, 453-464.

8. Brauner, A.; Fridman, O.; Gefen, O.; Balaban, N. Q. Distinguishing between resistance, tolerance and persistence to antibiotic treatment. *Nat. Rev. Microbiol.* **2016***, 14*, 320-330.

9. Claudi, B.; Spröte, P.; Chirkova, A.; Personnic, N.; Zankl, J.; Schürmann, N.; Schmidt, A.; Bumann, D. Phenotypic Variation of *Salmonella* in Host Tissues Delays Eradication by Antimicrobial Chemotherapy. *Cell* **2014***, 158*, 722-733.

10. Windels, E. M.; Michiels, J. E.; Fauvart, M.; Wenseleers, T.; Van den Bergh, B.; Michiels, J. Bacterial persistence promotes the evolution of antibiotic resistance by increasing survival and mutation rates. *ISME J* **2019***, 13*, 1239-1251.

11. Gaca, A. O.; Colomer-Winter, C.; Lemos, J. A. Many means to a common end: the intricacies of (p)ppGpp metabolism and its control of bacterial homeostasis. *J. Bacteriol.* **2015***, 197*, 1146-1156.

12. Corrigan, R. M.; Bellows, L. E.; Wood, A.; Gründling, A. ppGpp negatively impacts ribosome assembly affecting growth and antimicrobial tolerance in Gram-positive bacteria. *Proc. Natl. Acad. Sci. U. S. A.* **2016***, 113*, 1710.

13. Trastoy, R.; Manso, T.; Fernández-García, L.; Blasco, L.; Ambroa, A.; Pérez Del Molino, M. L.; Bou, G.; García-Contreras, R.; Wood, T. K.; Tomás, M. Mechanisms of Bacterial Tolerance and Persistence in the Gastrointestinal and Respiratory Environments. *Clin. Microbiol. Rev.* **2018***, 31*, 23.

14. Stewart, P. S.; Franklin, M. J.; Williamson, K. S.; Folsom, J. P.; Boegli, L.; James, G. A. Contribution of Stress Responses to Antibiotic Tolerance in Pseudomonas aeruginosa Biofilms. *Antimicrob. Agents Chemother.* **2015***, 59*, 3838-3847.

15. Battesti, A.; Majdalani, N.; Gottesman, S. The RpoS-Mediated General Stress Response in Escherichia coli. *Annu. Rev. Microbiol.* **2011***, 65*, 189-213.

16. Harms, A.; Maisonneuve, E.; Gerdes, K. Mechanisms of bacterial persistence during stress and antibiotic exposure. *Science* **2016***, 354*, aaf4268.

17. Ronneau, S.; Helaine, S. Clarifying the Link between Toxin-Antitoxin Modules and Bacterial Persistence. *J. Mol. Biol.* **2019***, 431*, 3462-3471.

18. Page, R.; Peti, W. Toxin-antitoxin systems in bacterial growth arrest and persistence. *Nat. Chem. Biol.* **2016***, 12*, 208-214.

19. Pandey, D. P.; Gerdes, K. Toxin-antitoxin loci are highly abundant in free-living but lost from host-associated prokaryotes. *Nucleic Acids Res.* **2005***, 33*, 966-976.

20. Lobato-Márquez, D.; Díaz-Orejas, R.; García-del Portillo, F. Toxin-antitoxins and bacterial virulence. *FEMS Microbiol. Rev.* **2016***, 40*, 592-609.

21. Srivastava, A.; Pati, S.; Kaushik, H.; Singh, S.; Garg, L. C. Toxin-antitoxin systems and their medical applications: current status and future perspective. *Appl. Microbiol. Biotechnol.* **2021***, 105*, 1803-1821.

22. Song, S.; Wood, T. K. Toxin/Antitoxin System Paradigms: Toxins Bound to Antitoxins Are Not Likely Activated by Preferential Antitoxin Degradation. *Adv. Biosys.* **2020***, 4*, 1900290.

23. Gerdes, K.; Wagner, E. G. H. RNA antitoxins. *Curr. Opin. Microbiol.* **2007***, 10*, 117-124.

24. Fozo, E. M.; Hemm, M. R.; Storz, G. Small toxic proteins and the antisense RNAs that repress them. *Microbiol. Mol. Biol. Rev.* **2008***, 72*, 579-89, Table of Contents.

25. Gerdes, K.; Bech, F. W.; Jørgensen, S. T.; Løbner-Olesen, A.; Rasmussen, P. B.; Atlung, T.; Boe, L.; Karlstrom, O.; Molin, S.; von Meyenburg, K. Mechanism of postsegregational killing by the hok gene product of the parB system of plasmid R1 and its homology with the relF gene product of the E. coli relB operon. *EMBO J.* **1986***, 5*, 2023-2029.

26. Fineran, P. C.; Blower, T. R.; Foulds, I. J.; Humphreys, D. P.; Lilley, K. S.; Salmond, G. P. The phage abortive infection system, ToxIN, functions as a protein-RNA toxin-antitoxin pair. *Proc. Natl. Acad. Sci. U. S. A.* **2009***, 106*, 894-899.

27. Hayes, F. Toxins-Antitoxins: Plasmid Maintenance, Programmed Cell Death, and Cell Cycle Arrest. *Science* **2003***, 301*, 1496-1499.

28. Leplae, R.; Geeraerts, D.; Hallez, R.; Guglielmini, J.; Drèze, P.; Van Melderen, L. Diversity of bacterial type II toxin-antitoxin systems: a comprehensive search and functional analysis of novel families. *Nucleic Acids Res.* **2011***, 39*, 5513-5525.

29. Masuda, H.; Tan, Q.; Awano, N.; Wu, K.; Inouye, M. YeeU enhances the bundling of cytoskeletal polymers of MreB and FtsZ, antagonizing the CbtA (YeeV) toxicity in Escherichia coli. *Mol. Microbiol.* **2012***, 84*, 979-989.

30. Aakre, C. D.; Phung, T. N.; Huang, D.; Laub, M. T. A Bacterial Toxin Inhibits DNA Replication Elongation through a Direct Interaction with the β Sliding Clamp. *Mol. Cell* **2013***, 52*, 617-628.

31. Wang, X.; Lord, D. M.; Cheng, H. Y.; Osbourne, D. O.; Hong, S. H.; Sanchez-Torres, V.; Quiroga, C.; Zheng, K.; Herrmann, T.; Peti, W.; Benedik, M. J.; Page, R.; Wood, T. K. A new type V toxin-antitoxin system where mRNA for toxin GhoT is cleaved by antitoxin GhoS. *Nat. Chem. Biol.* **2012***, 8*, 855-861.

32. Marimon, O.; Teixeira, J. M.; Cordeiro, T. N.; Soo, V. W.; Wood, T. L.; Mayzel, M.; Amata, I.; García, J.; Morera, A.; Gay, M.; Vilaseca, M.; Orekhov, V. Y.; Wood, T. K.; Pons, M. An oxygen-sensitive toxin-antitoxin system. *Nat. Commun.* **2016***, 7*, 13634.

33. Unterholzner, S. J.; Poppenberger, B.; Rozhon, W. Toxin–antitoxin systems. *Mob. Genet. Elements* **2013***, 3*, e26219.

34. Paul, P.; Sahu, B. R.; Suar, M. Plausible role of bacterial toxin–antitoxin system in persister cell formation and elimination. *Mol. Oral Microbiol.* **2019***, 34*, 97-107.

35. Korch, S. B.; Henderson, T. A.; Hill, T. M. Characterization of the hipA7 allele of Escherichia coli and evidence that high persistence is governed by (p)ppGpp synthesis. *Mol. Microbiol.* **2003***, 50*, 1199-1213.

36. Helaine, S.; Cheverton, A. M.; Watson, K. G.; Faure, L. M.; Matthews, S. A.; Holden, D. W. Internalization of Salmonella by macrophages induces formation of nonreplicating persisters. *Science* **2014***, 343*, 204-208.

37. Moyed, H. S.; Bertrand, K. P. hipA, a newly recognized gene of Escherichia coli K-12 that affects frequency of persistence after inhibition of murein synthesis. *J. Bacteriol.* **1983***, 155*, 768-775.

38. Shah, D.; Zhang, Z.; Khodursky, A. B.; Kaldalu, N.; Kurg, K.; Lewis, K. Persisters: a distinct physiological state of E. coli. *BMC Microbiol.* **2006***, 6*, 53.

39. Maisonneuve, E.; Shakespeare, L. J.; Jørgensen, M. G.; Gerdes, K. Bacterial persistence by RNA endonucleases. *Proc. Natl. Acad. Sci. U. S. A.* **2011***, 108*, 13206-13211.

40. Muthuramalingam, M.; White, J. C.; Bourne, C. R. Toxin-Antitoxin Modules Are Pliable Switches Activated by Multiple Protease Pathways. *Toxins (Basel)* **2016***, 8*, 10.3390/toxins8070214.

41. Verstraeten, N.; Knapen, W. J.; Kint, C. I.; Liebens, V.; Van den Bergh, B.; Dewachter, L.; Michiels, J. E.; Fu, Q.; David, C. C.; Fierro, A. C.; Marchal, K.; Beirlant, J.; Versées, W.; Hofkens, J.; Jansen, M.; Fauvart, M.; Michiels, J. Obg and Membrane Depolarization Are Part of a Microbial Bet-Hedging Strategy that Leads to Antibiotic Tolerance. *Mol. Cell* **2015***, 59*, 9-21.

42. Maisonneuve, E.; Castro-Camargo, M.; Gerdes, K. (p)ppGpp controls bacterial persistence by stochastic induction of toxin-antitoxin activity. *Cell* **2013***, 154*, 1140-1150.

43. Traxler, M. F.; Summers, S. M.; Nguyen, H.; Zacharia, V. M.; Hightower, G. A.; Smith, J. T.; Conway, T. The global, ppGpp-mediated stringent response to amino acid starvation in Escherichia coli. *Mol. Microbiol.* **2008***, 68*, 1128-1148.

44. Germain, E.; Castro-Roa, D.; Zenkin, N.; Gerdes, K. Molecular Mechanism of Bacterial Persistence by HipA. *Mol. Cell* **2013***, 52*, 248-254.

45. Neubauer, C.; Gao, Y. G.; Andersen, K. R.; Dunham, C. M.; Kelley, A. C.; Hentschel, J.; Gerdes, K.; Ramakrishnan, V.; Brodersen, D. E. The structural basis for mRNA recognition and cleavage by the ribosome-dependent endonuclease RelE. *Cell* **2009***, 139*, 1084-1095.

46. Cook, G. M.; Robson, J. R.; Frampton, R. A.; McKenzie, J.; Przybilski, R.; Fineran, P. C.; Arcus, V. L. Ribonucleases in bacterial toxin–antitoxin systems. *Biochim. Biophys. Acta - Gene Regul. Mech.* **2013***, 1829*, 523-531.

47. Lee, I.; Lee, S. J.; Chae, S.; Lee, K.; Kim, J.; Lee, B. Structural and functional studies of the Mycobacterium tuberculosis VapBC30 toxin-antitoxin system: implications for the design of novel antimicrobial peptides. *Nucleic Acids Res.* **2015***, 43*, 7624-7637.

48. Jørgensen, M. G.; Pandey, D. P.; Jaskolska, M.; Gerdes, K. HicA of *Escherichia coli* Defines a Novel Family of Translation-Independent mRNA Interferases in Bacteria and Archaea. *J. Bacteriol.* **2009***, 191*, 1191-1199.

49. Yeo, C. C. GNAT toxins of bacterial toxin–antitoxin systems: acetylation of charged tRNAs to inhibit translation. *Mol. Microbiol.* **2018***, 108*, 331-335.

50. Jurenas, D.; Garcia-Pino, A.; Van Melderen, L. Novel toxins from type II toxin-antitoxin systems with acetyltransferase activity. *Plasmid* **2017***, 93*, 30-35.

51. Wilcox, B.; Osterman, I.; Serebryakova, M.; Lukyanov, D.; Komarova, E.; Gollan, B.; Morozova, N.; Wolf, Y. I.; Makarova, K. S.; Helaine, S.; Sergiev, P.; Dubiley, S.; Borukhov, S.; Severinov, K. Escherichia coli ItaT is a type II toxin that inhibits translation by acetylating isoleucyl-tRNAIle. *Nucleic Acids Res.* **2018***, 46*, 7873-7885.

52. Yashiro, Y.; Yamashita, S.; Tomita, K. Crystal Structure of the Enterohemorrhagic Escherichia coli AtaT-AtaR Toxin-Antitoxin Complex. *Structure* **2019***, 27*, 476-484.e3.

53. Jurenas, D.; Chatterjee, S.; Konijnenberg, A.; Sobott, F.; Droogmans, L.; Garcia-Pino, A.; Van Melderen, L. AtaT blocks translation initiation by N-acetylation of the initiator tRNA(fMet). *Nat. Chem. Biol.* **2017***, 13*, 640-646.

54. McVicker, G.; Tang, C. M. Deletion of toxin–antitoxin systems in the evolution of Shigella sonnei as a host-adapted pathogen. *Nat. Microbiol.* **2016***, 2*, 16204.

55. Qian, H.; Yu, H.; Li, P.; Zhu, E.; Yao, Q.; Tai, C.; Deng, Z.; Gerdes, K.; He, X.; Gan, J.; Ou, H. Toxin–antitoxin operon kacAT of Klebsiella pneumoniae is regulated by conditional cooperativity via a W-shaped KacA–KacT complex. *Nucleic Acids Res.* **2019***, 47*, 7690-7702.

56. Qian, H.; Yao, Q.; Tai, C.; Deng, Z.; Gan, J.; Ou, H. Y. Identification and characterization of acetyltransferase-type toxin-antitoxin locus in Klebsiella pneumoniae. *Mol. Microbiol.* **2018***, 108*, 336-349.

57. Cheverton, A. M.; Gollan, B.; Przydacz, M.; Wong, C. T.; Mylona, A.; Hare, S. A.; Helaine, S. A Salmonella Toxin Promotes Persister Formation through Acetylation of tRNA. *Mol. Cell* **2016***, 63*, 86-96.

58. Rycroft, J. A.; Gollan, B.; Grabe, G. J.; Hall, A.; Cheverton, A. M.; Larrouy-Maumus, G.; Hare, S. A.; Helaine, S. Activity of acetyltransferase toxins involved in Salmonella persister formation during macrophage infection. *Nat. Commun.* **2018***, 9*, 1993.

59. Okoro, C. K.; Kingsley, R. A.; Connor, T. R.; Harris, S. R.; Parry, C. M.; Al-Mashhadani, M.; Kariuki, S.; Msefula, C. L.; Gordon, M. A.; de Pinna, E.; Wain, J.; Heyderman, R. S.; Obaro, S.; Alonso, P. L.; Mandomando, I.; MacLennan, C. A.; Tapia, M. D.; Levine, M. M.; Tennant, S. M.; Parkhill, J.; Dougan, G. Intracontinental spread of human invasive Salmonella Typhimurium pathovariants in sub-Saharan Africa. *Nat. Genet.* **2012***, 44*, 1215-1221.

60. Stanaway, J. D.; Parisi, A.; Sarkar, K.; Blacker, B. F.; Reiner, R. C.; Hay, S. I.; Nixon, M. R.; Dolecek, C.; James, S. L.; Mokdad, A. H.; Abebe, G.; Ahmadian, E.; Alahdab, F.; Alemnew, B. T. T.; Alipour, V.; Allah Bakeshei, F.; Animut, M. D.; Ansari, F.; Arabloo, J.;

Asfaw, E. T.; Bagherzadeh, M.; Bassat, Q.; Belayneh, Y. M. M.; Carvalho, F.; Daryani, A.; Demeke, F. M.; Demis, A. B. B.; Dubey, M.; Duken, E. E.; Dunachie, S. J.; Eftekhari, A.; Fernandes, E.; Fouladi Fard, R.; Gedefaw, G. A.; Geta, B.; Gibney, K. B.; Hasanzadeh, A.; Hoang, C. L.; Kasaeian, A.; Khater, A.; Kidanemariam, Z. T.; Lakew, A. M.; Malekzadeh, R.; Melese, A.; Mengistu, D. T.; Mestrovic, T.; Miazgowski, B.; Mohammad, K. A.; Mohammadian, M.; Mohammadian-Hafshejani, A.; Nguyen, C. T.; Nguyen, L. H.; Nguyen, S. H.; Nirayo, Y. L.; Olagunju, A. T.; Olagunju, T. O.; Pourjafar, H.; Qorbani, M.; Rabiee, M.; Rabiee, N.; Rafay, A.; Rezapour, A.; Samy, A. M.; Sepanlou, S. G.; Shaikh, M. A.; Sharif, M.; Shigematsu, M.; Tessema, B.; Tran, B. X.; Ullah, I.; Yimer, E. M.; Zaidi, Z.; Murray, C. J. L.; Crump, J. A. The global burden of non-typhoidal salmonella invasive disease: a systematic analysis for the Global Burden of Disease Study 2017. *Lancet Infect. Dis.* **2019***, 19*, 1312-1324.

61. Okoro, C. K.; Kingsley, R. A.; Quail, M. A.; Kankwatira, A. M.; Feasey, N. A.; Parkhill, J.; Dougan, G.; Gordon, M. A. High-resolution single nucleotide polymorphism analysis distinguishes recrudescence and reinfection in recurrent invasive nontyphoidal Salmonella typhimurium disease. *Clin. Infect. Dis.* **2012***, 54*, 955-963.

62. Walling, L. R.; Butler, J. S. Toxins targeting transfer RNAs: Translation inhibition by bacterial toxin-antitoxin systems. *Wiley Interdiscip. Rev. RNA* **2019***, 10*, e1506.

63. Modell, A. E.; Blosser, S. L.; Arora, P. S. Systematic Targeting of Protein-Protein Interactions. *Trends Pharmacol. Sci.* **2016***, 37*, 702-713.

64. Gagarinova, A.; Phanse, S.; Cygler, M.; Babu, M. Insights from protein-protein interaction studies on bacterial pathogenesis. *Expert Rev. Proteom.* **2017***, 14*, 779-797.

65. Bogan, A. A.; Thorn, K. S. Anatomy of hot spots in protein interfaces: Edited by J. Wells. *J. Mol. Biol.* **1998***, 280*, 1-9.

66. Kahan, R.; Worm, D. J.; de Castro, G. V.; Ng, S.; Barnard, A. Modulators of protein–protein interactions as antimicrobial agents. *RSC Chem. Biol.* **2021***, 2*, 387-409.

67. Sheng, C.; Dong, G.; Miao, Z.; Zhang, W.; Wang, W. State-of-the-art strategies for targeting protein–protein interactions by small-molecule inhibitors. *Chem. Soc. Rev.* **2015***, 44*, 8238-8259.

68. Arkin, M.; Tang, Y.; Wells, J. Small-Molecule Inhibitors of Protein-Protein Interactions: Progressing toward the Reality. *Chem. Biol.* **2014***, 21*, 1102-1114.

69. Scott, D. E.; Bayly, A. R.; Abell, C.; Skidmore, J. Small molecules, big targets: drug discovery faces the protein-protein interaction challenge. *Nat. Rev. Drug Discov.* **2016***, 15*, 533-550.

70. Bruzzoni-Giovanelli, H.; Alezra, V.; Wolff, N.; Dong, C. Z.; Tuffery, P.; Rebollo, A. Interfering peptides targeting protein-protein interactions: the next generation of drugs? *Drug Discov. Today* **2018***, 23*, 272-285.

71. Cardote, T. A. F.; Ciulli, A. Cyclic and Macrocyclic Peptides as Chemical Tools To Recognise Protein Surfaces and Probe Protein–Protein Interactions. *ChemMedChem* **2016***, 11*, 787-794.

72. Akram, O. N.; DeGraff, D. J.; Sheehan, J. H.; Tilley, W. D.; Matusik, R. J.; Ahn, J.; Raj, G. V. Tailoring Peptidomimetics for Targeting Protein–Protein Interactions. *Mol. Cancer Res.* **2014***, 12*, 967-978.

73. Dougherty, P. G.; Qian, Z.; Pei, D. Macrocycles as protein–protein interaction inhibitors. *Biochem. J.* **2017***, 474*, 1109-1125.

74. Qian, Z.; Dougherty, P. G.; Pei, D. Targeting intracellular protein–protein interactions with cell-permeable cyclic peptides. *Cur. Opin. Chem. Biol.* **2017***, 38*, 80-86.

75. Carro, L. Protein-protein interactions in bacteria: a promising and challenging avenue towards the discovery of new antibiotics. *Beilstein J. Org. Chem.* **2018***, 14*, 2881-2896.

76. Lu, D.; Keck, J. L. Structural basis of *Escherichia coli* single-stranded DNA-binding protein stimulation of exonuclease I. *Proc. Natl. Acad. Sci. USA* **2008***, 105*, 9169-9174.

77. Lu, D.; Bernstein, D. A.; Satyshur, K. A.; Keck, J. L. Small-molecule tools for dissecting the roles of SSB/protein interactions in genome maintenance. *Proc. Natl. Acad. Sci. U. S. A.* **2010***, 107*, 633-638.

78. Chilingaryan, Z.; Headey, S. J.; Lo, A. T. Y.; Xu, Z.; Otting, G.; Dixon, N. E.; Scanlon, M. J.; Oakley, A. J. Fragment-Based Discovery of Inhibitors of the Bacterial DnaG-SSB Interaction. *Antibiotics (Basel, Switzerland)* **2018***, 7*, 14.

79. Wijffels, G.; Dalrymple, B. P.; Prosselkov, P.; Kongsuwan, K.; Epa, V. C.; Lilley, P. E.; Jergic, S.; Buchardt, J.; Brown, S. E.; Alewood, P. F.; Jennings, P. A.; Dixon, N. E. Inhibition of protein interactions with the beta 2 sliding clamp of Escherichia coli DNA polymerase III by peptides from beta 2-binding proteins. *Biochemistry* **2004***, 43*, 5661-5671.

80. Yin, Z.; Whittell, L. R.; Wang, Y.; Jergic, S.; Liu, M.; Harry, E. J.; Dixon, N. E.; Beck, J. L.; Kelso, M. J.; Oakley, A. J. Discovery of lead compounds targeting the bacterial sliding clamp using a fragment-based approach. *J. Med. Chem.* **2014***, 57*, 2799-2806.

81. Kling, A.; Lukat, P.; Almeida, D. V.; Bauer, A.; Fontaine, E.; Sordello, S.; Zaburannyi, N.; Herrmann, J.; Wenzel, S. C.; König, C.; Ammerman, N. C.; Barrio, M. B.; Borchers, K.; Bordon-Pallier, F.; Brönstrup, M.; Courtemanche, G.; Gerlitz, M.; Geslin, M.; Hammann, P.; Heinz, D. W.; Hoffmann, H.; Klieber, S.; Kohlmann, M.; Kurz, M.; Lair, C.; Matter, H.;

Nuermberger, E.; Tyagi, S.; Fraisse, L.; Grosset, J. H.; Lagrange, S.; Müller, R. Targeting DnaN for tuberculosis therapy using novel griselimycins. *Science* **2015***, 348*, 1106.

82. Georgescu, R. E.; Yurieva, O.; Kim, S.; Kuriyan, J.; Kong, X.; O'Donnell, M. Structure of a small-molecule inhibitor of a DNA polymerase sliding clamp. *Proc. Natl. Acad. Sci. USA* **2008***, 105*, 11116-11121.

83. Yin, Z.; Whittell, L. R.; Wang, Y.; Jergic, S.; Ma, C.; Lewis, P. J.; Dixon, N. E.; Beck, J. L.; Kelso, M. J.; Oakley, A. J. Bacterial Sliding Clamp Inhibitors that Mimic the Sequential Binding Mechanism of Endogenous Linear Motifs. *J. Med. Chem.* **2015***, 58*, 4693-4702.

84. Wolff, P.; Oliéric, V.; Briand, J. P.; Chaloin, O.; Dejaegere, A.; Dumas, P.; Ennifar, E.; Guichard, G.; Wagner, J.; Burnouf, D. Y. Structure-Based Design of Short Peptide Ligands Binding onto the E. coli Processivity Ring. *J. Med. Chem.* **2011***, 54*, 4627-4637.

85. André, C.; Martiel, I.; Wolff, P.; Landolfo, M.; Lorber, B.; Silva da Veiga, C.; Dejaegere, A.; Dumas, P.; Guichard, G.; Oliéric, V.; Wagner, J.; Burnouf, D. Y. Interaction of a Model Peptide on Gram Negative and Gram Positive Bacterial Sliding Clamps. *ACS Infect. Dis.* **2019***, 5*, 1022-1034.

86. Kenny, C. H.; Ding, W.; Kelleher, K.; Benard, S.; Dushin, E. G.; Sutherland, A. G.; Mosyak, L.; Kriz, R.; Ellestad, G. Development of a fluorescence polarization assay to screen for inhibitors of the FtsZ/ZipA interaction. *Anal. Biochem.* **2003***, 323*, 224-233.

87. Sutherland, A. G.; Alvarez, J.; Ding, W.; Foreman, K. W.; Kenny, C. H.; Labthavikul, P.; Mosyak, L.; Petersen, P. J.; Rush III, T. S.; Ruzin, A.; Tsao, D. H. H.; Wheless, K. L. Structure-based design of carboxybiphenylindole inhibitors of the ZipA–FtsZ interaction. *Org. Biomol. Chem.* **2003***, 1*, 4138-4140.

88. Jennings, L. D.; Foreman, K. W.; Rush, T. S.; Tsao, D. H. H.; Mosyak, L.; Li, Y.; Sukhdeo, M. N.; Ding, W.; Dushin, E. G.; Kenny, C. H.; Moghazeh, S. L.; Petersen, P. J.; Ruzin, A. V.; Tuckman, M.; Sutherland, A. G. Design and synthesis of indolo[2,3-a]quinolizin-7-one inhibitors of the ZipA–FtsZ interaction. *Bioorg. Med. Chem. Lett.* **2004***, 14*, 1427-1431.

89. Tsao, D. H. H.; Sutherland, A. G.; Jennings, L. D.; Li, Y.; Rush, T. S.; Alvarez, J. C.; Ding, W.; Dushin, E. G.; Dushin, R. G.; Haney, S. A.; Kenny, C. H.; Karl Malakian, A.; Nilakantan, R.; Mosyak, L. Discovery of novel inhibitors of the ZipA/FtsZ complex by NMR fragment screening coupled with structure-based design. *Bioorg. Med. Chem.* **2006***, 14*, 7953-7961.

90. Ma, C.; Yang, X.; Kandemir, H.; Mielczarek, M.; Johnston, E. B.; Griffith, R.; Kumar, N.; Lewis, P. J. Inhibitors of Bacterial Transcription Initiation Complex Formation. *ACS Chem. Biol.* **2013***, 8*, 1972-1980.

91. Hinsberger, S.; Hüsecken, K.; Groh, M.; Negri, M.; Haupenthal, J.; Hartmann, R. W. Discovery of Novel Bacterial RNA Polymerase Inhibitors: Pharmacophore-Based Virtual Screening and Hit Optimization. *J. Med. Chem.* **2013***, 56*, 8332-8338.

92. Mielczarek, M.; Thomas, R. V.; Ma, C.; Kandemir, H.; Yang, X.; Bhadbhade, M.; Black, D. S.; Griffith, R.; Lewis, P. J.; Kumar, N. Synthesis and biological activity of novel mono-indole and mono-benzofuran inhibitors of bacterial transcription initiation complex formation. *Bioorg. Med. Chem.* **2015***, 23*, 1763-1775.

93. Ma, C.; Yang, X.; Lewis, P. J. Bacterial Transcription Inhibitor of RNA Polymerase Holoenzyme Formation by Structure-Based Drug Design: From in Silico Screening to Validation. *ACS Infect. Dis.* **2016***, 2*, 39-46.

94. Sartini, S.; Levati, E.; Maccesi, M.; Guerra, M.; Spadoni, G.; Bach, S.; Benincasa, M.; Scocchi, M.; Ottonello, S.; Rivara, S.; Montanini, B. New Antimicrobials Targeting Bacterial RNA Polymerase Holoenzyme Assembly Identified with an in Vivo BRET-Based Discovery Platform. *ACS Chem. Biol.* **2019***, 14*, 1727-1736.

95. Ahmed Ashraf, M. K.; Habib, M.; Haupenthal, J.; Rolf, W. H.; Empting, M. Hit evaluation of an α-helical peptide: Ala-scan, truncation and sidechain-to-sidechain macrocyclization of an RNA polymerase Inhibitor. *Biol. Chem.* **2019***, 400*, 333-342.

96. Ye, J.; Chu, A. J.; Lin, L.; Chan, S. T.; Harper, R.; Xiao, M.; Artsimovitch, I.; Zuo, Z.; Ma, C.; Yang, X. Benzyl and benzoyl benzoic acid inhibitors of bacterial RNA polymerase-sigma factor interaction. *Eur. J. Med. Chem.* **2020***, 208*, 112671.

97. Ye, J.; Chu, A. J.; Harper, R.; Chan, S. T.; Shek, T. L.; Zhang, Y.; Ip, M.; Sambir, M.; Artsimovitch, I.; Zuo, Z.; Yang, X.; Ma, C. Discovery of Antibacterials That Inhibit Bacterial RNA Polymerase Interactions with Sigma Factors. *J. Med. Chem.* **2020***, 63*, 7695-7720.

98. Ye, J.; Chu, A. J.; Lin, L.; Yang, X.; Ma, C. First-In-Class Inhibitors Targeting the Interaction between Bacterial RNA Polymerase and Sigma Initiation Factor Affect the Viability and Toxin Release of Streptococcus pneumoniae. *Molecules* **2019***, 24*.

99. Cossar, P. J.; Abdel-Hamid, M.; Ma, C.; Sakoff, J. A.; Trinh, T. N.; Gordon, C. P.; Lewis, P. J.; McCluskey, A. Small-Molecule Inhibitors of the NusB–NusE Protein–Protein Interaction with Antibiotic Activity. *ACS Omega* **2017***, 2*, 3839-3857.

100. Cossar, P. J.; Ma, C.; Gordon, C. P.; Ambrus, J. I.; Lewis, P. J.; McCluskey, A. Identification and validation of small molecule modulators of the NusB-NusE interaction. *Bioorg. Med. Chem. Lett.* **2017***, 27*, 162-167.

101. Yang, X.; Luo, M. J.; Yeung, A. C. M.; Lewis, P. J.; Chan, P. K. S.; Ip, M.; Ma, C. First-In-Class Inhibitor of Ribosomal RNA Synthesis with Antimicrobial Activity against Staphylococcus aureus. *Biochemistry* **2017***, 56*, 5049-5052.

102. Qiu, Y.; Chan, S. T.; Lin, L.; Shek, T. L.; Tsang, T. F.; Zhang, Y.; Ip, M.; Chan, P. K.; Blanchard, N.; Hanquet, G.; Zuo, Z.; Yang, X.; Ma, C. Nusbiarylins, a new class of antimicrobial agents: Rational design of bacterial transcription inhibitors targeting the interaction between the NusB and NusE proteins. *Bioorg. Chem.* **2019***, 92*, 103203.

103. Qiu, Y.; Chan, S. T.; Lin, L.; Shek, T. L.; Tsang, T. F.; Barua, N.; Zhang, Y.; Ip, M.; Chan, P. K.; Blanchard, N.; Hanquet, G.; Zuo, Z.; Yang, X.; Ma, C. Design, synthesis and biological evaluation of antimicrobial diarylimine and –amine compounds targeting the interaction between the bacterial NusB and NusE proteins. *Eur. J. Med. Chem.* **2019***, 178*, 214-231.

104. Chu, A. J.; Qiu, Y.; Harper, R.; Lin, L.; Ma, C.; Yang, X. Nusbiarylins Inhibit Transcription and Target Virulence Factors in Bacterial Pathogen Staphylococcus aureus. *Int. J. Mol. Sci.* **2020***, 21*.

105. Li, Y.; Zhu, X.; Zhang, J.; Lin, Y.; You, X.; Chen, M.; Wang, Y.; Zhu, N.; Si, S. Identification of a Compound That Inhibits the Growth of Gram-Negative Bacteria by Blocking BamA–BamD Interaction. *Front. Microbiol.* **2020***, 11*, 1252.

106. Vetterli, S. U.; Zerbe, K.; Müller, M.; Urfer, M.; Mondal, M.; Wang, S. Y.; Moehle, K.; Zerbe, O.; Vitale, A.; Pessi, G.; Eberl, L.; Wollscheid, B.; Robinson, J. A. Thanatin targets the intermembrane protein complex required for lipopolysaccharide transport in Escherichia coli. *Sci. Adv.* **2018***, 4*, eaau2634.

107. Moura, Elisabete C. C. M.; Baeta, T.; Romanelli, A.; Laguri, C.; Martorana, A. M.; Erba, E.; Simorre, J.; Sperandeo, P.; Polissi, A. Thanatin Impairs Lipopolysaccharide Transport Complex Assembly by Targeting LptC–LptA Interaction and Decreasing LptA Stability. *Front. Microbiol.* **2020***, 11*, 909.

108. Zhang, X.; Li, Y.; Wang, W.; Zhang, J.; Lin, Y.; Hong, B.; You, X.; Song, D.; Wang, Y.; Jiang, J.; Si, S. Identification of an anti-Gram-negative bacteria agent disrupting the interaction between lipopolysaccharide transporters LptA and LptC. *Int. J. Antimicrob. Agents* **2019***, 53*, 442-448.

109. Robinson, J. A.; Shankaramma, S. C.; Jetter, P.; Kienzl, U.; Schwendener, R. A.; Vrijbloed, J. W.; Obrecht, D. Properties and structure-activity studies of cyclic beta-hairpin peptidomimetics based on the cationic antimicrobial peptide protegrin I. *Bioorg. Med. Chem.* **2005***, 13*, 2055-2064.

110. Srinivas, N.; Jetter, P.; Ueberbacher, B. J.; Werneburg, M.; Zerbe, K.; Steinmann, J.; Van der Meijden, B.; Bernardini, F.; Lederer, A.; Dias, R. L.; Misson, P. E.; Henze, H.; Zumbrunn, J.; Gombert, F. O.; Obrecht, D.; Hunziker, P.; Schauer, S.; Ziegler, U.; Käch, A.; Eberl, L.; Riedel, K.; DeMarco, S. J.; Robinson, J. A. Peptidomimetic antibiotics target outer-membrane biogenesis in Pseudomonas aeruginosa. *Science* **2010***, 327*, 1010-1013.

111. Sader, H. S.; Flamm, R. K.; Dale, G. E.; Rhomberg, P. R.; Castanheira, M. Murepavadin activity tested against contemporary (2016-17) clinical isolates of XDR Pseudomonas aeruginosa. *J. Antimicrob. Chemother.* **2018***, 73*, 2400-2404.

112. Werneburg, M.; Zerbe, K.; Juhas, M.; Bigler, L.; Stalder, U.; Kaech, A.; Ziegler, U.; Obrecht, D.; Eberl, L.; Robinson, J. A. Inhibition of lipopolysaccharide transport to the outer membrane in Pseudomonas aeruginosa by peptidomimetic antibiotics. *Chembiochem* **2012***, 13*, 1767-1775.

113. Vetterli, S. U.; Moehle, K.; Robinson, J. A. Synthesis and antimicrobial activity against Pseudomonas aeruginosa of macrocyclic β-hairpin peptidomimetic antibiotics containing N-methylated amino acids. *Bioorg. Med. Chem.* **2016***, 24*, 6332-6339.

114. Andolina, G.; Bencze, L.; Zerbe, K.; Müller, M.; Steinmann, J.; Kocherla, H.; Mondal, M.; Sobek, J.; Moehle, K.; Malojčić, G.; Wollscheid, B.; Robinson, J. A. A Peptidomimetic Antibiotic Interacts with the Periplasmic Domain of LptD from Pseudomonas aeruginosa. *ACS Chem. Biol.* **2018***, 13*, 666-675.

115. Chan, W. T.; Espinosa, M.; Yeo, C. C. Keeping the Wolves at Bay: Antitoxins of Prokaryotic Type II Toxin-Antitoxin Systems. *Front. Mol. Biosci.* **2016***, 3*, 9.

116. Jaffé, A.; Ogura, T.; Hiraga, S. Effects of the ccd function of the F plasmid on bacterial growth. *J. Bacteriol.* **1985***, 163*, 841-849.

117. Engelberg-Kulka, H.; Glaser, G. Addiction Modules and Programmed Cell Death and Antideath in Bacterial Cultures. *Annu. Rev. Microbiol.* **1999***, 53*, 43-70.

118. Engelberg-Kulka, H.; Sat, B.; Reches, M.; Amitai, S.; Hazan, R. Bacterial programmed cell death systems as targets for antibiotics. *Trends Microbiol.* **2004***, 12*, 66-71.

119. Tanouchi, Y.; Lee, A. J.; Meredith, H.; You, L. Programmed cell death in bacteria and implications for antibiotic therapy. *Trends Microbiol.* **2013***, 21*, 265-270.

120. Kang, S.; Kim, D.; Lee, K.; Park, S. J.; Yoon, H.; Lee, S. J.; Im, H.; Lee, B. Functional details of the Mycobacterium tuberculosis VapBC26 toxin-antitoxin system based on a structural study: insights into unique binding and antibiotic peptides. *Nucleic Acids Res.* **2017***, 45*, 8564-8580.

121. Deep, A.; Tiwari, P.; Agarwal, S.; Kaundal, S.; Kidwai, S.; Singh, R.; Thakur, K. G. Structural, functional and biological insights into the role of Mycobacterium tuberculosis VapBC11 toxin–antitoxin system: targeting a tRNase to tackle mycobacterial adaptation. *Nucleic Acids Res.* **2018***, 46*, 11639-11655.

122. Sundar, S.; Rajan, M. P.; Piramanayagam, S. In Silico Derived Peptides for Inhibiting the Toxin–Antitoxin Systems of Mycobacterium tuberculosis: Basis for Developing Peptide-Based Therapeutics. *Int. J. Pept. Res. Ther.* **2019***, 25*, 1467-1475.

123. Kim, D. H.; Kang, S. M.; Park, S. J.; Jin, C.; Yoon, H. J.; Lee, B. J. Functional insights into the Streptococcus pneumoniae HicBA toxin-antitoxin system based on a structural study. *Nucleic Acids Res.* **2018***, 46*, 6371-6386.

124. Belitsky, M.; Avshalom, H.; Erental, A.; Yelin, I.; Kumar, S.; London, N.; Sperber, M.; Schueler-Furman, O.; Engelberg-Kulka, H. The *Escherichia coli* Extracellular Death Factor EDF Induces the Endoribonucleolytic Activities of the Toxins MazF and ChpBK. *Mol. Cell* **2011***, 41*, 625-635.

125. Ahn, D.; Lee, K.; Lee, S. J.; Park, S. J.; Yoon, H.; Kim, S.; Lee, B. Structural analyses of the MazEF4 toxin-antitoxin pair in Mycobacterium tuberculosis provide evidence for a unique extracellular death factor. *J. Biol. Chem.* **2017***, 292*, 18832-18847.

126. Kumar, S.; Kolodkin-Gal, I.; Engelberg-Kulka, H. Novel Quorum-Sensing Peptides Mediating Interspecies Bacterial Cell Death. *mBio* **2013***, 4*, 314.

127. Nigam, A.; Kumar, S.; Engelberg-Kulka, H. Quorum Sensing Extracellular Death Peptides Enhance the Endoribonucleolytic Activities of *Mycobacterium tuberculosis* MazF Toxins. *mBio* **2018***, 9*, 685.

128. Verma, S.; Kumar, S.; Gupta, V. P.; Gourinath, S.; Bhatnagar, S.; Bhatnagar, R. Structural basis of Bacillus anthracis MoxXT disruption and the modulation of MoxT ribonuclease activity by rationally designed peptides. *J. Biomol. Struct. Dyn.* **2015***, 33*, 606-624.

129. Agarwal, S.; Agarwal, S.; Bhatnagar, R. Identification and characterization of a novel toxin–antitoxin module from Bacillus anthracis. *FEBS Lett.* **2007***, 581*, 1727-1734.

130. Agarwal, S.; Mishra, N. K.; Bhatnagar, S.; Bhatnagar, R. PemK Toxin of Bacillus anthracis Is a Ribonuclease: an insight into its active site, structure, function. *J. Biol. Chem.* **2010***, 285*, 7254-7270.

131. Chopra, N.; Agarwal, S.; Verma, S.; Bhatnagar, S.; Bhatnagar, R. Modelling of the structure and interactions of the B. anthracis antitoxin, MoxX: deletion mutant studies highlight its modular structure and repressor function. *J. Comput. Aided Mol. Des.* **2011***, 25*, 275-291.

132. Mohammadzadeh, R.; Shivaee, A.; Ohadi, E.; Kalani, B. S. In Silico Insight into the Dominant Type II Toxin–Antitoxin Systems and Clp Proteases in Listeria monocytogenes and Designation of Derived Peptides as a Novel Approach to Interfere with this System. *Int. J. Pept. Res. Ther.* **2020***, 26*, 613-623.

133. Farhadi, T.; Hashemian, S. M.; Farhadi, Z. In Silico Designing of Peptidomimetics Enhancing Endoribonucleolytic Activities of Acinetobacter MazF Toxin as the Novel Anti-bacterial Candidates. *Int. J. Pept. Res. Ther.* **2020***, 26*, 1061-1071.

134. Lioy, V. S.; Rey, O.; Balsa, D.; Pellicer, T.; Alonso, J. C. A toxin–antitoxin module as a target for antimicrobial development. *Plasmid* **2010***, 63*, 31-39.

135. Fernández-Bachiller, M. I.; Brzozowska, I.; Odolczyk, N.; Zielenkiewicz, U.; Zielenkiewicz, P.; Rademann, J. Mapping Protein-Protein Interactions of the Resistance-Related Bacterial Zeta Toxin-Epsilon Antitoxin Complex ($\varepsilon_2\zeta_2$) with High Affinity Peptide Ligands Using Fluorescence Polarization. *Toxins (Basel)* **2016***, 8*, 222.

136. Gao, X.; Mu, Z.; Qin, B.; Sun, Y.; Cui, S. Structure-Based Prototype Peptides Targeting the Pseudomonas aeruginosa Type VI Secretion System Effector as a Novel Antibacterial Strategy. *Front. Cell. Infect. Microbiol.* **2017***, 7*, 411.

137. Li, T.; Yin, N.; Liu, H.; Pei, J.; Lai, L. Novel Inhibitors of Toxin HipA Reduce Multidrug Tolerant Persisters. *ACS Med. Chem. Lett.* **2016***, 7*, 449-453.

138. Baneyx, F. Recombinant protein expression in Escherichia coli. *Curr. Opin. Biotechnol.* **1999***, 10*, 411-421.

139. Structural Genomics Consortium; China Structural Genomics Consortium; Northeast Structural Genomics Consortium; Gräslund, S.; Nordlund, P.; Weigelt, J.; Hallberg, B. M.; Bray, J.; Gileadi, O.; Knapp, S.; Oppermann, U.; Arrowsmith, C.; Hui, R.; Ming, J.; dhe-Paganon, S.; Park, H. W.; Savchenko, A.; Yee, A.; Edwards, A.; Vincentelli, R.; Cambillau, C.; Kim, R.; Kim, S. H.; Rao, Z.; Shi, Y.; Terwilliger, T. C.; Kim, C. Y.; Hung, L. W.; Waldo, G. S.; Peleg, Y.; Albeck, S.; Unger, T.; Dym, O.; Prilusky, J.; Sussman, J. L.; Stevens, R. C.; Lesley, S. A.; Wilson, I. A.; Joachimiak, A.; Collart, F.; Dementieva, I.; Donnelly, M. I.; Eschenfeldt, W. H.; Kim, Y.; Stols, L.; Wu, R.; Zhou, M.; Burley, S. K.; Emtage, J. S.; Sauder, J. M.; Thompson, D.; Bain, K.; Luz, J.; Gheyi, T.; Zhang, F.; Atwell, S.; Almo, S. C.; Bonanno, J. B.; Fiser, A.; Swaminathan, S.; Studier, F. W.; Chance, M. R.; Sali, A.; Acton, T. B.; Xiao, R.; Zhao, L.; Ma, L. C.; Hunt, J. F.; Tong, L.; Cunningham, K.; Inouye, M.; Anderson, S.; Janjua, H.; Shastry, R.; Ho, C. K.; Wang, D.; Wang, H.; Jiang, M.; Montelione, G. T.; Stuart, D. I.; Owens, R. J.; Daenke, S.; Schütz, A.; Heinemann, U.; Yokoyama, S.; Büssow, K.; Gunsalus, K. C. Protein production and purification. *Nat. Methods* **2008***, 5*, 135-146.

140. Sterckx, Y. G. -.; De Gieter, S.; Zorzini, V.; Hadži, S.; Haesaerts, S.; Loris, R.; Garcia-Pino, A. An efficient method for the purification of proteins from four distinct toxin–antitoxin modules. *Protein Expr. Purif.* **2015***, 108*, 30-40.

141. Garcia-Pino, A.; Christensen-Dalsgaard, M.; Wyns, L.; Yarmolinsky, M.; Magnuson, R. D.; Gerdes, K.; Loris, R. Doc of prophage P1 is inhibited by its antitoxin partner Phd through fold complementation. *J. Biol. Chem.* **2008***, 283*, 30821-30827.

142. Li, G. Y.; Zhang, Y.; Chan, M. C.; Mal, T. K.; Hoeflich, K. P.; Inouye, M.; Ikura, M. Characterization of dual substrate binding sites in the homodimeric structure of Escherichia coli mRNA interferase MazF. *J. Mol. Biol.* **2006***, 357*, 139-150.

143. Ovchinnikov, S. V.; Bikmetov, D.; Livenskyi, A.; Serebryakova, M.; Wilcox, B.; Mangano, K.; Shiriaev, D. I.; Osterman, I. A.; Sergiev, P. V.; Borukhov, S.; Vazquez-Laslop, N.; Mankin, A. S.; Severinov, K.; Dubiley, S. Mechanism of translation inhibition by type II GNAT toxin AtaT2. *Nucleic Acids Res.* **2020***, 48*, 8617-8625.

144. Khambhati, K.; Bhattacharjee, G.; Gohil, N.; Braddick, D.; Kulkarni, V.; Singh, V. Exploring the Potential of Cell-Free Protein Synthesis for Extending the Abilities of Biological Systems. *Front. Bioeng. Biotechnol.* **2019***, 7*, 248.

145. Cregg, J. M.; Cereghino, J. L.; Shi, J.; Higgins, D. R. Recombinant protein expression in Pichia pastoris. *Mol. Biotechnol.* **2000***, 16*, 23-52.

146. Kitagawa, M.; Ara, T.; Arifuzzaman, M.; Ioka-Nakamichi, T.; Inamoto, E.; Toyonaga, H.; Mori, H. Complete set of ORF clones of Escherichia coli ASKA library (a complete set of E. coli K-12 ORF archive): unique resources for biological research. *DNA Res.* **2005***, 12*, 291-299.

147. Ito, K.; Murakami, R.; Mochizuki, M.; Qi, H.; Shimizu, Y.; Miura, K.; Ueda, T.; Uchiumi, T. Structural basis for the substrate recognition and catalysis of peptidyl-tRNA hydrolase. *Nucleic Acids Res.* **2012***, 40*, 10521-10531.

148. Giudice, E.; Gillet, R. The task force that rescues stalled ribosomes in bacteria. *Trends Biochem. Sci.* **2013***, 38*, 403-411.

149. Chaga, G.; Hopp, J.; Nelson, P. Immobilized metal ion affinity chromatography on Co2+-carboxymethylaspartate-agarose Superflow, as demonstrated by one-step purification of lactate dehydrogenase from chicken breast muscle. *Biotechnol. Appl. Biochem.* **1999***, 29 (Pt 1)*, 19-24.

150. Fairhead, M.; Howarth, M. Site-specific biotinylation of purified proteins using BirA. *Methods Mol. Biol.* **2015***, 1266*, 171-184.

151. Stites, W. E. Protein−Protein Interactions: Interface Structure, Binding Thermodynamics, and Mutational Analysis. *Chem. Rev.* **1997***, 97*, 1233-1250.

152. Wells, J. A.; McClendon, C. L. Reaching for high-hanging fruit in drug discovery at protein–protein interfaces. *Nature* **2007***, 450*, 1001-1009.

153. Lee, K. Y.; Lee, B. J. Structure, Biology, and Therapeutic Application of Toxin-Antitoxin Systems in Pathogenic Bacteria. *Toxins (Basel)* **2016***, 8*, 10.3390/toxins8100305.

154. Nathan, F.; Goormaghtigh Frédéric; Van, M. L.; William, M. Type II Toxin-Antitoxin Systems: Evolution and Revolutions. *J. Bacteriol. , 202*, 763.

155. Zhang, S.; Wang, Q.; Quan, S.; Yu, X.; Wang, Y.; Guo, D.; Peng, L.; Feng, H.; He, Y. Type II toxin–antitoxin system in bacteria: activation, function, and mode of action. *Biophys. Rep.* **2020***, 6*, 68-79.

156. Loris, R.; Marianovsky, I.; Lah, J.; Laeremans, T.; Engelberg-Kulka, H.; Glaser, G.; Muyldermans, S.; Wyns, L. Crystal structure of the intrinsically flexible addiction antidote MazE. *J. Biol. Chem.* **2003***, 278*, 28252-28257.

157. Madl, T.; Van Melderen, L.; Mine, N.; Respondek, M.; Oberer, M.; Keller, W.; Khatai, L.; Zangger, K. Structural basis for nucleic acid and toxin recognition of the bacterial antitoxin CcdA. *J. Mol. Biol.* **2006***, 364*, 170-185.

158. Oberer, M.; Zangger, K.; Gruber, K.; Keller, W. The solution structure of ParD, the antidote of the ParDE toxin antitoxin module, provides the structural basis for DNA and toxin binding. *Protein Sci.* **2007***, 16*, 1676-1688.

159. Cherny, I.; Gazit, E. The YefM antitoxin defines a family of natively unfolded proteins: implications as a novel antibacterial target. *J. Biol. Chem.* **2004***, 279*, 8252-8261.

160. Li, G. Y.; Zhang, Y.; Inouye, M.; Ikura, M. Structural mechanism of transcriptional autorepression of the Escherichia coli RelB/RelE antitoxin/toxin module. *J. Mol. Biol.* **2008***, 380*, 107-119.

161. Brown, B. L.; Lord, D. M.; Grigoriu, S.; Peti, W.; Page, R. The *Escherichia coli* Toxin MqsR Destabilizes the Transcriptional Repression Complex Formed between the Antitoxin MqsA and the *mqsRA* Operon Promoter * *J. Biol. Chem.* **2013***, 288*, 1286-1294.

162. De Jonge, N.; Garcia-Pino, A.; Buts, L.; Haesaerts, S.; Charlier, D.; Zangger, K.; Wyns, L.; De Greve, H.; Loris, R. Rejuvenation of CcdB-Poisoned Gyrase by an Intrinsically Disordered Protein Domain. *Mol. Cell* **2009***, 35*, 154-163.

163. Overgaard, M.; Borch, J.; Gerdes, K. RelB and RelE of Escherichia coli form a tight complex that represses transcription via the ribbon-helix-helix motif in RelB. *J. Mol. Biol.* **2009***, 394*, 183-196.

164. Khoo, S. K.; Loll, B.; Chan, W. T.; Shoeman, R. L.; Ngoo, L.; Yeo, C. C.; Meinhart, A. Molecular and Structural Characterization of the PezAT Chromosomal Toxin-Antitoxin System of the Human Pathogen *Streptococcus pneumoniae J. Biol. Chem.* **2007***, 282*, 19606-19618.

165. Dao-Thi, M.; Van Melderen, L.; De Genst, E.; Afif, H.; Buts, L.; Wyns, L.; Loris, R. Molecular Basis of Gyrase Poisoning by the Addiction Toxin CcdB. *J. Mol. Biol.* **2005***, 348*, 1091-1102.

166. Garcia-Pino, A.; Balasubramanian, S.; Wyns, L.; Gazit, E.; De Greve, H.; Magnuson, R. D.; Charlier, D.; van Nuland, Nico A. J.; Loris, R. Allostery and Intrinsic Disorder Mediate Transcription Regulation by Conditional Cooperativity. *Cell* **2010***, 142*, 101-111.

167. Winther, K. S.; Gerdes, K. Regulation of enteric vapBC transcription: induction by VapC toxin dimer-breaking. *Nucleic Acids Res.* **2012***, 40*, 4347-4357.

168. Vedadi, M.; Arrowsmith, C. H.; Allali-Hassani, A.; Senisterra, G.; Wasney, G. A. Biophysical characterization of recombinant proteins: a key to higher structural genomics success. *J. Struct. Biol.* **2010***, 172*, 107-119.

169. Niesen, F. H.; Berglund, H.; Vedadi, M. The use of differential scanning fluorimetry to detect ligand interactions that promote protein stability. *Nat. Protoc.* **2007***, 2*, 2212-2221.

170. Vedadi, M.; Niesen, F. H.; Allali-Hassani, A.; Fedorov, O. Y.; Finerty, P. J.,Jr; Wasney, G. A.; Yeung, R.; Arrowsmith, C.; Ball, L. J.; Berglund, H.; Hui, R.; Marsden, B. D.; Nordlund, P.; Sundstrom, M.; Weigelt, J.; Edwards, A. M. Chemical screening methods to identify ligands that promote protein stability, protein crystallization, and structure determination. *Proc. Natl. Acad. Sci. U. S. A.* **2006***, 103*, 15835-15840.

171. Jameson, D. M.; Seifried, S. E. Quantification of protein-protein interactions using fluorescence polarization. *Methods* **1999***, 19*, 222-233.

172. Du, Y.; Moulick, K.; Rodina, A.; Aguirre, J.; Felts, S.; Dingledine, R.; Fu, H.; Chiosis, G. High-throughput screening fluorescence polarization assay for tumor-specific Hsp90. *J. Biomol. Screen.* **2007***, 12*, 915-924.

173. Reindl, W.; Gräber, M.; Strebhardt, K.; Berg, T. Development of high-throughput assays based on fluorescence polarization for inhibitors of the polo-box domains of polo-like kinases 2 and 3. *Anal. Biochem.* **2009***, 395*, 189-194.

174. Strutt, J. W. On the dynamical theory of gratings. *Proc. Math. Phys. Eng.* **1907***, 79*, 399-416.

175. Wood, R. W. XXVII. Diffraction gratings with controlled groove form and abnormal distribution of intensity. *London Edinburgh Philos. Mag. J. Sci.* **1912***, 23*, 310-317.

176. Liedberg, B.; Lundström, I.; Stenberg, E. Principles of biosensing with an extended coupling matrix and surface plasmon resonance. *Sensors Actuators B: Chem.* **1993***, 11*, 63-72.

177. Zhang, L. M.; Uttamchandani, D. Optical chemical sensing employing surface plasmon resonance. *Electron. Lett.* **1988***, 24*, 1469 -1470

178. Akimoto, T.; Sasaki, S.; Ikebukuro, K.; Karube, I. Effect of incident angle of light on sensitivity and detection limit for layers of antibody with surface plasmon resonance spectroscopy. *Biosens. Bioelectron.* **2000***, 15*, 355-362.

179. Stenberg, E.; Persson, B.; Roos, H.; Urbaniczky, C. Quantitative determination of surface concentration of protein with surface plasmon resonance using radiolabeled proteins. *J. Colloid Interface Sci.* **1991***, 143*, 513-526.

180. Arnesen, T. Towards a Functional Understanding of Protein N-Terminal Acetylation. *PLOS Biology* **2011***, 9*, e1001074.

181. Merrifield, R. B. Solid Phase Peptide Synthesis. I. The Synthesis of a Tetrapeptide. *J. Am. Chem. Soc.* **1963***, 85*, 2149-2154.

182. Liu, B.; Poolman, B.; Boersma, A. J. Ionic Strength Sensing in Living Cells. *ACS Chem. Biol.* **2017***, 12*, 2510-2514.

183. Maguire, M. E.; Cowan, J. A. Magnesium chemistry and biochemistry. *Biometals* **2002***, 15*, 203-210.

184. Passioura, T.; Suga, H. A RaPID way to discover nonstandard macrocyclic peptide modulators of drug targets. *Chem. Commun.* **2017***, 53*, 1931-1940.

185. Huang, Y.; Wiedmann, M. M.; Suga, H. RNA Display Methods for the Discovery of Bioactive Macrocycles. *Chem. Rev.* **2019***, 119*, 10360-10391.

186. Suga, H. Max-Bergmann award lecture:A RaPID way to discover bioactive nonstandard peptides assisted by the flexizyme and FIT systems. *J. Pep. Sci.* **2018***, 24*, e3055.

187. Studier, F. W. Protein production by auto-induction in high-density shaking cultures. *Protein Expr. Purif.* **2005***, 41*, 207-234.

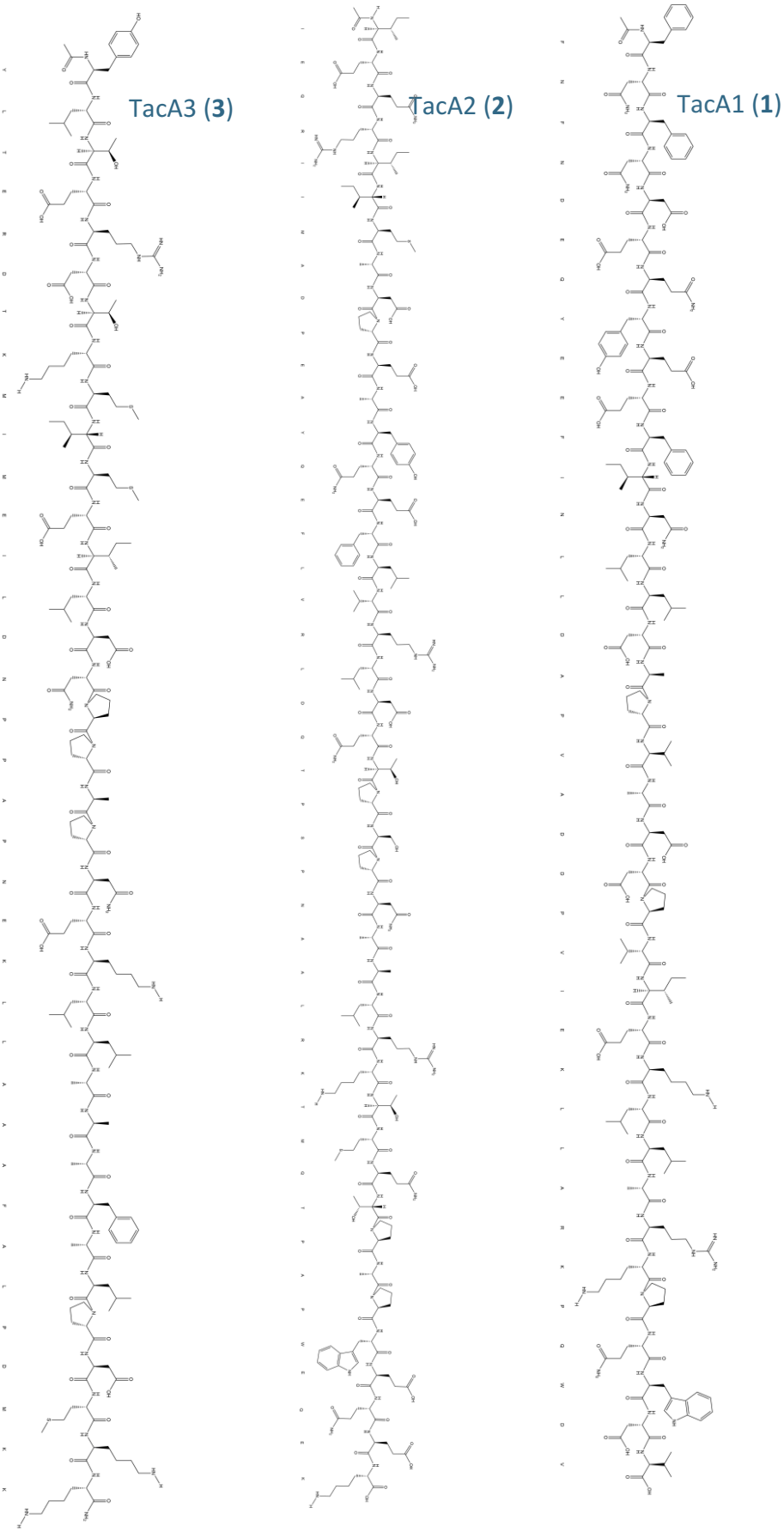
188. Gasteiger, E.; Hoogland, C.; Gattiker, A.; Duvaud, S.; Wilkins, M. R.; Appel, R. D.; Bairoch, A. Protein Identification and Analysis Tools on the ExPASy Server. In *The Proteomics Protocols Handbook*; Walker, J. M., Ed.; Humana Press: Totowa, NJ, 2005; pp 571-607.

189. Heyduk, T.; Ma, Y.; Tang, H.; Ebright, R. H. Fluorescence anisotropy: Rapid, quantitative assay for protein-DNA and protein-protein interaction. *Meth. Enzymol.* **1996***, 274*, 492-503.

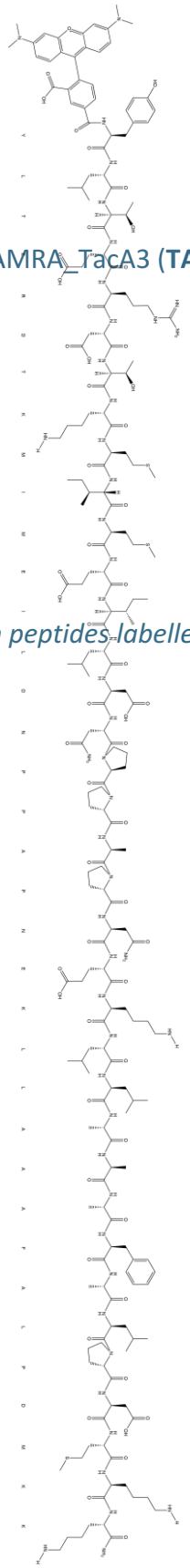
APPENDIX

Sequencing		
	pQE65	TGAGCGGATAACAATTTCACACAG
	pQE276	GGCAACCGAGCGTTCTGAAC
	P29SENrev	GCCTTTCGTTTTATTTGA
DNA Ligation		
	FP1_TacT1_pQE80LC	CACGAAGTGGGACGTGTAACAGCACC
	RP1_TacT1_pQE80LC	GTAAGCTTACTATTGAGGGAGCCTAAGGAACAATG
	FP2_TacT1_pQE80LC	GGCTCCCTCAATAGTAAGCTTACAATTGGTGGTACATAG
	RP2_TacT1_pQE80LC	GTTACACGTCCCACTTCGTGCCATTCGATTTTCTG
	FP1_TacT2_pQE80LC	GAATGGCACGAAATGATCTCCACCCCTGAGC
	RP1_TacT2_pQE80LC	GTAAGCTTATTAAACACTCTCCACCAAATCCCC
	FP2_TacT2_pQE80LC	GTGGAGAGTGTTTAATAAGCTTACAATTGGTGGTACATAG
	RP2_TacT2_pQE80LC	GAGATCATTTCGTGCCATTCGATTTTCTG
	FP1_TacT3_pQE80LC	GAATGGCACGAAATGATGTTTACAGACTGGCATGAGG
	RP1_TacT3_pQE80LC	GCTTATCATAACCTACCAGATGCAGATAAAGCAG
	FP2_TacT3_pQE80LC	GCATCTGGTAGGTTATGATAAGCTTACAATTGGTGGTAC
	RP2_TacT3_pQE80LC	GTAAACATCATTTCGTGCCATTCGATTTTC
Mutagenesis		
	TacT1_F140Y_fwrd	GCCAAAAATTTCTACATTCACCATGG
	TacT1_F140Y_rev	TTCTTCGGTAAGTGCATG
	TacT2_F137Y_fwrd	CGGGAATTTTATCAGCGGGTGGG
	TacT2_F137Y_rev	CGCTTCATCCGACAGGGC
	TacT3_F143Y_fwrd	GACTGGTACAAAGGATTTGGCG
	TacT3_F143Y_rev	GCAGACCTGTTTATTTTTGGCATC

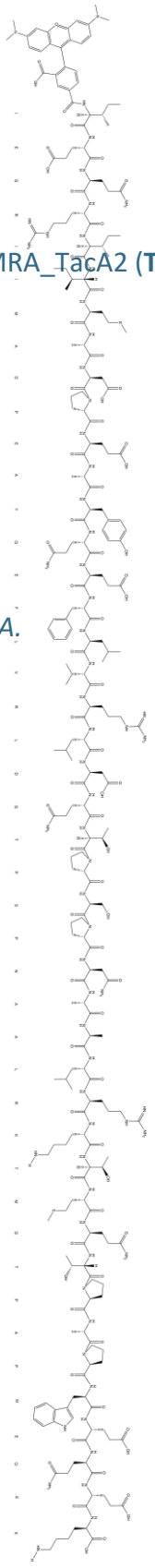
Table S1: *Primers used for sequencing and DNA hi-fi ligation.*



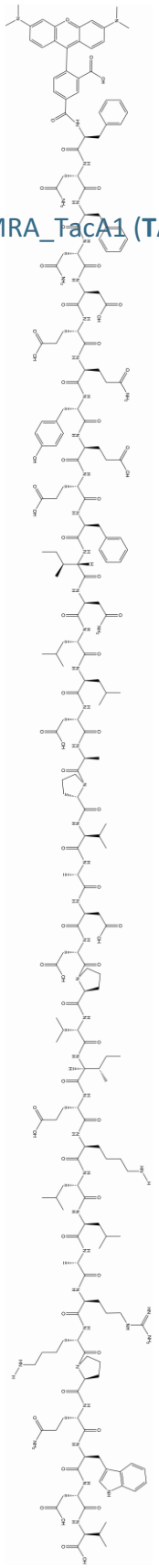
*minimum antitoxin peptides **1-3**.*



TAMRA_TacA3 (**TAMRA_3**)



TAMRA_TacA2 (**TAMRA_2**)



TAMRA_TacA1 (**TAMRA_1**)

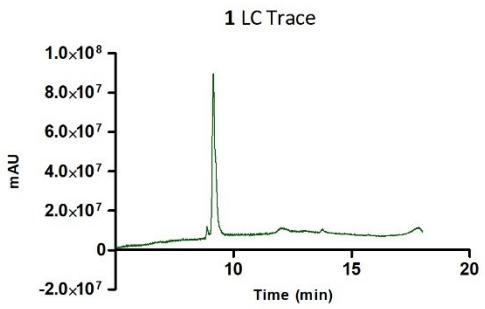
of minimum antitoxin peptides labelled with TAMRA.

Peptide	Purity	Mass
1	100%	3mg
2	100%	2.5mg
3	99.8%	4mg
TAMRA_1	100%	5mg
TAMRA_2	99.8%	2mg
TAMRA_3	99%	1.5mg

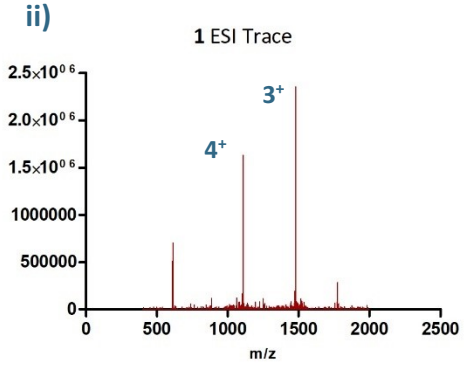
Table S 1: *Purities and mass of minimum antitoxin peptides*

a)

i)

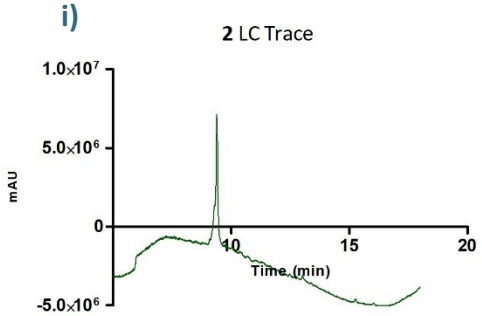


ii)

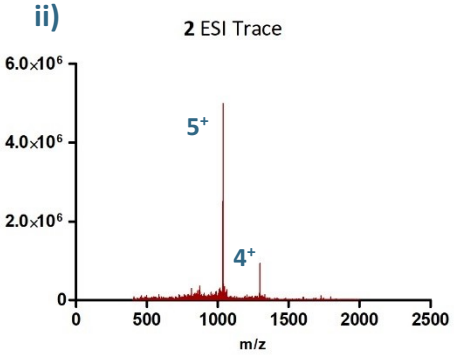


b)

i)

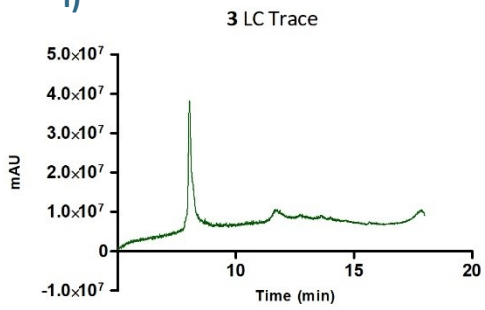


ii)

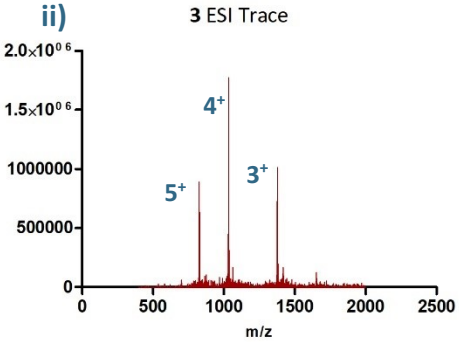


c)

i)



ii)



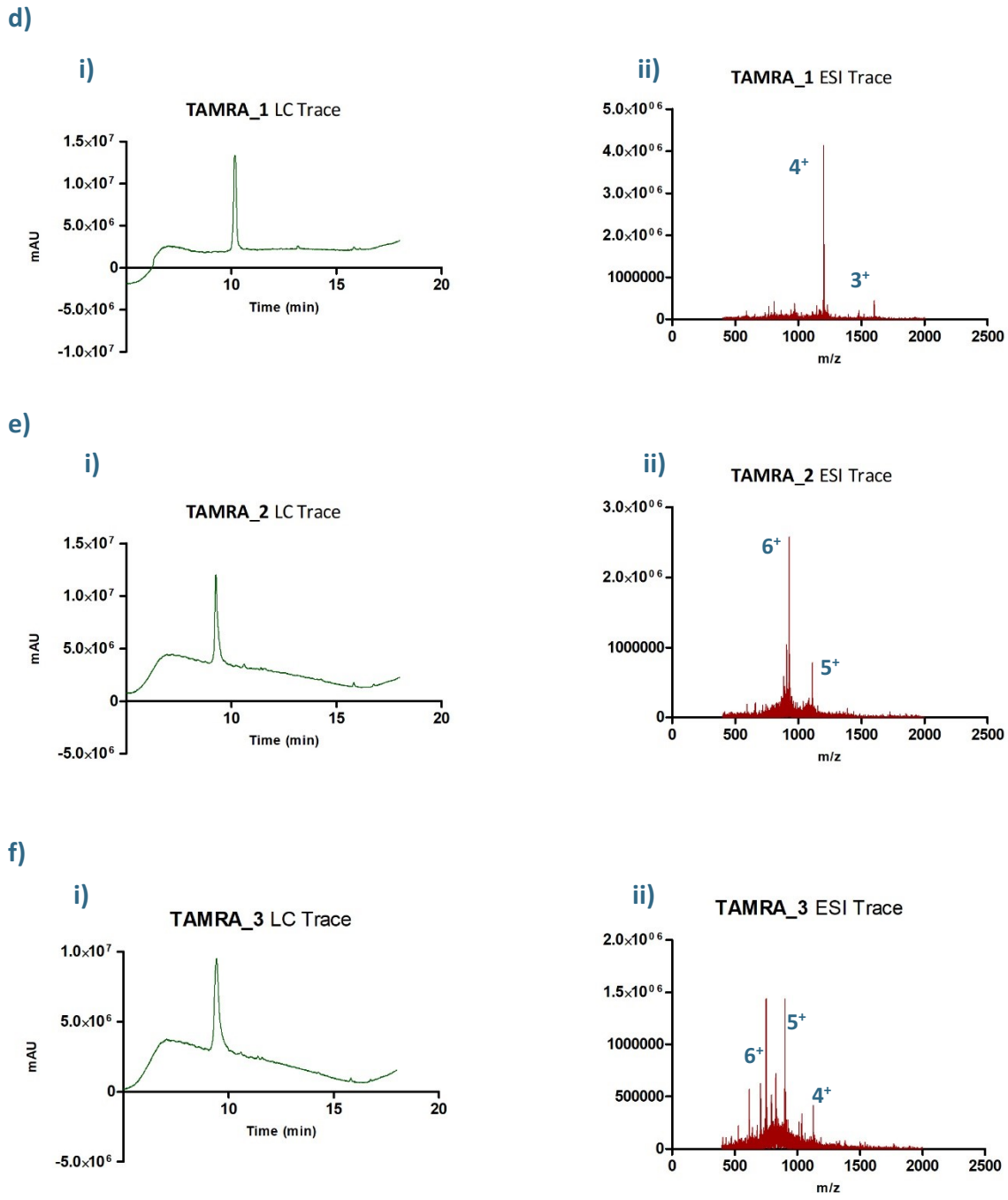
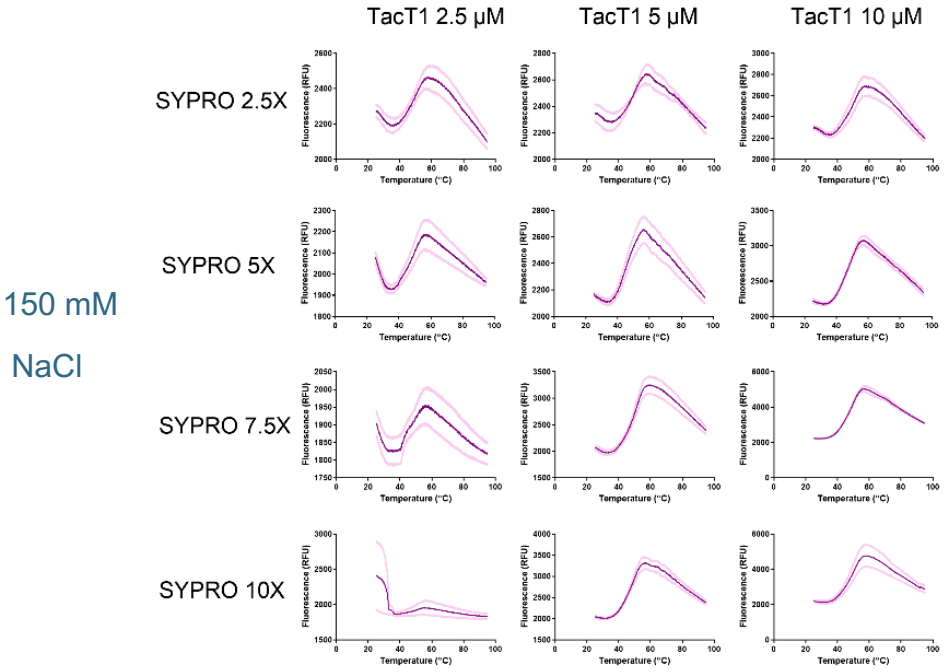
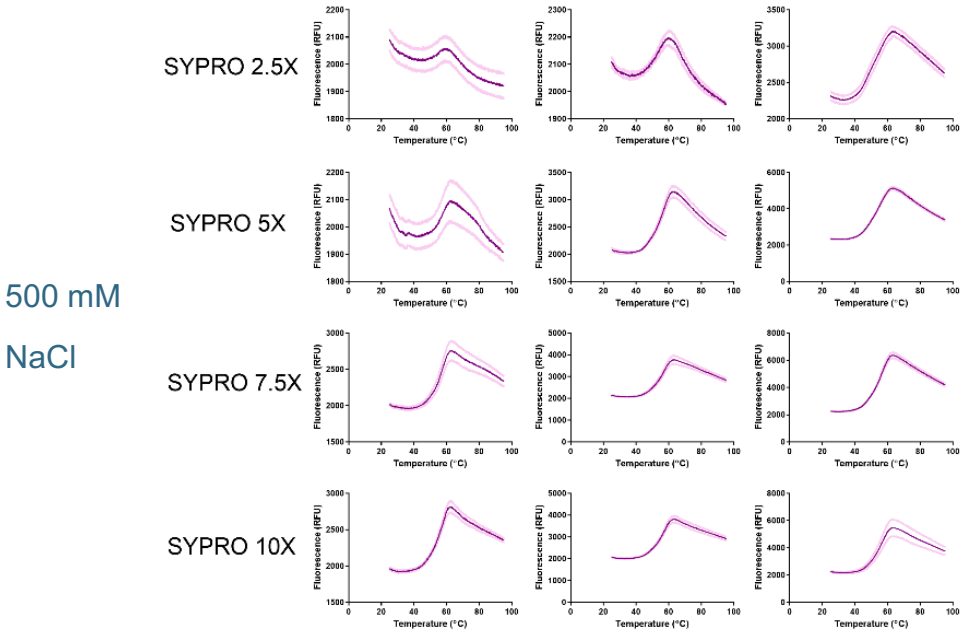


Figure S 3: UV chromatograms at 280 nm (i) and ESI traces of purified peptides (ii)*. A single peak was observed in UV chromatograms corresponding to the desired product* ***a.i) 1; b.i) 2; c.i) 3*** *and* ***d.i) TAMRA_1; e.i) TAMRA_2*** *and* ***f.i) TAMRA_3.*** *The peaks in the mass spectrograms correspond to the charged peptide ions* ***a.ii)*** *Expected mass of* ***1*** *was 4434.4 Da, the following ions were observed: 4^+ (1109.9) and 3^+ (1478.1)****; b.i)*** *Expected mass of* ***2*** *was 5183.9 Da, the following ions were observed: 5^+ (1037.8) and 4^+ (1296.6)****; c.i)*** *Expected mass of* ***3*** *was 4130.9 Da, the following ions were observed: 5^+ (827.4), 4^+ (1033.1) and 3^+ (1377.8);* ***d.i)*** *Expected mass of* ***TAMRA_1*** *was 4806.4 Da, the following ions were observed: 4^+ (1202.9) and 3^+ (1602.5)****; e.i)*** *Expected mass of* ***TAMRA_2*** *was 5555.3 Da, the following ions were observed: 6^+ (926.7) and 5^+ (1111.7) and* ***f.i)*** *Expected mass of* ***TAMRA_3*** *was 4502.3 Da, , the following ions were observed: 6^+ (750.9) and 5^+ (901.7) and 4^+ (1125.9)*

a)


TacT1 2.5 µM
TacT1 5 µM
TacT1 10 µM
SYPRO 2.5X
SYPRO 5X
SYPRO 7.5X
SYPRO 10X
150 mM NaCl
Fluorescence (RFU)
Temperature (°C)


SYPRO 2.5X
SYPRO 5X
SYPRO 7.5X
SYPRO 10X
500 mM NaCl
Fluorescence (RFU)
Temperature (°C)

b)

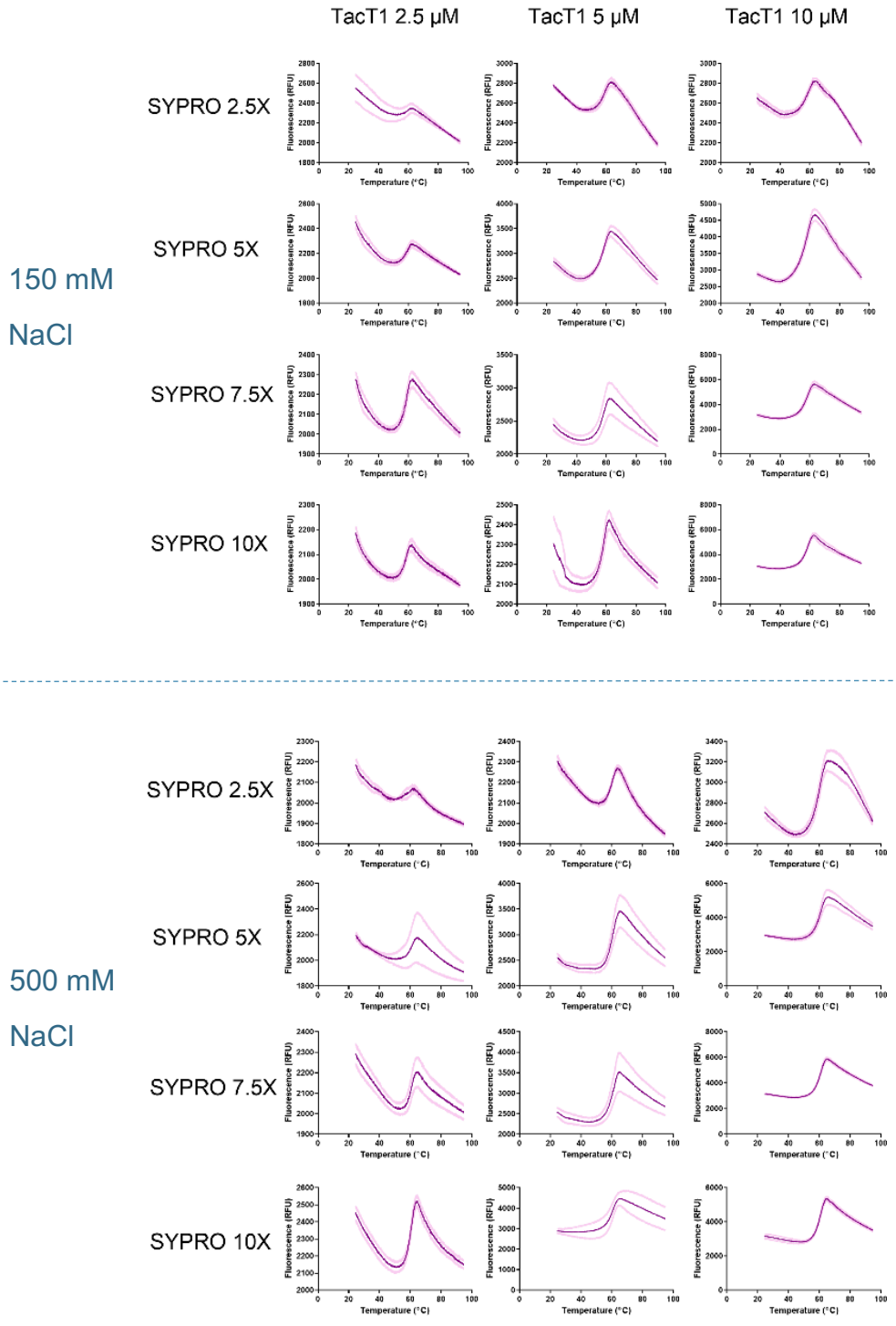

TacT1 2.5 µM
TacT1 5 µM
TacT1 10 µM
SYPRO 2.5X
SYPRO 5X
SYPRO 7.5X
SYPRO 10X
150 mM NaCl
500 mM NaCl
Fluorescence (RFU)
Temperature (°C)

***Figure S4: DSF with TacT2 and TacT3 proteins at different conditions**. The change in fluorescence of **a)** TacT2 and **b)** TacT3 proteins (2.5-10 µM) in solution in the presence of SYPRO-Orange dye (2.5 – 10 X (1:2000 -1:500)) with increasing temperatures between 25-95°C. Measured in two buffers at different salt concentrations 150 mM and 500 mM NaCl. The average of triplicate measurements is shown with the dark purple line and the standard deviation shown with light purple lines.*